We are IntechOpen,
the world's leading publisher of
Open Access books
Built by scientists, for scientists

6,900
Open access books available

185,000
International authors and editors

200M
Downloads

Our authors are among the

154
Countries delivered to

TOP 1%
most cited scientists

12.2%
Contributors from top 500 universities

BOOK CITATION INDEX
CLARIVATE ANALYTICS
INDEXED

WEB OF SCIENCE™

Selection of our books indexed in the Book Citation Index
in Web of Science™ Core Collection (BKCI)

Interested in publishing with us?
Contact book.department@intechopen.com

Thermodynamics of Protein Structure Formation and Function

Dan W. Urry

Bioelastics Inc., Vestavia Hills, Alabama
USA

1. Introduction

1.1 The birth of thermodynamics with the development of the steam-powered heat engine

Thermodynamics was born of the need to improve efficiency of the steam-powered heat engine in order that flooded salt mines of England could become more productive. The *water-to-vapor phase transition* provides the physical property whereby the steam-powered heat engine functions. Heat flows into the engine at the 100°C of the phase transition to effect a dramatic volume expansion. *For the steam-powered heat engine, heating causes expansion to perform mechanical work*. Principal contributors to the initial development of thermodynamics were Nicolas Léonard Sadi Carnot (1824), French physicist and military engineer who died of cholera in 1832 at the age of 36 and William Thomson (Lord Kelvin), a physicist and engineer of the University of Glasgow, whose contribution was in the period of 1840 to 1855 (Smith, 1977).

Looking back at this remarkable development, Prigogine and Stengers (1984a) state, under the section heading of "Heat, the Rival of Gravitation" that "Out of all this common knowledge, nineteenth-century science concentrated on the single fact that combustion produces heat and that heat may lead to an increase in volume; as a result, combustion produces work. Fire leads, therefore, to a new kind of machine, the heat engine, the technological innovation on which industrial society was founded." Heating water at 100°C converts water to steam, a phase transition, to an increase in disorder (in entropy). Perhaps Lord Kelvin's statement of the Second Law of Thermodynamics is most relevant to our concerns, which is "It is impossible to convert heat completely into work in a cyclic process." Greater efficiencies in the conversion of heat into work become possible when heat is poured into a system at the temperature of a transition. Biology utilizes a unique and unfailing two-component phase transition of protein-in-water, and biology does so with a particularly empowering twist made possible by the accuracy and diversity of its protein sequences.

1.2 The aqueous protein-based heat engine of biology

The heat engine of biology comprises a two-component system of protein-in-water. Heating the fully hydrated (soluble) protein effects a phase separation of hydrophobic association (an association of oil-like side chains) that results in contraction. As depicted in Figure 1A, a model protein of the repeating pentamer sequence, (glycyl-valyl-glycyl-valyl-prolyl)$_{251}$, in water (cross-linked by γ-irradiation to form a transparent elastic-contractile sheet) is swollen

below the temperature of the transition and contracts on heating to raise the temperature from below to above the that of the phase transition. As seen in Fig. 1B, on heating the strip becomes transiently opaque, while contracting to lift a weight in the performance of mechanical work. *For the protein-in-water heat engine of biology, heating causes contraction to perform mechanical work.*
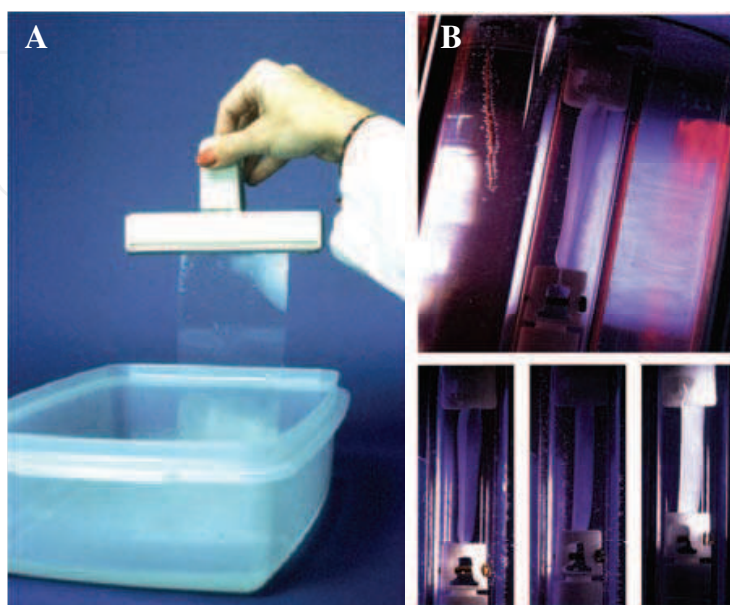

Fig. 1. An aqueous protein-based heat engine of biology, a water swollen sheet and a contracting strip of the cross-linked $(GVGVP)_{251}$, which is the basic elastic-contractile model protein of our study
A. Water-swollen transparent sheet below the temperature of the onset of the phase transition.
B. Upper: Aqueous chamber at a tilt containing a thermocouple and a strip, the heat engine, stretched by an attached weight. Lower: As the temperature is raised through that of the phase transition, the protein in water heat engine performs the work of lifting a weight by contraction. From Urry, 1995 with permission of Ann States Photography.

For warm-blooded animals, however, temperatures change very little. Importantly in these cases, the protein-in-water heat engine does not require heating to raise the temperature from below to above the temperature of the reversible phase separation of hydrophobic association in water to drive contraction. Instead contraction by hydrophobic association occurs by lowering the transition temperature from above to below body temperature, as attached biological functional groups are converted to their more hydrophobic states. The transition temperature is lowered by means of chemical or electrochemical energy inputs that convert a functional group from a more-polar to a more-hydrophobic state, such as occurs on charge neutralization or otherwise removal of charge. In mammals, when the temperature of the phase separation is lowered from above to below 37°C, contraction occurs as low entropy hydrophobic hydration becomes higher entropy bulk water (See section **9**: Summarizing Comments).
In your author's view, only when this increase in entropy (of pentagonal rings of hydrophobic hydration becoming less-ordered bulk water) is explicitly taken into consideration, can treatments of biological energy conversion involving changes in hydrophobic association in water be consistent with the Second Law of Thermodynamics.

That this performance of work, seen on charge neutralization, still represents an underlying protein-based heat engine is easily demonstrated. Here we note a family of model protein compositions that is considered in more detail below in Section **6**. At pH 7.5 in phosphate buffered saline, the glutamic acid (E, Glu) residue in **Model protein i**, (GVGVP GVGVP GEGVP GVGVP GVGVP GVGVP)$_{36}$GVGVP, is ionized as the carboxylate (-COO⁻). This designed ECMP contracts when the temperature is raised from 55 to 70°C. For **Model protein i** lowering the pH to 3 forms the uncharged carboxyl (-COOH) and under this circumstance contraction occurs on raising the temperature from 15 to 30°C. Thus, at pH 7.5 **Model protein i** is a protein-in-water heat engine that contracts with a transition centered near 60°C, and at pH 3 **Model protein i** is a protein-in-water heat engine that contracts with a transition centered between 20 and 25°C. Thus, at pH 7.5 **Model protein i** *performs thermo-mechanical transduction* at elevated temperature, and at pH 3 **Model protein i** *performs thermo-mechanical transduction* below physiological temperature.

Also, **Model protein i**, at physiological temperature (37°C) and physiological pH, dissolves in water or occurs as a swollen cross-linked matrix. At 37°C, on lowering the pH to 3 the dissolved solution phase separates by hydrophobic association and the swollen cross-linked matrix contracts by hydrophobic association, with release of water, *to perform chemo-mechanical transduction*. Numerous functional groups of biology, attached to designed ECMP, drive contraction on conversion from their more polar state to their more hydrophobic state. Neutralization of charge results in formation of more hydrophobic hydration (See Figs. 10C and 12), with a negative δΔH and a larger positive δ[-TΔS] (See Eqn. 4 of section **6.1.1** and associated discussion). This requires that the phase transition, where $\Delta H_t = T_t \Delta S_t$, occurs at a lower temperature. This ΔT_t-mechanism of energy conversion derives from input energies that shift the onset temperature, T_t, of phase transitions. The T_t-based Hydrophobicity Scale, of all amino acid residues in their different functional states (as applicable) and of additional functional groups, allows for the phenomenological design of ECMP capable of performing diverse free energy transductions (Urry, 2006a).

Experimental evaluations - 1) of the change in Gibbs free energy for hydrophobic association, **ΔG$_{HA}$**, to obtain a **ΔG$_{HA}$**-based Hydrophobicity Scale (Urry, 2004), 2) of an apolar-polar repulsive free energy of hydration, ΔG_{ap}, where charge disrupts hydrophobic hydration, and 3) of the mechanism of protein elasticity – allow insight into protein function, design of ECMP as transductional drug delivery/diseased cell targeting vehicles, and of many other medical and non-medical applications (Urry, 2006a; Urry et al., 2010).

1.3 Biology's inverse temperature transition, the rival of gravitation

Thus, for the biological world we note the Prigogine and Stengers (1984a) assertion that for the industrial world "Heat, the Rival of Gravitation" drives the phase transition of a more-ordered, condensed state of bulk water to the more-disordered, expanded gaseous state of steam to *achieve mechanical work by expansion*. And we extend it here to the biological world and argue that "Heat, the Rival of Gravitation" drives a phase transition to increased protein order by association of hydrophobic (oil-like) groups within and between protein chains to *achieve mechanical work by contraction*, (Urry, 1995; 1997; 2006a; Urry et al, 2010).

Central to understanding this phenomenon is that hydrophobic hydration is low entropy, structured water. Before the protein-in-water transition occurs, structured water arranges as pentagonal rings in association with hydrophobic groups (Stackelberg & Müller, 1951; 1954; Teeter, 1984), as may be seen in Fig. 2. During the phase transition of hydrophobic
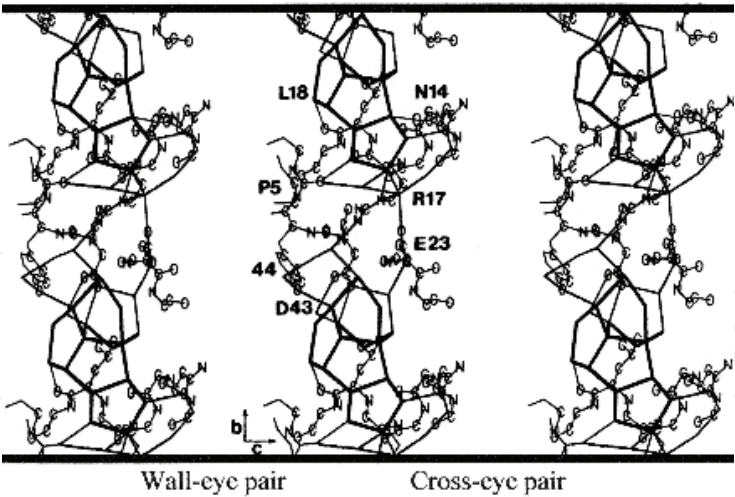
Fig. 2. Stereo views of residual pentagonal rings of hydrophobic hydration in association with hydrophobic moieties of L18 (leucine) and R17 (arginine) residues, after hydrophobic association of the small protein, crambin. From Teeter, 1984 with permission of M. M. Teeter.

association, the pentagonal rings of water of hydrophobic hydration become more-disordered as pentagonal rings of water become higher entropy bulk water (Urry et al., 1997). This decrease in order of water, i.e., increase in entropy, overwhelms in magnitude the increase in order on protein association, i.e., decrease in entropy, as hydrophobic groups of protein associate in the process of contraction (See section **6.1.3**). To emphasize this distinction, the ECMP-based phase transition to greater order of the model protein on raising the temperature is called an _inverse temperature transition_, (ITT). This is protein ordering on heating through the ITT of the ECMP, which ordering can be seen microscopically as the formation of twisted filaments that associate to form fibrils and fibers (Urry, 1992) and can even be seen with cyclic analogues of the model proteins as reversible crystallization on heating (Urry et al. 1978; Cook et al. 1980).
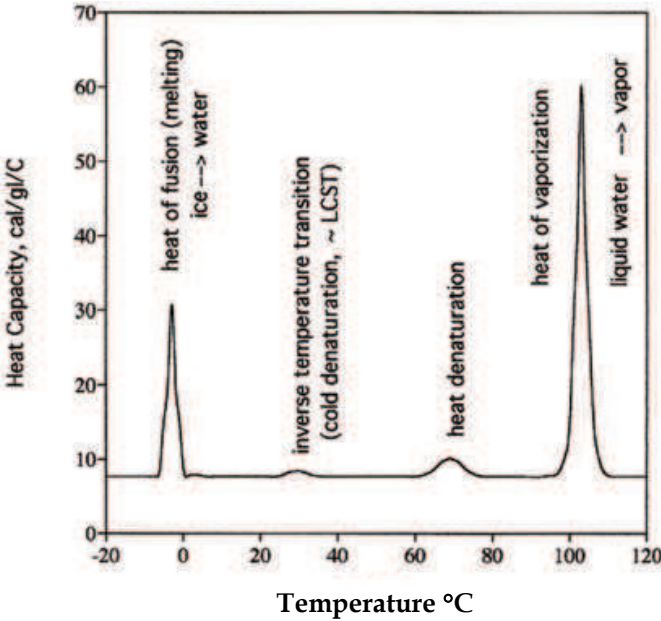

Fig. 3. Representation of endothermic phase transitions of $(GVGVP)_{251}$- in-water. From Figure 5.2 of Urry, 2006a.

Thus, without explicit consideration of water, which goes from being more-ordered to being less-ordered on raising the temperature from below to above the phase transition, the ITT of the protein-in-water heat engine of biology would seem to contradict the Second Law of Thermodynamics. But in fact, the heat driven increase in disorder (in entropy) as pentagonal rings of hydrophobic hydration become less-ordered bulk water is greater than the increase in order (decrease in entropy) as the model protein associates. Thus, in spite of the increase in order of the protein component, the ITT of ECMPs, is endothermic like those of the other transitions of water-to-vapor and ice-to-water, as water goes to a state of higher entropy of Fig. 3.

In summary, the water-to-vapor phase transition results in a dramatic increase in entropy of water and thereby enables the steam engine of the 19th Century Industrial Revolution to perform work by expansion. More profoundly, in your author's view, biology's inverse temperature transition results in a remarkable increase in entropy of water as pentagonal rings of hydrophobic hydration become higher entropy bulk water - whether driven by thermal energy input to raise the temperature through the phase transition or by chemical and other energy inputs that lower the temperature of the phase transition to hydrophobic association from above to below the operating temperature. This enables the diverse protein-based machines that sustain living organisms to perform work by contraction (Urry, 1995, 1997, 2006a; Urry et al., 2010).

1.4 Contrast between the arrow-of-time for the universe and the arrow-of-time for biology

Expressing his high esteem for the Second Law of Thermodynamics Eddington (1958) stated, "The law that entropy always increases – the second law of thermodynamics – holds, I think, the supreme position among the laws of Nature." With entropy measuring the increase in disorder, i.e., the increase in randomness, Eddington put forth the concept of "times arrow," (now commonly referred to as the arrow-of-time) using the argument, "Let us draw an arrow arbitrarily. If as we follow the arrow we find more and more of the random element in the state of the world, then the arrow is pointing towards the future; if the random element decreases the arrow points toward the past. That is the only distinction known to physics. I shall use the phrase 'times arrow' to express this one-way property of time which has no analogue in space. It is a singularly interesting property from a philosophical standpoint."

Considering the arrow-of-time, Toffler (1984), in the Forward to "Order Out of Chaos: Man's New Dialogue with Nature," (Prigogine & Stengers, 1984), addressed the dichotomy presented by biology with, "Imagine the problems introduced by Darwin and his followers! For evolution, far from pointing toward reduced organization and diversity, points in the opposite direction. Evolution proceeds from simple to complex, from 'lower' to 'higher' forms of Life, from undifferentiated to differentiated structures. And, from a human point of view, all is quite optimistic. The (biological) universe gets 'better' organized as it ages, continually advancing to a higher level as time sweeps by." The Toffler Forward set the stage for the Prigogine & Stengers thesis from the discipline of non-equilibrium thermodynamics, under which circumstances less-ordered systems may spontaneously give rise to complex more-ordered systems. Again quoting from Prigogine & Stengers, (1984b), "We can speak of a new coherence, of a mechanism of 'communication' among molecules. But this type of communication can arise only in far-from-equilibrium conditions. It is quite interesting that such communication seems to be the rule in the world of biology. It may in fact be taken as the very basis of the definition of a biological system."

Your author has previously argued (See the Epilogue of Urry, 2006a) that, while the energy required to produce the great macromolecules of biology is very large, the macromolecules themselves are not-so-far-from-equilibrium, due to discarding of 8 kcal/mol-residue with the addition of each residue. Yet repulsive free energies within complementary protein sequences can drive association between them. For further discussion of this issue see section **2**.

1.5 The components of this paper

Our perspective of the thermodynamics of protein structure formation and function unfolds below in seven parts: 1) Description of a key step in the biosynthesis of biomacromolecules, the nucleic acids and proteins, whereby biology achieves order out of chaos. The key step simply exemplifies an energy-fed reversal of biology's otherwise vaunted exception to the universal arrow-of-time. 2) Development of a model system of elastic-contractile model proteins (ECMPs) with which to establish the thermodynamics of hydration and of elasticity in protein function. 3) Phenomenological demonstration of a family of 15 pair-wise energy conversions achievable by designed ECMP capable of a thermally driven inverse temperature transition (ITT) to increased order by hydrophobic association. Thereby numerous inputs of intensive variables of the free energy - mechanical force, pressure, chemical potential, temperature, electrochemical potential, and electromagnetic radiation - act on different functional groups to change the temperature of the ITT. 4) Development of the thermodynamics of protein hydration (ΔG_{HA} and ΔG_{ap}) and of elasticity (the internal energy, f_E, and entropy, f_S, components of force) as established by designed ECMP. 5) Noting how the Genetic Code (which is common to all characterized life on earth) facilitates protein-based machine evolution, new energy sources and improved machine efficiencies are, thereby, shown to be accessible at no increase in the energy required to produce new and/or more efficient protein machines. 6) The thermodynamics of protein hydration (ΔG_{HA} and ΔG_{ap}) and of elasticity (f_E and f_S) are shown to be operative in biology's protein-based machines. 7) Application of the thermodynamics of Eyring's Absolute Rate Theory to the essential functions of trans-membrane transport processes of biology allows that the single image of the Gibbs free energy profile for ion passage from one side to the other of a cell membrane through a conduit of protein is sufficient to calculate trans-membrane ion currents as a function of ion activity and trans-membrane potential. This means of analysis, extrapolated to an array of essential biological trans-membrane transport processes, points to a future of a remarkable Eyring legacy, even to the trans-membrane transport processes of the energy factory of the living cell, the mitochondria of the animal kingdom and the chloroplasts of the plant kingdom.

2. How does biology reverse the universal arrow-of-time to achieve its order out of chaos?

In an early consideration relevant to biology's reversal of the universal arrow-of-time, Schrödinger (1944a) reasoned, "… we had to evade the tendency to disorder by 'inventing the molecule', in fact, an unusually large molecule which has to be a masterpiece of highly differentiated order.…" Almost a decade later Sanger (Sanger, 1952; Sanger & Thompson, 1953a; 1953b) demonstrated that proteins have specified sequences. *The means whereby biology achieves specified sequences for large chain molecules and the Genetic Code (See section 5) provide the solution as to how biology reverses the universal arrow-of-time, given sufficient energy*

supply. Anticipating construction of biological molecules different from anything as yet characterized by 1944, Schrödinger (1944b) further reasoned, "…from all that we have learnt about the structure of living matter, we must be prepared to find it working in a manner that cannot be reduced to the ordinary laws of physics." With remarkable foresight, he then went on to say, "… not on the grounds that there is any 'new force' or what not, directing the behaviour of the single atoms within a living organism, but because the construction is different from anything we have yet tested in the physical laboratory."

Indeed, a protein, in general, is in the words of Schrödinger (1944a) "an unusually large molecule" and always "a masterpiece of highly differentiated order." For a protein is a polymer, a polypeptide, in which each peptide unit may be formed of any one of 20 chemically and structurally diverse amino acid residues. So differentiated is the order that a 100 residue protein with the possibility of any one of twenty amino acid residues in each position gives the probability of a particular sequence as one in 10^{131}.

The key process in biology's reversal of the universal arrow-of-time resides within the synthesis of the magnificent macromolecules of biology, the nucleic acid and protein chain molecules of biology. These polymers exhibit precise sequences of subunits. The repeating units derive from four distinct nucleotides in each of the deoxyribonucleic acids (DNAs) and the ribonucleic acids (RNAs) and from 20 distinct amino acid residues of proteins. *Once these remarkably accurate sequences of diverse amino acids are obtained, three dimensional structure and function follow.* The primary structure, for example the accurate sequence of diverse amino acids of a protein, dictates protein folding and assembly, i.e., dictates three-dimensional structure (Anfinsen, 1973). Also, by the analysis reviewed here, the changes in structure that result in function, arise out of discrete energy inputs acting on biological functional groups attached to protein to bring about changes in hydrophobic association and often coupled with elastic deformation. Accordingly, an understanding, of how biology achieves order out of chaos and reverses the universal arrow-of-time, has as its basis an understanding of the thermodynamics whereby precise protein sequences are obtained, the Genetic Code, and the thermodynamics of protein function. In your author's view, central to understanding the energy conversions that constitute protein function are knowledge of the thermodynamics of hydrophobic hydration, elasticity, and Eyring Rate Theory.

2.1 A common key step whereby biology achieves order out of chaos in the biosynthesis for each of its great macromolecules – DNA, RNA, and protein

During construction of the nucleic acids and proteins of biology, the growing polymers are not-so-far-from-equilibrium. While protein and nucleic acid biosyntheses do require a very large amount of energy, the completed chain is *never*-very-far-from-equilibrium. The addition of each single amino acid residue for protein synthesis or of a triplet nucleotide codon of nucleic acid synthesis per amino acid, consumes ~24 kcal/mol of free energy. Discarding 24 kcal/mol to the environment, on adding each triplet codon to the growing nucleic acid and each amino acid residue to the growing protein chain, reproducibly produces accurate sequences. *A precise sequence dictates the three-dimensional structure of a protein in water for a given state of the functional groups of the sequence and of functional groups otherwise bound to the protein. And changes in state of the associated functional groups result in structural changes that give rise to function.*

In the biosynthesis of protein the activation of each amino acid (AA) and transfer to tRNA by aminoacyl-tRNA synthetase is given as follows: AA + ATP + tRNA = AA-tRNA + AMP +
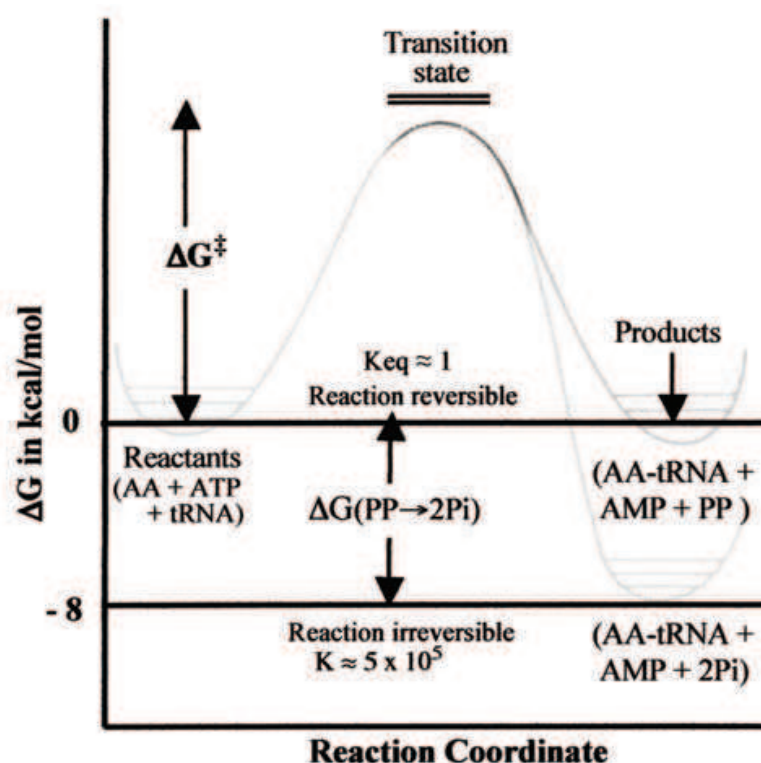
Fig. 4. Free energy profile for the reaction of amino acid (AA) plus ATP plus tRNA to produce the activated amino acid, i.e., AA-tRNA, ready for selective addition to the growing protein chain. The reaction may be seen in two steps: 1) The formation of AA-tRNA + AMP + PP, which is perfectly reversible with an equilibrium constant of one and the ratio of reactant to product of 1:1, 2) The enzymatic breakdown of pyrophosphate, PP → 2Pi + 8 kcal/mol, results in an irreversible overall reaction, i.e., K ≈ 5x10⁵. This very large cost of 800 kcal/mol-residue activation for production of a 100-residue-protein provides the free energy required for the peptide bond formation. There is yet another 1500 kcal-mol-(AA-tRNA) to bring the 100 AA-tRNA molecules out of disarray into alignment (see Eqns. 3b and 3c). Thus, some 2300 kcal/mol-residues added to take 100 amino acids (AA) out of chaos and to form a 100-residue protein of specified sequence.

PP(pyrophosphate), where AA stands for amino acid, ATP for adenosine triphosphate, tRNA for transfer-RNA, AA-tRNA for the activated amino acid as aminoacyl–tRNA energy-wise readied for addition to the growing protein chain, and PP for pyrophosphate. The equilibrium constant for this reaction required for attachment of each amino acid residue to tRNA is of the order of 1, i.e., K ≈ 1. The reactants and products occur at a ratio of approximately one. Due to the presence of an abundance of pyrophosphatase, catalytic breakdown of pyrophosphate immediately ensues, i.e., PP → 2Pi (inorganic phosphate) + 8kcal/mol. At each step of residue activation, a free energy of 8 kcal is released per mole of residue activated. As shown in **Figure 4**, this lowers the free energy of products by 8 kcal/mol. Based on this activation step alone, only one error would be made during the addition of some 500,000 residues. The free energy of pyrophosphate hydrolysis of 8 kcal/mol-residue-activated for addition to the growing chain immediately dissipates into the environment and is no longer associated with the process of chain growth. (For further discussion see Chapter 4 Likelihood of Life's Protein Machines: Extravagant in Construction Yet Efficient in Function of Urry, 2006a).

"Thus, (rather than employing far-from-equilibrium conditions) biology produces its macromolecules by means of an energetically extravagant, step-by-step, methodical march out of chaos" (See the Epilogue of Urry, 2006a).

2.1.1 Replication of DNA by G-C and A-T base pairings

Three steps lead to the biosynthesis of protein. These are: replication, wherein the strand of DNA that encodes protein sequence is duplicated for a daughter cell; transcription, the conversion of DNA into the equivalent sequence of RNA, and translation, the conversion of the ribonucleic acid sequence into the specified protein sequence. Beginning with replication of DNA, i.e.,

$$\text{parent DNA} \rightarrow \text{replication} \rightarrow \text{DNA of daughter cell} \qquad (1)$$

An overall expression for DNA replication may be written as,

$$pATP + qGTP + rTTP + sCTP = DNA + (p + q + r + s)PP \qquad (1a)$$

where A (adenine), G (guanine), T (thymine) and C (cytosine) are the four bases, and the nucleotides - AMP (adenosine monophosphate), GMP (guanosine monophosphate), TMP (thymidine monophosphate), CMP (cytidine monophosphate) are the repeating units added one-by-one to form DNA. This applies to the synthesis of each strand of DNA to duplicate the DNA double helix. For biosynthesis of a 100-residue protein, the sum, (p + q + r + s) = 300.

A codon, which is a specific sequence of three bases, in general, encodes for one of the 20 amino acid residues, and there is a redundancy of codons for most amino acids. For example, there are four codons that encode for G (glycine, Gly) and a different four codons encode for V (valine, Val), and yet another set of four codons encode for P (proline, Pro), for A (alanine, Ala), and for L (leucine, Leu). On the other hand only one codon encodes for W (tryptophan, Trp) and six codons encode for R (arginine, Arg). The Genetic Code is a table that lists the codons that encode for each amino acid. As discussed in Section **5** below, the Genetic Code is arranged remarkably well for evolution of diverse and efficient protein-based machines that utilize modulation of inverse temperature transitions for function.

Again reaction (1a) occurs at near equilibrium for each nucleotide addition, but an abundant pyrophosphatase by way of reaction (1b) catalyzes the breakdown of pyrophosphate, PP, into 2 inorganic phosphates, 2Pi, and in the process releases 8 kcal/mol of energy to be dissipated into the environment, including heat that is no longer to be associated with the growing biomacromolecule.

$$(p + q + r + s)PP \rightarrow \text{pyrophosphatase} \rightarrow 2(p + q + r + s)Pi + (p + q + r + s) \times 8 \text{ kcal/mole} \qquad (1b)$$
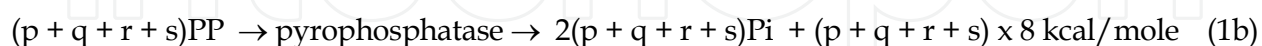
Thus, when encoding for a 100-residue protein, which requires a sequence of 300 nucleotides, there would be a free energy of (300 x 8) kcal/mol-residue released into the environment, that is, 2400 kcal/mol-300 base daughter cell DNA, which by transcription gives a 300 base strand of RNA, see Eqns. (2), as required for production of a 100-residue protein.
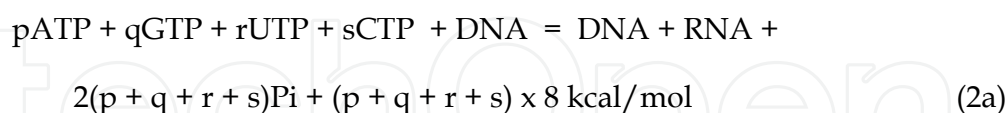
2.1.2 Transcription of DNA to produce RNA by G-C and A-U base pairings

The four bases of RNA are – adenine (A), guanine (G), uracil (U), and cytosine (C**)** – and the added nucleotide residues are – adenosine monophosphate (AMP), guanosine monophosphate (GMP), uridine monophosphate (UMP), and cytidine monophosphate

(CMP). The reaction constitutes transcribing a strand of deoxyribonucleic acid, DNA, into a strand of RNA. The statement of which may be given as Eqn. (2), i.e.,

$$DNA \rightarrow transcription \rightarrow RNA \tag{2}$$

The stoichiometry of the reaction may be given as,

$$pATP + qGTP + rUTP + sCTP + DNA = DNA + RNA +$$

$$2(p + q + r + s)Pi + (p + q + r + s) \times 8 \text{ kcal/mol} \tag{2a}$$

Again, to encode for a 100-residue protein would mean (300 x 8) kcal/mol, or again 2400 kcal/mol being released to the surrounding solution.
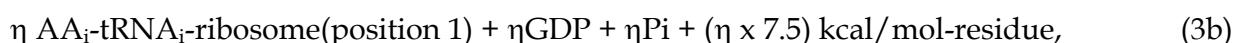
2.1.3 Translation of RNA to produce protein

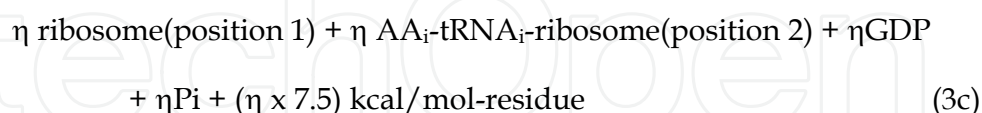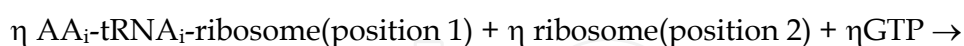The translation of an RNA sequence into protein of $\eta = 100$, i.e.,

$$RNA \rightarrow translation \rightarrow protein \tag{3}$$

stated in terms of four reactions: a) The activation of an amino acid residue, AA_i, to its specific $tRNA_i$, discussed above, wherein AA_i, ATP, and $tRNA_i$ react to give AA_i-$tRNA_i$, AMP, and 2Pi with release of 8 kcal/mol-residue, i.e.,

$$\eta \, AA_i + \eta \, tRNA_i + \eta \, ATP \rightarrow \eta \, AA_i\text{-}tRNA_i + \eta \, AMP + 2\eta \, Pi + (\eta \times 8) \text{ kcal/mol-residue.} \tag{3a}$$
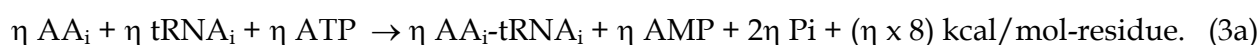
Eqn. (3a) represents a selectivity step where the correct amino acid is attached to its appropriate tRNA that contains the correct triplet codon for the amino acid being attached in an activated state. The amino acid selectivity process continues in the following reactions.

$$\eta \, AA_i\text{-}tRNA_i + \eta \, ribosome(position\ 1) + \eta \, GTP \rightarrow$$

$$\eta \, AA_i\text{-}tRNA_i\text{-}ribosome(position\ 1) + \eta GDP + \eta Pi + (\eta \times 7.5) \text{ kcal/mol-residue,} \tag{3b}$$

transfer to ribosome (position 2)

$$\eta \, AA_i\text{-}tRNA_i\text{-}ribosome(position\ 1) + \eta \, ribosome(position\ 2) + \eta GTP \rightarrow$$

$$\eta \, ribosome(position\ 1) + \eta \, AA_i\text{-}tRNA_i\text{-}ribosome(position\ 2) + \eta GDP$$

$$+ \eta Pi + (\eta \times 7.5) \text{ kcal/mol-residue} \tag{3c}$$

and finally the activated amino acid, AA_i-$tRNA_i$, bound at ribosome position 2, is added to the growing protein chain in its designated position in the sequence, i.e.,

$$\eta \, AA_i\text{-}tRNA_i\text{-}ribosome(position\ 2) \rightarrow \eta \, tRNA_i + \eta \, AA_i \text{ in protein} \tag{3d}$$
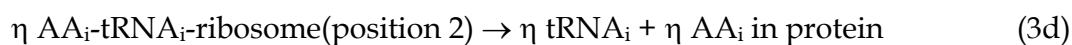
The cost in terms of Gibbs free energy to add a single amino acid to the growing protein chain is (8 + 2 x 7.5) kcal/mol-residue, and the cost of producing a 100-residue protein would be 2300 kcal/mol-100-residue protein.

As given above, the probability for a precise sequence of a 100-residue protein, with the possibility of one of 20 amino acid residues in each position, i.e., $(1/20)^{100} = 10^{-131}$. When the equilibrium constant is one, i.e., $K = 10^{-\Delta G/2.3RT} = 1$, ΔG is 0, and there is the probability of an

equal number of reactants and products. When the probability of a product is one chance in 10^{-131} for the occurrence of the product, one may write that $K = 10^{-\Delta G/2.3RT} = 10^{-131}$, or $\Delta G/2.3RT = 131$. Solving for the Gibbs free energy, $\Delta G = 131 \times 2.3RT = 186$ kcal/mole-100-residue protein. Calculated in this manner the efficiency of the synthesis of the 100-residue protein becomes $186/2300 = 0.08$, i.e., an efficiency of the order of some 8%.

As will be noted below, protein-based motors can function at very high efficiencies. The F_1-ATPase (the F_1-motor of ATP synthase acting in reverse) has been calculated as approaching 100% (Kinosita et al., 2000). This has led to the exclamation that Life's protein machines are *extravagant in construction yet efficient in function* (See Chapter 4 of Urry, 2006a). (Some of the 1500 kcal/mol pays for a repulsive free energy between hydrophobic and charged groups.)

2.2 Precise primary structure, i.e., sequence, dictates three dimensional structure and function!

As argued above, a high price in terms of Gibbs free energy is paid in order to obtain polymers of precise sequence. Consequences of this severe price for precise sequence are the beautiful functional structures of biology. The more diverse the "side chains" of the repeating sequence, the more diverse are the functional capabilities. This is why the nucleic acids with but four similar repeating nucleotides each with the capacity of base pairing, i.e., A-T and G-C of poly(deoxyribonucleic acid) DNA and U-T and G-C of poly(ribonucleic acid), RNA, are suitable for sequence replication and transcription as considered above in terms of free energy required to produce precise sequences in Eqns. (1) and (2).

At the root of the structuring that becomes a living organism is the primary structure of DNA, the poly(deoxyribonucleic acid). DNA provides the sequence of bases that ultimately specify the precise sequence of protein. Protein sequence utilizes 20 structurally diverse residues that may be broadly classified as aromatic and aliphatic hydrophobic residues, as negatively and positively charged residues, and as neutral residues with non-ionizable polar functional moieties, capable, for example, of hydrogen-bonding. Overlapping with the latter two groups is cysteine with its –SH functional group that is commonly used in disulfide, -S-S-, cross-linking on formation of cystine.

Again, the probability of a precise sequence, with the possibility of one specific residue out of 20 residues in each position of even a relatively small 100-residue protein, becomes $(1/20)^{100} = 10^{-131}$, that is, one out 10^{131} sequences (See Chapter 4 of Urry, 2006a). This truly enormous number of possible sequences allows for an extraordinary number of protein three-dimensional structures with which to perform the diverse work (functions) required to sustain a cell.

2.2.1 Protein performs the work of constructing and maintaining the cell

The precise sequence of a protein, under physiological conditions, dictates the three-dimensional structure of the protein itself and whether it associates with like subunits to form an oligomeric protein comprised of symmetrically related subunits and/or with unlike subunits to form more complex protein structures. A remarkable example is ATP synthase of more than 20 subunits ($10a$, $2b$, 3α, 3β, γ, ε). This rotary protein motor combines ADP (adenosine diphosphate) and Pi (inorganic phosphate) to make 32 of the 36 ATP (adenosine triphosphate) molecules on complete oxidation of a single molecule of glucose to 6 CO_2 plus 6 H_2O. Recall, ATP is the biological energy currency utilized to perform the work that sustains and propagates the living cell.

Assemblies of subunits, such as those of the three-fold rotary F_1-motor of ATP synthase, are dominated by hydrophobic inter-subunit interactions (Privalov, 1990) under the control of temperature and biological functional groups that can occur in two or more functional states. The more polar (e.g., charged) state, disrupts hydrophobic association and the more apolar (the more hydrophobic) favors hydrophobic association, each in a cooperative manner.

2.2.2 Familiar insights into the changes in hydrophobic associations that give rise to function

Insight begins with the familiar adage, "Oil and water don't mix!" Of course, they simply phase separate. But if oil-like and polar (e.g., water-like) groups are constrained to coexist along a polymer chain, they can't phase separate. Instead, the oil-like groups, dispersed along the polymer chain, self-associate by chain folding and by association with other chain segments, and, thereby, separate from water. But once the most favorable, the lowest free energy state, is obtained at a given temperature and pressure, only substantial changes in solvent or such as phosphorylation can change the state.

A related and more interesting adage becomes, "Oil and vinegar don't mix!" The solute of vinegar is principally acetic acid, which can exist in two states, i.e., $CH_3\text{-}COOH \leftrightarrows CH_3\text{-}COO^- + H^+$, the very polar charged state, $CH_3\text{-}COO^-$, and the less-polar (more-hydrophobic) uncharged state, $CH_3\text{-}COOH$. Again as for oil and water, phase separation dominates the mixture of oil and vinegar. When hydrophobic and ionizable groups are forced by sequence to coexist as demonstrated with certain designed ECMP, it has been shown by means of substantial physical characterization of ECMP containing a glutamic acid (E, Glu) residue with the R-group of $-CH_2\text{-}CH_2\text{-}COOH$ that the formation of the more polar state of $-CH_2\text{-}CH_2\text{-}COO^-$ disrupts hydrophobic association (See for example Urry et al., 1997). It will be seen below, using the crystal structure of the closed conformation of the full-length KcsA potassium ion channel (Uysal et al., 2009) that the absence of carboxylate is seen associated with hydrophobic association that opens the channel, whereas the presence of carboxylate is seen associated with hydrophobic dissociation (Urry et al., 2010) and a closed channel. And the pH dependence of the conductance of the KcsA K^+-channel of Thompson et al. (2008) demonstrates conductance to turn off on the titration of glutamic acids to form charged glutamates.

Particularly, when the oil-like and charged groups are constrained to coexist by protein structure, they can be shown to reach out for hydration unperturbed by the other, that is, there is a competition for hydration between hydrophobic and charged residues (See for example Urry et al., 1997). This results in an *apolar-polar repulsive free energy of hydration*, ΔG_{ap}. (See Section **6.2.6** below and Urry, 1992; 1997).

2.2.3 Biological polymers of reproducible precise sequence add a new wrinkle to the "*laws of physics*"

Anticipating construction of biological molecules different from anything as yet characterized at the time, Schrödinger (1944b) further reasoned, "…from all that we have learnt about the structure of living matter, we must be prepared to find it (living matter) working in a manner that cannot be reduced to the ordinary laws of physics." With remarkable foresight, he then went on to say, "… not on the grounds that there is any 'new force' or what not, directing the behaviour of the single atoms within a living organism, but

because the construction is different from anything we have yet tested in the physical laboratory." Different constructions arise due to the capacity of biology to synthesize long proteins of precise sequence. This is because near physiological temperature the fundamental activation reaction, essentially independent of amino acid structure, has an equilibrium constant, K, of $10^{5.7}$. This translates into the order of one error in a half a million residue additions. Again, assuming that the twenty different residues possible at each position had an equal probability of being added, there would be 10^{131} different sequences possible for a 100-residue protein. This results in protein constructions that were simply inconceivable prior to the elucidation protein sequences and protein biosynthesis.

Again as Schrödinger (1944a) stated, "... living matter, while not eluding the 'laws of physics' as established up to date, is likely to involve 'other laws of physics' hitherto unknown, which, however, once they have been revealed, will form just as integral a part of this science as the former." As indicated above, the *new wrinkle to the "laws of physics"* derives from *an apolar-polar repulsive free energy of hydration, ΔG_{ap},* that can be seen with the disparate side-chains (e.g., hydrophobic and charged) constrained to coexist along the precise sequence of which a protein chain is comprised.

It has been seen above that the reproducibly-achieved precise protein sequence (with an error as small as of one in one-half million residue additions) is achieved at an extraordinary cost in energy, and as such is consistent with the Second Law of Thermodynamics. It is not yet understood, however, just how the protein biosynthetic apparatus came into existence with which to achieve this protein construction so essential to the existence of life as we understand it.

2.3 Is the construction and maintenance of the biosynthetic apparatus for protein in accordance with the Second Law of Thermodynamics?

The biomacromolecular composition of the biosynthetic apparatus for production of protein requires RNA to specify protein sequence and protein catalysis to transcribe DNA into RNA, to produce tRNA, to attach amino acid (AA_i) to $tRNA_i$, i.e., to produce AA_i-$tRNA_i$, and to catalyze the steps in which the correct AA_i of an AA_i-$tRNA_i$ becomes attached to the correct position in the growing protein chain. The energy required for the latter, some 15 kcal/mol amino acid residue added of Eqns (3b) and (3c) in addition to precise protein sequence also pays for repulsive free energies that occur between disparate residues. DNA, RNA and protein chains of precise sequence are all simultaneously required in the first instance to achieve replication, transcription, translation to protein. How the initial biosynthetic apparatus came into existence is unknown. Once the ribosomal biosynthetic apparatus has been assembled with its accessory enzymes and nucleic acids all available, however, synthesis of protein does not contravene the Second Law of Thermodynamics.

3. A model protein system with which to establish thermodynamics of protein structure formation and function!

3.1 The composition of the basic model protein, (GVGVP)$_n$

Our model protein system, with which to establish thermodynamic elements of protein function, originates from the mammalian elastic protein, elastin, as a repeating pentapeptide sequence, (GVGVP)$_n$ with n ≤ 15, depending on the species. A polypeptide chain may be represented as [-NH-CHR-CO-]$_n$ or as [-CO-NH-CHR-]$_n$ where the side chain (the R-group) of G (Gly, glycine) is the hydrogen atom, -H, the R-group of V (Val, valine) is –CH(CH$_3$)$_2$,

and the R-group of P (Pro, proline) is N_i–CH_2-CH_2-CH_2–C_i^α, i.e., three CH_2 groups spanning from the nitrogen atom, N, to the α-carbon of the same residue, i. Therefore, all side chains in $(GVGVP)_n$ are either the hydrophobic aliphatic hydrocarbons or the near neutral hydrogen atom and the only polar group is the recurring dipolar peptide moiety, -CO-NH-. Chemically and biologically synthesized $(GVGVP)_n$, with n ranging up to 200 or more, may be modified with sparse substitution of V by one or more functional groups, such as the carboxyls of glutamic and aspartic acids and the amino function of lysine (K, Lys), and additional biological functional groups such as redox functions, other prosthetic groups, phosphate, etc. Also, V residues may be replaced by the more hydrophobic F (Phe or phenylalanine) systematically to raise the hydrophobicity with the result of increased positive cooperativity giving an increased efficiency of energy conversion. These modified $(GVGVP)_n$ are called *designed* elastic-contractile model proteins (ECMP).

3.2 The molecular structure of the basic model protein, $(GVGVP)_n$

Figure 5A schematically represents the molecular structure of the basic model protein, $(GVGVP)_n$, as a series of VPGV β-turns with G spacers. Extending the spacer G residue to the adjacent V residue α-carbons, the VGV segment allows dynamic torsional oscillations of the intervening two peptide moieties. The damping of the amplitude of these peptide torsional oscillations gives rise to the librational entropy mechanism of protein elasticity (Urry et al., 1982d).
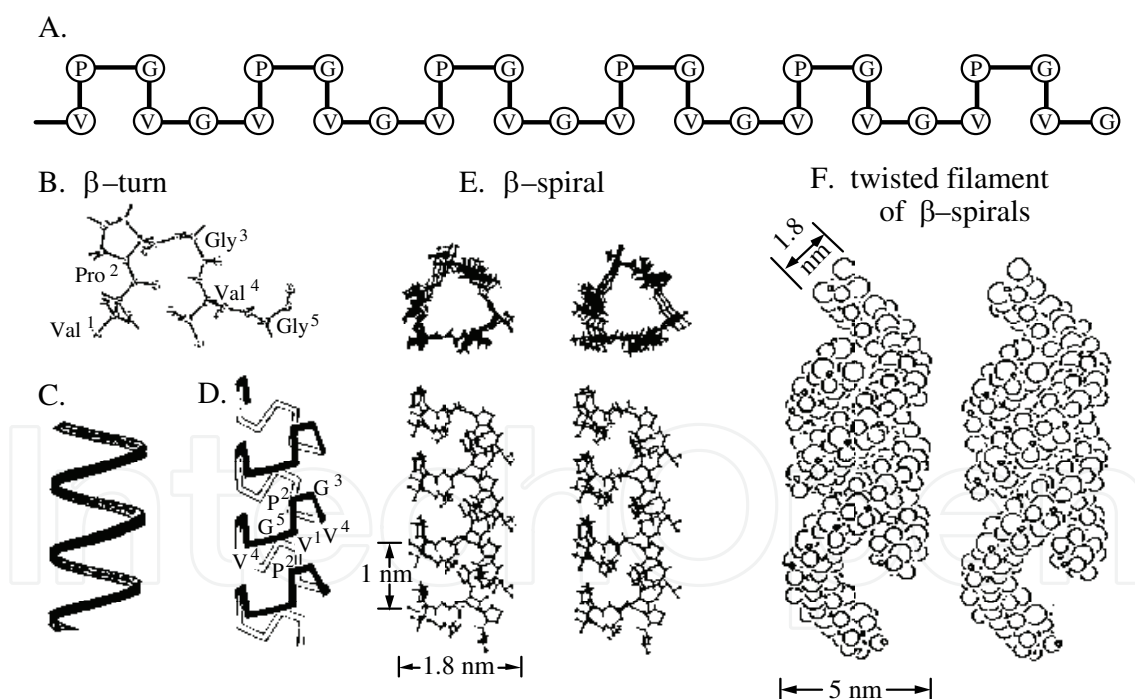

Fig. 5. Molecular structure of the elastic-contractile model protein, $(GVGVP)_n$. The structure is seen with repeating β-turns separated by dynamic suspended segments that wrap-up into associating β-spirals and exhibit simultaneous "near ideal" elasticity and phase transitional behavior from water to associate by hydrophobic interactions.
B. β-turn from the crystal structure of cyclo$(GVGVP)_3$ (Cook et al. 1980) which is the cyclic correlate of the linear β-spiral of D and E (Urry et al., 1981; Venkatachalam, et al. 1981; Venkatachalam and Urry, 1981). F. Adapted from Urry et al., 1982d.
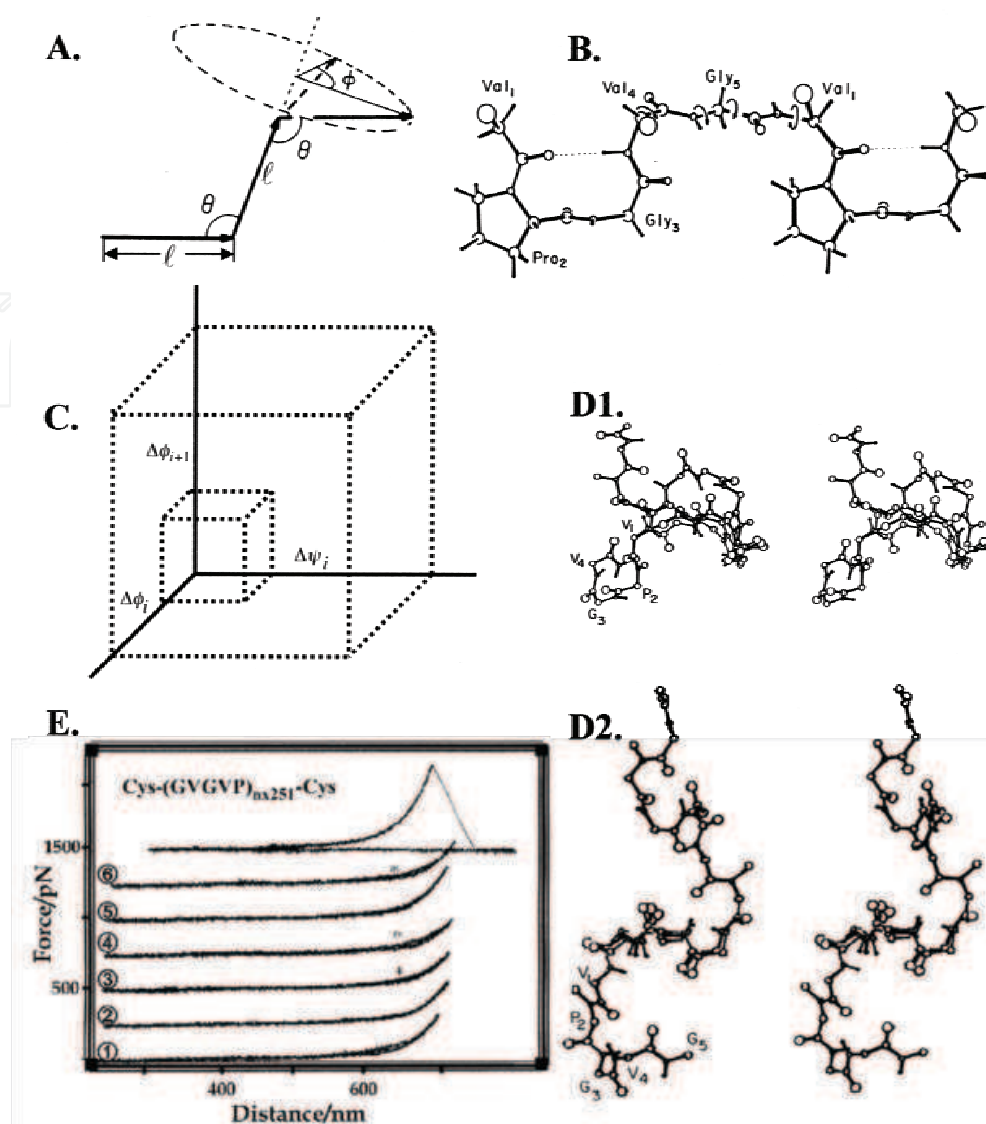
Fig. 6. Elements for understanding the nature of elasticity of the basic elastic-contractile model protein, (GVGVP)$_n$.

A. The structural elements for propagation of a rudimentary chain (Eyring, 1932). Bond length (ℓ), backbone bond angle (θ), torsion, or dihedral, angle (ϕ) due to rotation about bonds (Adapted from Urry, 1982).

B. Unrolled perspective of the β-spiral of (GVGVP)$_n$ showing suspended segments where peptide moieties are free to undergo large amplitude oscillations (peptide librations) involving the paired (ψ_4 & ϕ_5) and ψ_5 & ϕ_1 torsion angles. (From Urry, 1983)

C. Representation of entropy as a volume in configuration space, with axes plotting amplitude of torsion angle oscillations. As the volume increases due to larger torsion angle oscillations, a greater entropy can be calculated. (From Urry et al., 2010).

D1. One turn of the β-spiral with 2.7 β-turns per turn of spiral and an h of 3.5 Å showing the large torsion angle oscillations between the first and second β-turns. D2. On extension to an h of 8.0 Å, note damped oscillations. (From Urry & Venkatachalam, 1983).

E. Single-chain force-extension/relaxation curves, development of force during pulling in the z-direction of an AFM device with scans labelled from the bottom as Adapted from Urry et al., 2002.

The details of the β-turn are seen in **Figure 5B**, as obtained from the crystal structure of cyclo(GVGVP)$_3$ (Cook et al. 1980), which is the cyclic conformational correlate of the linear β-spiral conformation, as shown experimentally and computationally (Urry et al. 1981; Venkatachalam, et al. 1981; Venkatachalam and Urry, 1981). The linear β-spiral conformation is represented in increasing detail in **Figures 5C, D,** and **E** (Urry, 1990; 1991). Based on optical diffraction of negatively stained electron micrographs from incipient aggregates of dilute solutions (Volpin et al., 1976), three β-spirals of (GVGVP)$_n$ are thought to form twisted filaments as represented in **Figure 5F** (Urry et al., 1982d).

3.3 The unique properties of the basic model protein, (GVGVP)$_n$: "Near ideal" elasticity and phase transitional behavior

It is extraordinary that the basic model protein system, (GVGVP)$_n$ in water, simultaneously exhibits "near ideal" elasticity and thermally-elicited phase transitional behavior. To emphasize this unique and useful combination of properties, protein-based polymers based on (GVGVP)$_n$ have been given the descriptive name of elastic-contractile model proteins (ECMPs).

3.3.1 The "near ideal" elasticity of the basic model protein, (GVGVP)$_n$

An understanding of the "near ideal" elasticity of (GVGVP)$_n$ may be gained by discussing the component parts of Fig. 6, above. In particular, the curves of Fig. 6E utilized the basic atomic force microscope (AFM) (Hugel, 2003; Urry et al. 2002). Instead of imaging structures on a surface by rastering in the x- and y-dimensions, the cantilever tip moves in the z-direction with a long chain molecule spanning from the cantilever tip to the substrate surface to give a stress-strain curve that measures single-chain elasticity.

Ideal elasticity occurs when the plot of the force versus relaxation curve exactly overlays the force versus extension curve. Within the sensitivity (the noise level) of the measured stress-strain curves of Fig. 6E, the extension and relaxation traces of curves ② and ⑤ overlap. For curves ② and ⑤, therefore, the energy expended on extension is entirely recovered on relaxation, that is, these curves provide examples of ideal elasticity exhibited by extension and relaxation of a single-chain of Cys-(GVGVP)$_{502}$.-Cys. (Note: The Cys (cysteine, C) residues are present to achieve chemical (sulfhydryl) attachment to the cantilever tip of the AFM and for sulfhydryl attachment to the substrate surface.)

On the other hand curves ①, ③, ④, and ⑥ of Fig. 6E exhibit a higher noise level and in the original data separation is detectable as extension becomes greater than 600 nm. In these cases the extension curve is slightly higher than the relaxation curve, i.e., the cost in energy for extension is greater than the energy recovered on relaxation. Extension curves that occur at higher force levels than the relaxation curves are said to exhibit a hysteresis, which is an energy loss.

As seen in Fig. 4 of Urry et al. 2002 for Cys-(GVGIP)$_{260}$-Cys, the energy expended for extension is several times that recovered on relaxation. This is due in part to the greater hydrophobicity of (GVGIP) than of (GVGVP). The increase in the change in Gibbs free energy for hydrophobic association, ΔG_{HA}, results in a greater propensity for association with non-load bearing chain segments. A higher force on extension is required to disrupt these associations. The greater expenditure of energy to extend and disrupt these hydrophobic associations is not recovered on relaxation.

When the single-chain force-extension studies on Cys-(GVGIP)$_{260}$-Cys occur at very high dilution, however, essentially near ideal elasticity can be obtained. A slight hysteresis of

each of the curves, ①, ③, ④, and ⑥ of Fig. 6E, may be due to the chain folding back on itself, as time was allowed at low extension to increase the likelihood of backfolding (Hugel, 2003). As seen in Fig. 5E, the translation along the spiral axis for each complete turn is 1nm, and one complete turn requires three pentamers. Also, note in Fig. 6D1 that it is one turn of spiral, i.e., three pentamers, that is used in the calculation of the damping of torsion angle oscillations on extension by 130% from a value of 1 nm to 2.3 nm. Using the insight of Fig. 6C and the decrease in amplitude of torsion angle oscillation on extension, the change in entropy, ΔS, can be calculated by the equation, $\Delta S = R \ln[\Pi_i \Delta \phi_i^e \Delta \psi_i^e / \Pi_i \Delta \phi_i^r \Delta \psi_i^r]$.

The total elastomeric force, f_T plotted in Figure 6E, is the sum of an entropic component of force, f_S, and an internal energy component of force, f_E, i.e., $f_T = f_S + f_E$. The entropic component of elastic force is calculated as $f_S = -T(\partial S/\partial L)_{VT}$, where ∂S is calculated from the above expression for ΔS and ∂L derives from the 130% extension as used in Fig. 6D2. The sources of f_E derive from the reversible deformation of the angle, θ, and of the bond length, ℓ, both of Fig. 6A. (See section **6.2.10**, below.)
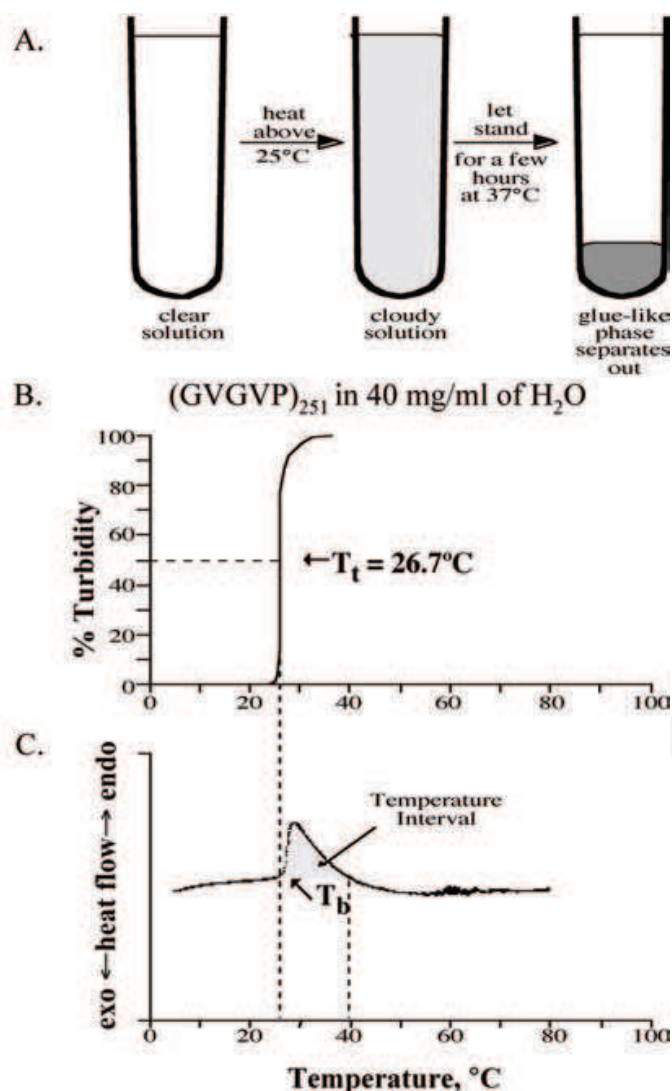

Fig. 7. Characterization of the (GVGVP)$_n$-in-water inverse temperature transition, using temperature dependence of turbidity and differential scanning calorimetry. From Urry, 1997.

3.3.2 The phase transitional behavior of the basic model protein, (GVGVP)$_n$

The basic elastic-contractile model protein, (GVGVP)$_n$, is miscible with water in all proportions below the onset temperature of the inverse temperature transition (ITT), i.e., the solutions are clear below 25°C. As depicted in Fig. 7A for concentrations of less than 400 mg/ml, on raising the temperature above 25°C, the clear aqueous solution becomes cloudy, and on standing phase separation occurs to form a viscoelastic state of 63% water and 37% model protein by weight, which constitutes a one molar concentration of pentamers, (GVGVP), of approximately 400 mg/ml (Urry et al., 1985).

As shown in Fig. 7B, when the phase separation process is followed spectroscopically, the onset of turbidity of a 40 mg/ml solution of (GVGVP)$_{251}$ begins at about 25°C. Turbidity continues on to a maximal value, 100% turbidity. The value of T_t is taken at 50% turbidity to give in this case a value of **26.7°C**, which value is bold-faced in this case to indicate that it is for the homopolypentapeptide, (GVGVP)$_n$, i.e., for a polypentapeptide for which the mole fraction, f_V, is one. In characterizations below, whenever values are for a general polypentapeptide, (GXGVP) as in poly[f_V(GVGVP), f_X(GXGVP)], the quantities are not bold-faced until the data for several values of f_X have been determined and then extrapolate to f_X = 1. At f_X = 1, i.e., for (GXGVP)$_n$, the values, the thermodynamic quantities for the homopolypentapeptide, are to be bold-faced. All quantities for f_X = 1 are then compared for the development of the **T_t**- and **ΔG_{HA}**-Hydrophobicity Scales. The values of **ΔG_{HA}** are similarly obtained from differential scanning calorimetry (DSC) data.

The DSC curve for (GVGVP)$_{251}$ in 40 mg/ml of water is given in Fig. 7C. The onset of the endothermic transition, indicated as **T_b**, is essentially the same as that of **T_t** of Fig. 7B. While these values tend to be used interchangeably, a distinction is retained in the data of **Table 1**, below. The temperature interval over which the phase transition occurs is approximated as in Fig. 7C. If the scan could be done more slowly the temperature interval would be much narrower, as seen in Urry et al., 1985, where there was no limit on time for completion of the phase separation. The question of scan rate becomes a question of the stability and sensitivity of the DSC equipment, which presents a challenge for the low heats of the inverse temperature transition.

4. Energy conversions of designed elastic-contractile model proteins are those of living organisms!

4.1 Phenomenology of model protein-based free energy transduction.

Phenomenological demonstration of a family of 15 pair-wise energy conversions becomes possible by means of designed ECMP capable of a thermally driven inverse temperature transition to increased model protein order by hydrophobic association. The family of pair-wise energy conversions possible by designed elastic-contractile model proteins are identified by the six intensive variables of the free energy – mechanical force, pressure, chemical potential, temperature, electro-chemical potential, and electromagnetic radiation. As seen in Fig. 1, the basic sequence (GVGVP)$_n$ on γ-irradiation cross-linking of its phase separated state can be formed as elastic sheets that perform *thermo-mechanical transduction*, i.e., "pumping iron," contracting on raising the temperature from below to above that of the phase separation and relaxing on lowering the temperature from above to below that of phase separation.

On sparse replacement of one V residue, every 30 or 50 residues, by a glutamic acid or a lysine residue and cross-linking, the resulting elastic sheet performs *chemo-mechanical transduction*.
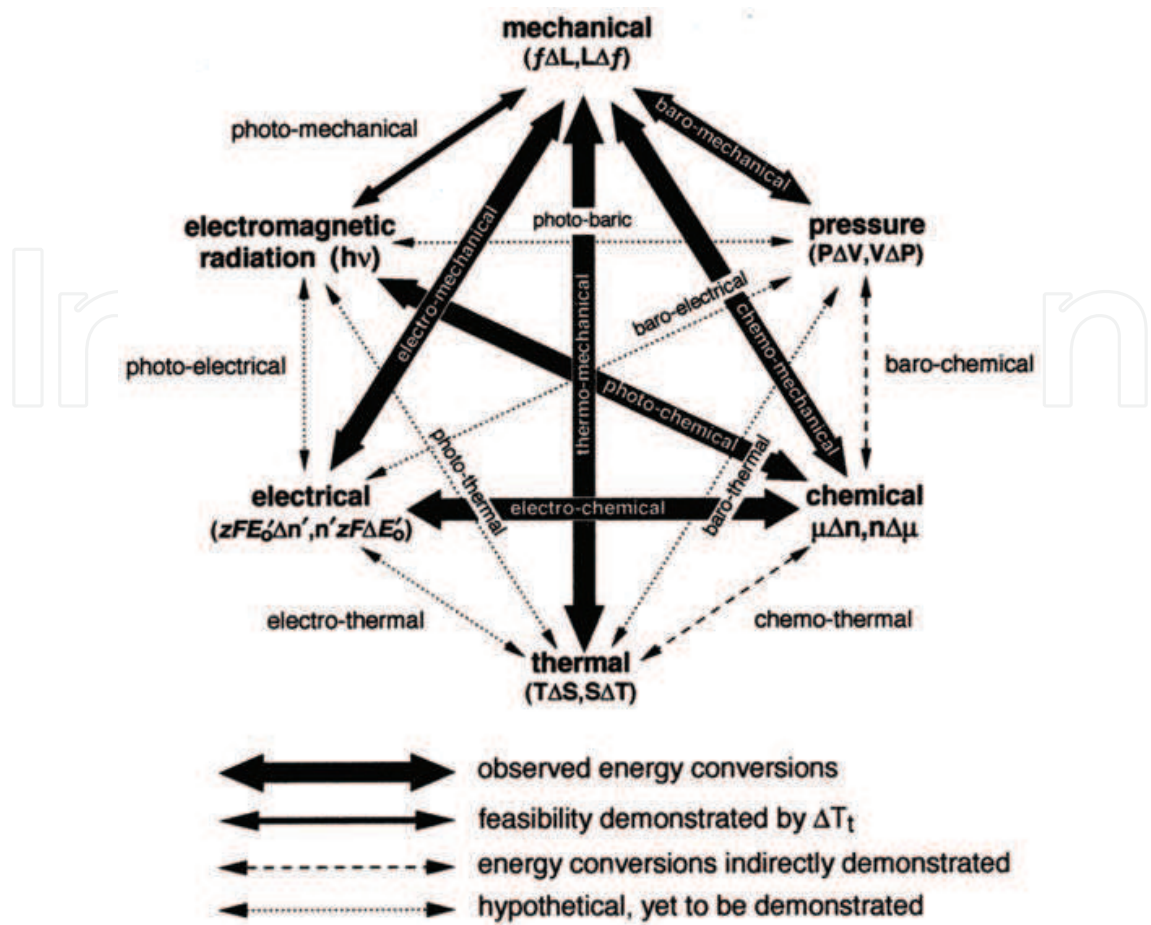
Fig. 8. The phenomenological ΔT_t-mechanism of free energy transduction using designed elastic-contractile model proteins (ECMPs). Application of pressure increases T_t and drives relaxation. Introduction of a chemical energy that neutralizes charge lowers T_t and drives contraction. Raising the temperature from below to above the transition drives contraction. Reduction of a redox function lowers T_t to drive contraction. The absorption of near ultraviolet light by a designed ECMP with attached azobenzene and cinnamide drive a *trans* to *cis* isomerization and raises the value of T_t. From Urry, 1997.

On attaching a redox group to the amino function of a lysine side chain, reduction drives contraction and oxidation effects relaxation in the performance of *electro-mechanical transduction*. Moreover, on replacing two V residues, per ECMP repeating unit, by both an acid/base function and a redox function allows that reduction of the redox function shifts the pK of the acid/base function causing the uptake of proton, thus achieving *electro-chemical transduction*. This becomes the "pumping of protons," e.g., the release of proton on oxidation, in phenomenological analogy to the electron transport chain of the inner mitochondrial membrane where oxidation of redox groups pumps protons into the inner membrane space. The examples noted here demonstrate phenomenology of three (mechanical force, chemical potential, and electrochemical potential) of the six intensive variables of the free energy for which ECMP can be designed to achieve free energy transduction.

Whenever a ΔT_t occurs and the operating temperature lies between the two values, on going from the higher value of T_t to the lower value of T_t, hydrophobic association occurs with the result of driving contraction.

4.2 Five phenomenological axioms for ΔT_t-based free energy transduction by designed model proteins

AXIOM 1: The manner in which a guest amino acid residue, or chemical modification thereof, alters the temperature, T_t, of a hydrophobic folding and/or assembly transition provides a measure of its hydrophobicity. A decrease in T_t represents an increase in hydrophobicity and an increase in T_t represents a decrease in hydrophobicity.

AXIOM 2: Raising the temperature from below to above T_t results in hydrophobic folding and/or assembly and can be used to perform useful mechanical work by contraction.

This represents the phenomenological aqueous elastic-contractile model protein heat engine of biology.

Example: Thermo-mechanical transduction

AXIOM 3: At constant temperature, lowering the value of T_t from above to below an operating temperature, i.e., increasing the hydrophobicity by changing a functional group from its more polar state to its more hydrophobic state results in contraction by hydrophobic folding and/or assembly and can be used to perform useful mechanical work, as in the lifting a weight.

Examples: Chemo↔mechanical transduction   Electro↔mechanical transduction

                  Baro↔mechanical transduction   Photo↔mechanical transduction

AXIOM 4: Any two distinct functional groups each with more and less hydrophobic states and each responsive to different variables can be coupled one to the other by being part of the same hydrophobic folding and assembly domain.

Examples: Electro↔chemical transduction   Electro↔thermal transduction

                  Baro↔electrical transduction   Photo↔voltaic transduction

                  Thermo↔chemical transduction   Photo↔thermal transduction

                  Baro↔thermal transduction   Baro↔chemical transduction

                  Photo↔baric transduction   Photo↔chemical transduction

                  Chemo↔chemical transduction   *Electro↔electrical transduction*

                  Electromagnetic radiation-1 ↔ Electromagnetic radiation-2 transduction

The italicized energy conversions represent three additional pair-wise free energy transductions for a total now of eighteen possible pair-wise free energy transductions using the above described ΔT_t-mechanism.

AXIOM 5: The energy conversions of AXIOMS 2, 3 and 4 can be demonstrated to be more efficient when carried out under the influence of more hydrophobic domains. This poising or biasing is observed in titrations by increased positive cooperativity. See Figs. 5.34 and 5.36 (Urry, 2006a), Figs. 14B and 15, and **Table** 3 below and associated discussions.

4.3 The ΔT_t-Mechanism for free energy transduction using designed elastic-contractile model proteins (ECMP) based on (GVGVP)$_n$

The temperatures, $\mathbf{T_{b(t)}}$ of **Table 1** column 2, represent either $\mathbf{T_t}$, the temperature for the onset of the inverse temperature transition (ITT) as defined by the onset of turbidity as shown in Fig. 7B, or $\mathbf{T_b}$, the temperature for the onset of the ITT as determined using differential scanning calorimetry (DSC) by the onset of the endothermic transition as

Residue X	$T_{b(t)}$ °C	$\Delta G°_{HA}(\chi)$/kcal/mol pentamer
Trp	-105	− 7.00
Phe	-45	− 6.15
Tyr	-75	− 5.85
His°	-10(T_t)	− 4.80 (from graph)
Leu	5	− 4.05
Ile	10	− 3.65
Val	26	− 2.50
Met	15	− 1.50
His$^+$	30 (T_t)	− 1.90 (from graph)
Cys	30 (T_t)	− 1.90 (from graph)
Glu(COOH)	20 (2)	− 1.30 (− 1.50)
Pro	40	− 1.10
Ala	50	− 0.75
Thr	60	− 0.60
Asp(COOH)	40	− 0.40
Lys(NH$_2$)	40 (38)	− 0.05 (− 0.60)
Asn	50	− 0.05
Gly	55	0.00
Ser	60	+ 0.55
Arg	60 (T_t)	+ 0.80 (from graph)
Gln	70	+ 0.75
Tyr(ϕ-O$^-$)	140	+ 1.95
Asp(COO$^-$)	170 (T_t)	≈ + 3.4 (from graph)
Lys(NH$_3^+$)	(104)	(+ 2.94)
Glu(COO$^-$)	(218)	(+ 3.72)
Ser(PO$_4^=$)	860 (T_t)	≈ + 8.0 (from graph)

Data within parentheses utilized microbial preparations of poly(30 mers), e.g., (GVGVP GVGVP GXGVP GVGVP GVGVP GVGVP)$_n$, with n ≈ 40. The notation (from graph) indicates that the value of T_t from Table 4 was used with the sigmoid curve of Fig. 13 to estimate $\Delta G°_{HA}(X)$. Adapted from Urry, 2004).

Table 1: Hydrophobicity Scale in terms of $\Delta G°_{HA}$, the change Gibbs free energy of hydrophobic association, for amino acid residue (X) of chemically synthesized poly[f_v(GVGVP), f_x(GXGVP)], 40 mg/ml, mw ≈ 100 kDa in 0.15 N NaCl, 0.01 M phosphate, using the net heat of the inverse temperature transition, ΔH_t ≈ $\Delta G°_{HA}$, per (GXGVP), determined at $f_x = 0.2$ and extrapolated to $f_x = 1$.

defined in Fig. 7C. In general column 2 of **Table 1** lists values for T_b; where T_t is used, it is indicated by (T_t) being placed to the right of the number. Poly[f_v(GVGVP),f_x(GXGVP)] gives the general ECMP composition where f_v and f_x are the mole fractions in the polymer of the defined pentamer repeats and $f_v + f_x = 1$. Experimentally, data are obtained for different low values of f_x and the data points define a straight line that is extrapolated to $f_x = 1$. When bold-faced, as for T_t or T_b, the result is for the homopolypentapeptide, (GXGVP)$_n$, which value may, for the more hydrophobic residues, be below 0°C or the value may be greater than 100°C for the more polar, charged residues.

For the biosynthetically prepared composition (GVGVP GVGVP GEGVP GVGVP GVGVP GVGVP)$_{36}$(GVGVP), for the glutamate state, -COO$^-$, in 0.15 NaCl and pH 2.5, T_t and T_b are 58°C, and for the glutamic acid state, -COOH, in 0.15 NaCl at pH 6.6, T_t and T_b are 22°C, i.e., $\Delta T_t = \Delta T_b = 36$°C. Using **Table 1**, the difference between the two states is 218 – 20 = 198 for (GEGVP)$_n$, which for the above composition six pentamer repeats per (GEGVP) gives a similar value, 198/6 = 33°C.

When using the γ-irradiation cross-linked matrix, X^{20}-(GVGVP GVGVP GEGVP GVGVP GVGVP GVGVP)$_{36}$(GVGVP), the elastic strip is swollen at pH 3 and 20°C and contracts on raising the temperature to 40°C; this is *thermo-mechanical transduction*. While holding the temperature constant at 40°C, however, at neutral pH the cross-linked matrix is swollen, but on lowering the pH to 3, (i.e., raising the chemical potential (inputting the chemical energy) of proton, $\Delta\mu_H$, the designed elastic-contractile model protein contracts and can perform mechanical work. This is *chemo-mechanical transduction*. The bold arrows of Fig. 8 between the mechanical and thermal energies, labeled thermo-mechanical, and between chemical and mechanical energies, labeled chemo-mechanical, represent the above-described free energy transductions.

The above represent explicit examples of the **ΔT_t-mechanism** for free energy transduction by means of designed elastic-contractile model proteins (ECMPs), as further discussed in sections **4.1** and **4.2**.

5. The genetic code provides easy access to new energy sources and improved efficiency!

All characterized life has the same Genetic Code, and it plays a central role in the thermodynamics of evolution of protein-based machines as seen through the prism of the energy converting mechanism of ECMP. Due to the Genetic Code, an ECMP, capable of performing thermo-mechanical transduction, can readily be designed to access a new energy source. For example, substitution (mutation) of a single base in 150 bases encoding for (GVGVP)$_{10}$ converts a heat engine (a machine), capable of thermo-mechanical transduction, into a chemically driven engine capable of chemo-mechanical transduction. A different single-base mutation can increase the efficiency of the designed ECMP-based machine.

The triplet codon for placing V in the sequence of a protein is fourfold redundant. Any one of four triplet codons GUU, GUC, GUA, and GUG encode for the valine (V, Val) residue. By a single-base mutation in the second position of either of two triplet codons, GUA $\rightarrow$ GAA or GUG $\rightarrow$ GAG, V is replaced by E, (glutamic acid, Glu) to introduce the carboxyl function, i.e., –CH$_2$-CH$_2$-COO$^-$ + H$^+$ $\leftrightarrows$ –CH$_2$-CH$_2$-COOH. Adding the proton to a carboxylate drives contraction with the consequence of *chemo-mechanical transduction*. A single-base mutation in the second position of either of another two triplet codons for V, GUU $\rightarrow$ GAU or GUC $\rightarrow$ GAC, become two ways to replace V by the D (aspartic acid, asp) residue with a slightly different carboxyl function, i.e., – CH$_2$-COO$^-$ + H$^+$ $\leftrightarrows$ –CH$_2$-COOH similarly to drive for *chemo-mechanical transduction*.

Significantly, a single mutation in the base of the first position of the triplet codon of V, e.g., GUU $\rightarrow$ UUU, gives the much more hydrophobic F (phenylalanine, Phe) residue with the consequence of an increased efficiency of energy conversion. Also three of the V triplet codons, GUU, GUC, and GUA, by single mutations in the first position to AUU, AUC, and AUA, give rise to the slightly more hydrophobic isoleucine (I, Ile) with one CH$_2$ more than V to modestly increase efficiency of energy conversion. Then a single-base mutation of the

isoleucine triplet codon of AUA to AAA gives the amino function of lysine, $-NH_3^+ \leftrightarrows -NH_2 +$ H^+, where removal of a proton from the $-NH_3^+$ group to give $-NH_2$ provides another means with which to achieve *chemo-mechanical transduction*. But importantly, it provides a positive charge, which, with increase in hydrophobicity, increases the binding capacity of redox functions such as NAD (nicotinamide adenine dinucleotide) and FAD (flavin adenine dinucleotide) with their negative diphosphate linkage to give the *electro-mechanical* and *electro-chemical transductions* of the electron transport chain of the inner mitochondrial membrane.

These simple single-base mutations produce new and improved protein-based machines either to access new energies or to increase the efficiency of function of an existing protein-based machine. Significantly, the new or improved protein-based machines are biosynthesized *without any increase in the energy required to access a new energy source or to produce a more efficient machine*. When a single mutation with no increase in cost of energy to produce the new protein results in a new machine capable of accessing a new energy source and/or a more efficient machine, it becomes apparent why the arrow-of-time for the biological world would be one that, in the words of Toffler (1984), "… proceeds from simple to complex, from 'lower' to 'higher' forms of Life, from undifferentiated to differentiated structures."

The preceding represent elemental means whereby living organisms can naturally evolve from lower to higher forms of life using the mechanism of energy conversion identified on characterization of designed ECMP. *In fact, it would seem that the Genetic Code itself was arranged in order for the living organism to evolve from primitive to more advanced and more complex forms using the energy converting mechanism demonstrated by the elastic-contractile model proteins (ECMP) - as long as there are adequate energy sources and building materials available.* (For a more complete discussion, see Chapter 6: On the Evolution of Protein-based Machines: Toward Complexity of Structure and Diversity of Function of Urry, 2006a).

6. Designed ECMP provide the thermodynamics of protein hydration and of elasticity!

Thermodynamics of protein hydration ($\Delta \mathbf{G_{HA}}$ and ΔG_{ap}) and of elasticity (the internal energy, f_E, and entropy, f_S, components of force) can be established by designed ECMP. The thermodynamics of protein hydration are obtained using differential scanning calorimetry (DSC) of the phase separation process. Whereas acid/base and redox titrations, as a function of V $\rightarrow$ F increases in hydrophobicity, provide means of measuring ΔG_{ap}. DSC data provide the heat of the phase transition, $\Delta \mathbf{H_t}$, which on derivation, using the relationship at the phase transition of $\Delta \mathbf{H_t} \approx T_t \Delta \mathbf{S_t}$, yields the critical quantity, the change in Gibbs free energy for hydrophobic association, $\Delta \mathbf{G_{HA}}$, as the difference, $\Delta \mathbf{H_t}$(GVGVP) - $\Delta \mathbf{H_t}$(GXGVP), where X is the substitution being characterized (Urry, 2004; 2006a). The result is the $\Delta \mathbf{G_{HA}}$-based Hydrophobicity Scale obtained for all amino acid residues, including their different functional states, where relevant, and for many biological prosthetic groups in their different functional states. As the hydrophobic R-groups are completely hydrated before the transition and essentially fully dehydrated after phase separation, the values of $\Delta \mathbf{G_{HA}}$, so obtained, may be considered to be maximal values. And this needs to be taken into consideration when interpreting a particular structural change attending protein function, e.g., in the extent of hydrophobic association experienced.

Thus, the thermodynamics of protein hydration have been obtained as the free energies of interaction, $\Delta \mathbf{G_{HA}}$ and ΔG_{ap}, and have been established by physico-chemical characterizations of designed ECMP.

6.1 Thermodynamics of the protein-in-water heat engine of biology

The protein-in-water heat engine of biology functions on the same general physical principle as the steam-powered heat engine of the birth of thermodynamics, which principle is the increase in entropy of water, when heat is applied at the temperature of a phase transition. Dramatic expansion of the bulk-water-to-vapor phase transition near the 100°C gives the increase in entropy of water for the steam-powered heat engine, whereas conversion of three-dimensionally interconnected pentagonal rings of water to bulk water gives the increase in entropy of water for the protein-in-water heat engine of biology. There is analogy to water dipole moments o three-dimensionally interconnected hexagonal rings of ice reorienting to become bulk water during the melting transition of relevance to Eyring's Significant Structure Theory of Water (Hobbs et al., 1966).

Significantly, while the phase transition of the melting of ice is quite fixed near 0°C, the transition temperature (T_t) of the inverse temperature transition (ITT) of protein-in-water can be shifted over much of the available aqueous range of water.

Lowering the temperature of the ITT utilizes non-random three-dimensional protein structures to which functional groups are bound. Conversion of functional groups by chemical or electrochemical energy input from a more-polar (e.g., charged) state to a more hydrophobic state, increases pentagonally-arranged water molecules, otherwise destructured by orientation toward charge. This lowers T_t from above to below the operating temperature and drives contraction by hydrophobic association (See Fig. 12 below). By this change in state of an attached biological functional group, the protein-in-water heat engine of biology functions as a protein-in-water chemical (or electrochemical) engine.

The physical process is competition for hydration. Nascent charges destroy pentagonal rings of hydrophobic hydration, as they recruit hydrophobic hydration for their own hydration, which raises T_t, disrupts hydrophobic association, and reverses contraction. Apolar and polar groups lower their free energies by reaching out for hydration unperturbed by the other. This expresses as an apolar-polar repulsive free energy of hydration, ΔG_{ap}.

6.1.1 Hydration of the hydrophobic CH$_2$ group is exothermic (Butler, 1937)

Butler examined the water solubility of the series of linear alcohols – methanol (CH_3-OH), ethanol (CH_3-CH_2-OH), n-propanol (CH_3-CH_2-CH_2-OH), n-butanol (CH_3-CH_2-CH_2-CH_2-OH), and n-pentanol (CH_3-CH_2-CH_2-CH_2-CH_2-OH) – and found the exothermic heat of dissolution to increase for each added CH_2, at the rate of $\Delta H/CH_2$ = –1.5 kcal/mol. Remarkably, dissolution of the CH_2 in water is a favorable heat releasing reaction. Hydrophobic hydration forms with the release of heat! Why then does the solubility of these linear alcohols decrease as the number of CH_2 moieties increase until n-octanol with seven CH_2 groups is insoluble? The answer is seen in the [–$T\Delta S$] term of the Gibbs free energy of dissolution, Eqn. (4).

$$\Delta G(\text{dissolution}) = \Delta H - T\Delta S. \tag{4}$$

Namely, the [–$T\Delta S$] term increases positively (unfavorably) for the Butler series as [–$T\Delta S$]/CH_2 = + 1.7 kcal/mol. A positive ΔG(dissolution) means insolubility; too many CH_2 moieties exposed to water means insolubility. Before too many hydrophobic groups are exposed to water, however, they may compete for hydration with more polar groups. Thus, the exothermicity on forming the pentagonal rings of hydrophobic hydration (See Fig. 2) is
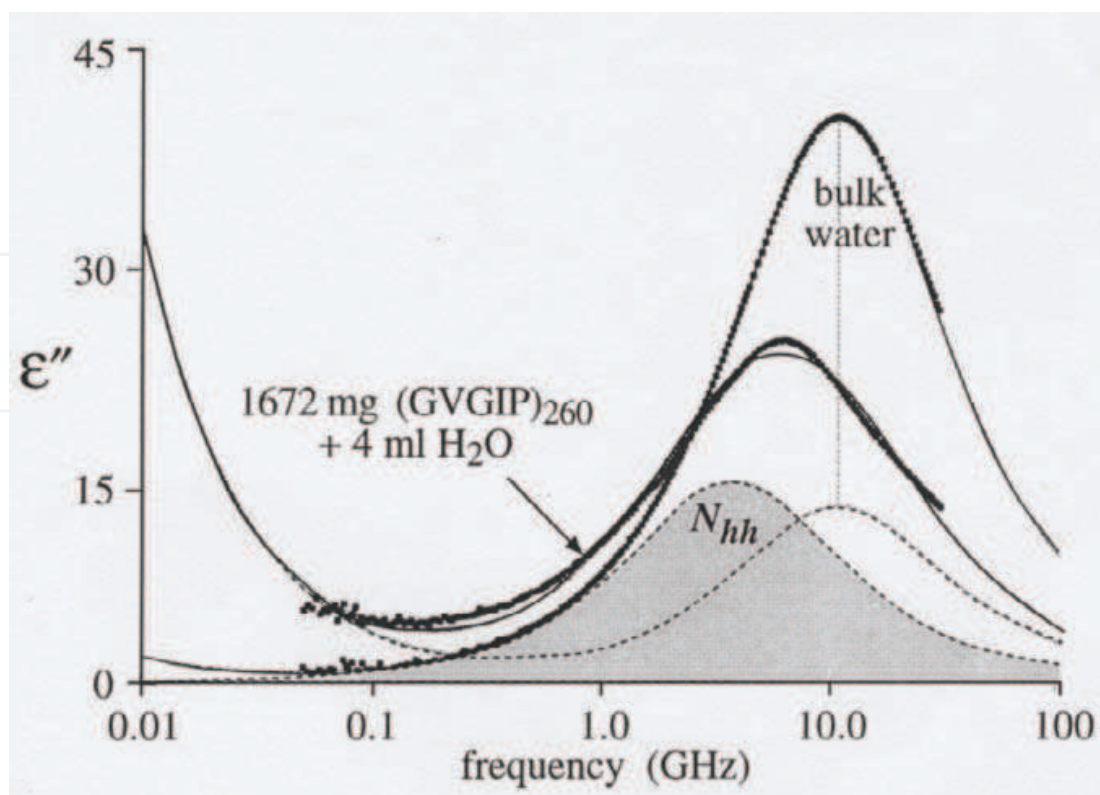
Fig. 9. Imaginary part of the dielectric permittivity of bulk water and of 1672 mg $(GVGIP)_{260}$ dissolved in 4 ml of water at 7°C. The curve for $(GVGIP)_{260}$ in water is resolved into two components, one for bulk water and one for water interacting with the model protein, $(GVGIP)_{260}$, which number of interacting water molecules is designated as N_{hh}. From Urry et al., 1997a.

the basis for a competition with polar groups for hydration. This competition for hydration is documented below in Figs. 10C and 12.

6.1.2 Hydrophobic hydration as characterized by microwave dielectric relaxation

As seen in Fig. 9, the imaginary part of the microwave dielectric relaxation spectrum of bulk water demonstrates an intense absorption just above 10 GHz. The spectrum for a solution of 1672 mg $(GVGIP)_{260}$ in 4 ml of water at 7°C, also seen in Fig. 9, has a broader absorption at lower frequency. On resolving the curve for bulk water just above 10 GHz, a second absorption occurs at a lower frequency, which represents water interacting with the ECMP, $(GVGIP)_{260}$.

The magnitude of N_{hh} is plotted in Fig. 10A as a function of dilution, which N_{hh} is found to increase until it plateaus near 5 mg/ml for both $(GVGIP)_{260}$ and $(GVGVP)_{251}$. The temperature dependence of N_{hh} in Fig. 10B, shows the magnitude of N_{hh} for $(GVGIP)_{260}$ to drop rather abruptly essentially to zero as the temperature passes through the interval of the inverse temperature transition (ITT) for $(GVGIP)_{260}$. Similarly for $(GVGVP)_{251}$, as the temperature passes through the temperature interval of the ITT for $(GVGVP)_{251}$, approximated in Fig. 7C, the magnitude of N_{hh} for $(GVGVP)_{251}$ drops to near zero. On the basis of the data of Fig. 10B, N_{hh} represents the numbers of water molecules of hydrophobic hydration (Urry et al. 1997a). The residual N_{hh} for (GVGVP) in Fig.10B is analogous to the residual pentagonal rings of water for hydrophobically associated crambin of Fig. 2.
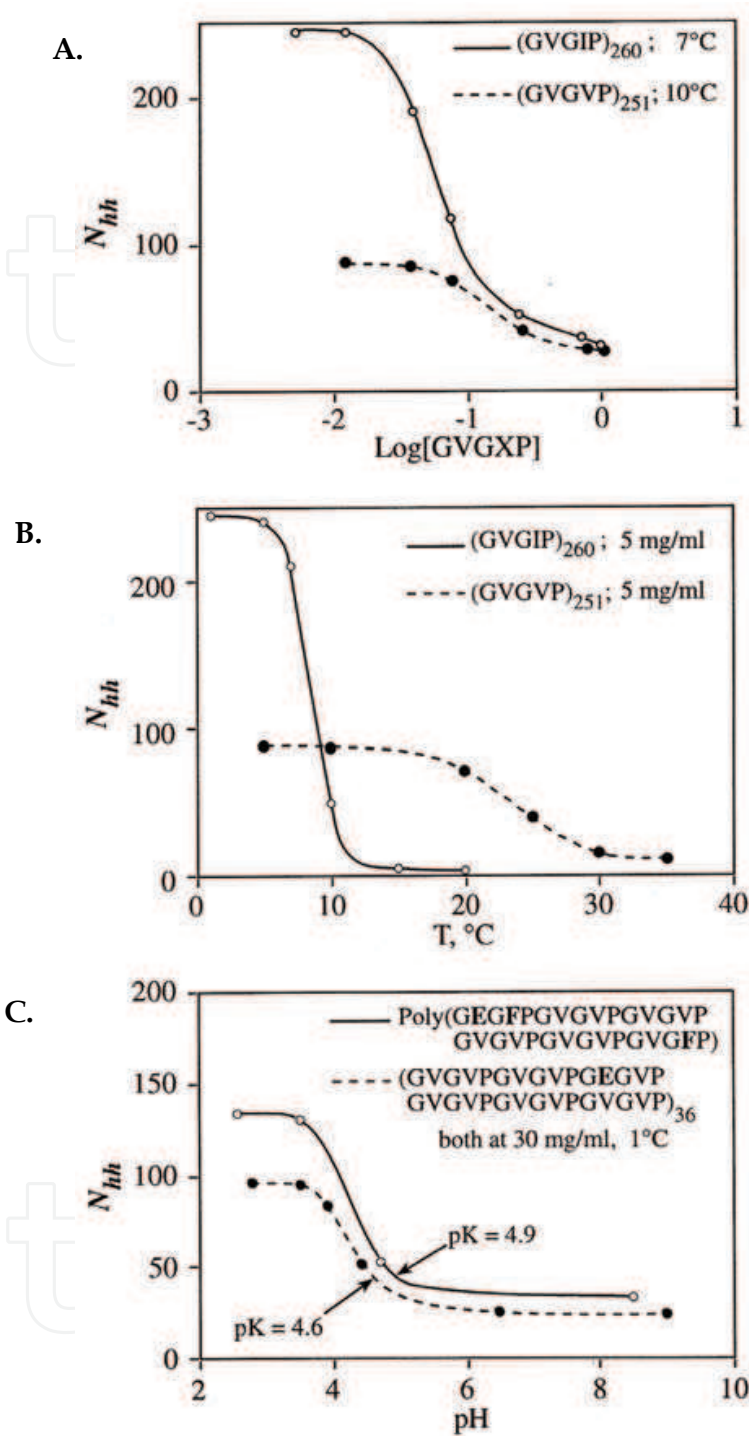
Fig. 10. Microwave dielectric relaxation studies on a unique water interacting with the basic and a designed ECMP. **A**. Demonstrates that on dilution this unique water increases. **B**. Shows that this unique water disappears as hydrophobic association develops, i.e., this identifies *Nhh* as hydrophobic hydration. **C**. Shows *Nhh*, the amount of hydrophobic hydration, to decrease as charged carboxylates form. Indeed, a competition for hydration has been directly observed between hydrophobic and carboxylates, (-COO$^-$). From Urry et al., 1997a.

Having found N_{hh} to represent the number of waters of hydrophobic hydration, the issue of the competition for hydration between charged groups and hydrophobic groups is addressed in Fig. 10C at 30 mg/ml and 1°C by means of the designed ECMP, (GVGVP GVGVP GEGVP GVGVP GVGVP GVGVP)$_{36}$ and the more hydrophobic, poly(GEGFP GVGVP GVGVP GVGVP GVGVP GVGFP), with n of approximately 40. Both designed ECMPs contain the glutamic acid (Glu, E) residue, such that at low pH the functional group of the E-residue will be –COOH. As reported in Fig. 10C, on raising the pH, N_{hh}, decreases as the charged carboxylate groups, -COO⁻, form with increased pK as 2V → 2F per 30 mer (Urry et al., 1997a).

Thus, the data of Fig. 10C directly demonstrate the competition for hydration between hydrophobic groups and charged groups. As charged -COO⁻ form, they cooperate to disrupt the cyclically-arranged dipoles of pentagonal rings of water as the dipoles realign toward charge, not unlike charged plates reorient water dipoles in Eyring's Significant Structure Theory of Water (Hobbs et al., 1966; Jhon & Eyring, 1976). As hydrophobic and charged groups compete for limited water, they move away from each other in order to achieve hydration unperturbed by the other resulting in an apolar-polar repulsive free energy of hydration, ΔG_{ap} (Urry, 1992; 1997). In Fig. 14B ΔG_{ap} is seen as hydrophobic-induced pK shifts!

6.1.3 Thermodynamics of the inverse temperature transition

At a given temperature within the interval of the inverse temperature transition, the system of ECMP in water is at equilibrium; the chemical potential of the hydrophobically dissociated molecules in solution, μ_{HD}, is the same as the chemical potential of the phase separated, hydrophobically associated molecules, μ_{HA}. Since $\mu_{HD} = \mu_{HA}$, $\Delta G = 0$, and for the inverse temperature transition, ITT,

$$\Delta H_t \approx T_t \Delta S_t. \tag{5}$$

where the subscript, t, stands for the transition characterized in Fig. 7. Neglecting the very small heat capacity of the ECMP and of water over the temperature interval, the heat of the ITT for (GVGVP) for the transition of Fig. 7C will be given as **ΔH_t(GVGVP)**, where the bold-faced **ΔH_t** means per mole of pentamer, (GVGVP), within (GVGVP)$_{251}$.

As seen in Fig. 7C, the ITT is an endothermic transition, that is, ΔH_t is positive. Therefore, by Eqn. (5) ΔS_t is positive. The entropy increases as the phase separation occurs. Yet in this protein-in-water, two-component system, the protein becomes more ordered, i.e., ΔS_t(protein) is negative. The only other component of the ITT, water, must be the component that gives rise to the positive ΔS_t. And specifically, the hydrophobic hydration, N_{hh}, of Figs. 9 and 10B, is the water that becomes less-ordered bulk water, i.e., $\Delta S_t(N_{hh} \rightarrow$ bulk water) represents the positive entropy change that drives the ITT. During the transition the model protein becomes restricted in its motion on hydrophobic association and even becomes structured with formation of filaments, fibrils and fibers (Urry, 1992), that is, ΔS_t(model protein) is negative. So we write,

$$\Delta S_t(N_{hh} \rightarrow \text{bulk water}) > \Delta S_t(\text{total system}) + \Delta S_t(\text{model protein}) > 0 \tag{6}$$

and

$$\Delta S_t(N_{hh} \rightarrow \text{bulk water}) > \Delta S_t(\text{total system}) >> 0 \tag{7}$$

By Eqns. (5) and (6), it is apparent for the two-component ITT, that the component, ΔH_t(model protein) $\approx T_t \Delta S_t$(model protein). Also, ΔH_t(model protein) would be an exothermic component within a larger endothermic component. Accordingly, it is interesting to report that temperature modulated differential scanning calorimetry (TMDSC) separates out such an exothermic component that is one-quarter to one-third the magnitude of the endothermic component (Rodríguez-Cabello et al., 2004). As hydrophobic association occurs, a van der Waals' interaction energy is expected to result in an exothermic component to the ITT, in this case arising largely from London's dispersion forces (See Eyring, et al. 1958).

When developing a Hydrophobicity Scale based on ΔG_{HA}, the change in Gibbs free energy for hydrophobic association, no attempt will be made to separate out the exothermic component, as the van der Waals' energy due principally to dispersion forces would be part of all hydrophobic associations. It is interesting to note in the plot of T_b versus ΔH_t of Fig. 13 below that all of the amino acid residues containing aliphatic side chains and even the glycine residue where the $-CH_2-$ is in the backbone fall on a straight line, whereas the aromatic residues give a much steeper slope and a greater heat (See Fig. 13, section **6.2.4**).
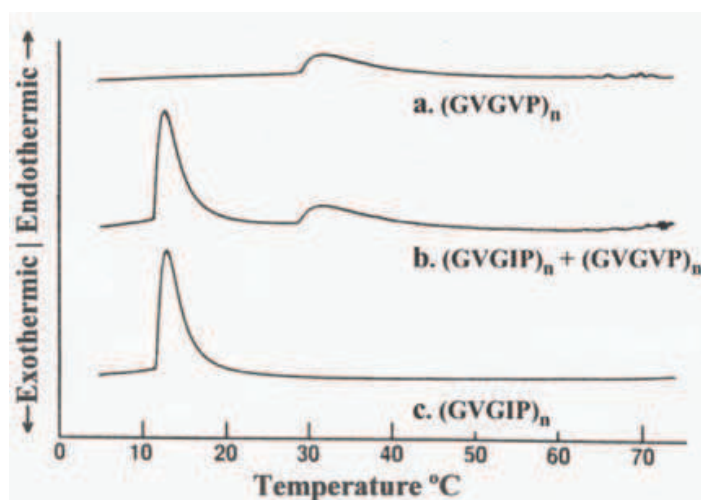

Fig. 11. Differential scanning calorimetry curves of $(GVGVP)_n$ and $(GVGIP)_n$ in water. Demonstrated are heats of ΔH_t(GVGVP) = 1.2 kcal/mol-(GVGVP) and ΔH_t(GVGIP) = 3.0 kcal/mol-(GVGIP). Scanning the aqueous mixture shows the ECMP to self associate, i.e., to demix, which suggests an hierarchical hydrophobic folding of protein. Adapted from Urry et al., 1997a.

6.2 The changes in Gibbs free energy underlying the protein-in-water heat engine of biology

6.2.1 The hierarchy of hydrophobic association demonstrated by demixing of ECMP on raising the temperature

The side chains of V, $-CH(CH_3)_2$, and I, $-CH_2-CH(CH_3)_2$ differ by a single $-CH_2-$. Similarly, the pentamers, (GVGVP) and (GVGIP) differ only by a single $-CH_2-$. In particular, the molecular weights of the pentamer units are 409 Daltons for (GVGVP) and 423 Daltons for (GVGIP). Just a 3.4% increase in molecular weight lowers the onset temperature by 15°C and increases the heat of the transition by 240%. By considering the aliphatic groups only, 2V(86D), 2G(28D), and P(42D) gives 156 Daltons for (GVGVP) and V(43D), 2G(28D), P(42D),

and I(57D) gives 170 Daltons for (GVGIP), which is a small 11% increase in mass of hydrophobic moieties to be responsible for a 2.4 fold increase in heat of the transition. It was also seen in Fig. 10B that the added -CH$_2$- of (GVGIP) resulted in a slightly larger 2.8 fold increase based on the estimated number of waters of hydrophobic hydration, N_{hh}.

Another important feature occurs in the DSC data of Fig. 11. When the temperature is scanned for an equimolar mixture of (GVGVP)$_n$ and (GVGIP)$_n$ in water, starting some 5°C or more below the lowest T_t, there is a complete demixing of the polypentamers that differ by but one -CH$_2$- moiety per pentamer. This represents a remarkable separation capacity and surely has an impact on details of hydrophobic associations as proteins fold.

It is interesting that the inverse temperature transition, which is driven by the increase in entropy as pentagonal rings of hydrophobic hydration become higher entropy bulk water, can achieve the decrease in entropy of complete separation of a mixture of polymers as seen in the middle curve of Fig. 11. This effect has also been used in the purification of microbially-prepared ECMP (See Fig. 5 of McPherson et al., 1996). In particular, during the purification of (GVGVP)$_{251}$ from an *E-coli* lysate, an endotoxin impurity was observed with a phase separation of its own that overlapped with the temperature interval for (GVGVP)$_{251}$. The endotoxin impurity could be largely separated from (GVGVP)$_n$ by centrifugation at 23°C, facilitating later complete removal of the small amount of remaining endotoxin.

6.2.2 Experimental dependence of both T$_t$ and ΔH$_t$ on the amount of hydrophobic hydration, *Nhh*

In Fig. 10A and B the increase in hydrophobic hydration, N_{hh}, is a factor of 2.8 on going from (GVGVP)$_n$ to (GVGIP)$_n$ resulting from the increase of but a single CH$_2$ per pentamer. From yet another experiment, the endothermic heat of the transition in water for (GVGIP)$_n$, i.e., **ΔH$_t$**(GVGIP) = 2.61 kcal/mol-(GVGIP), is larger by a factor of 2.4 than that for (GVGVP)$_n$, i.e., **ΔH$_t$**(GVGVP) = 1.07 kcal/mol-(GVGVP) (Luan et al. 1990; Luan & Urry, 1991). *The magnitude of the increase in hydrophobic hydration due to the added CH$_2$ appears to be larger than the magnitude of the increase in the heat of the transition, which effect results in the lowered value of T$_t$ as ΔH$_t$ ≈ T$_t$ΔS$_t$.* A similar correlation, in this case an inverse correlation, is observed between the increase in N_{hh} and the decrease in T$_t$ for **Model protein ii** and for **Model protein I** of Fig. 12A and B.

The formation of the charged carboxylate (-COO⁻) of the glutamic acid residue (Glu, E) decreases N_{hh}, the amount of hydrophobic hydration, as seen in Fig. 10C. In addition to the addition of a proton to neutralize the charged carboxylate, the capacity of the carboxylate charge to destructure hydrophobic hydration is moderated by ion-pairing, as with a Ca^{2+} ion. The increase in hydrophobicity, measured by the increase in number of molecules of hydrophobic hydration, N_{hh}, for a transition driven by chemical energy is demonstrated in Fig. 12 by titration of Ca^{2+} into the ECMP-water two component system. As Ca^{2+} ion-pairs with glutamic acid residues, the value of **T$_t$** decreases and the waters of hydrophobic hydration increase in an inverse relationship (See Fig. 12).

Noting the considerations of section **6.1.3**, the experimental endothermic heat given as per mole pentamer, **ΔH$_t$**(GVGVP), is comprised of two components, the *major heat absorbed* as $N_{hh} \rightarrow$ bulk water for GVGVP and the *smaller heat released* as van der Waals contacts develop as hydrophobic association proceeds between repeats of (GVGVP) (See Rodríguez-Cabello et al., 2004). These two components are given as in Eqn. (8),
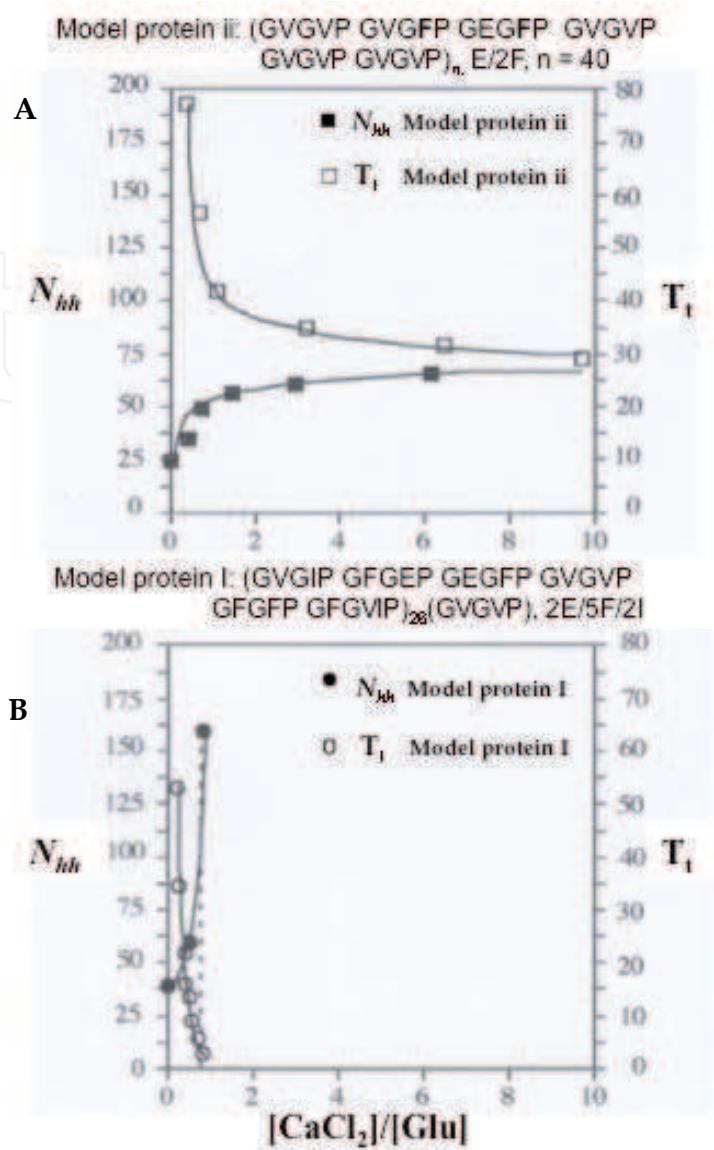
Fig. 12. Inverse correlation of T_t, the temperature of the inverse temperature transition, ITT, and N_{hh}, the number of waters of hydrophobic hydration. Independent of the steepness of the $[Ca^{2+}]$ binding to carboxylate, the values for T_t mirror the values for N_{hh}. *Increases in hydrophobic hydration, N_{hh}, lower T_t, the temperature of the ITT!* This and the correlation of ΔH_t and N_{hh} seen on comparison of data in Figs. 10 and 11 are consistent with the definition of ΔG_{HA} of Eqn. (12) below. From Urry, 2006a.

$$\Delta H_t = \Delta H_t'(\text{heat absorbed as } N_{hh} \rightarrow \text{bulk water per GVGVP})$$

$$+ \Delta H_t''(\text{heat released due to contacts between GVGVP}) \qquad (8)$$

By Eqn. (5), $\Delta H_t \approx T_t \Delta S_t$, the $T_t(\text{GVGVP})\Delta S_t(\text{GVGVP})$ term for the phase transition can be written,

$$T_t\Delta S_t = T_t\Delta S_t'(N_{hh} \rightarrow \text{bulk water per GVGVP}) +$$

$$T_t\Delta S_t''(\text{contacts between GVGVP decrease entropy}) \qquad (9)$$

Again there are the equivalent two components, the *larger positive entropy change* per mole pentamer, $\Delta S_t'$, as hydrophobic hydration, N_{hh}, per mole pentamer becomes less-ordered bulk water and *the smaller negative entropy change*, $\Delta S_t''$, as (GVGVP) become constrained by hydrophobic association.

Keeping in mind the two equivalent per pentamer, (GVGVP), components within Eqn. (8) and Eqn. (9), Eqn. (5) can simply be written for (GVGVP) as,

$$\Delta H_t(GVGVP) \approx T_t(GVGVP)\Delta S_t(GVGVP) \tag{10}$$

6.2.3 Derivation of the change in Gibbs free energy for hydrophobic association, ΔG_{HA}, due to a substitution of V by X

Required is an expression for the change in Gibbs free energy resulting from a change of a single R-group in the (GVGVP) pentamer. The differences in Fig. 12 between the inverse temperature transitions exhibited by GVGVP)$_n$ and (GVGIP)$_n$ represent the desired quantity, ΔG_{HA}, i.e., the change in the Gibbs free energy for hydrophobic association, in this example, due to the addition of a single CH_2-group. The unique position X between two G residues, GXG, allows each amino acid residue, including chemical adducts to carboxyl (e.g., Glu and Asp) and amino functions, to occur with retention of the fundamental elastic and phase transitional properties. Accordingly, Eqn (9) is restated for (GXGVP), i.e.,

$$\Delta H_t(GXGVP) \approx T_t(GXGVP)\Delta S_t(GXGVP). \tag{11}$$

Subtraction of Eqn. (11) from Eqn. (10) gives,

$$\Delta H_t(GVGVP) - \Delta H_t(GXGVP) \approx T_t(GVGVP)\Delta S_t(GVGVP) - T_t(GXGVP)\Delta S_t(GXGVP). \tag{12}$$

The term on the right-hand side of Eqn. (12) expresses the sought after change in Gibbs free energy for the (GVGVP)-in-water phase transition of hydrophobic association, ΔG_{HA}, on substitution of V by X, that is,

$$\Delta G_{HA}(GVGVP \rightarrow GXGVP) = T_t(GVGVP)\Delta S_t(GVGVP) - T_t(GXGVP)\Delta S_t(GXGVP). \tag{13}$$

Eqn. (13) represents the change in Gibbs free energy due to the increase in entropy as pentagonal rings of water become bulk water minus the smaller decrease in entropy as the model protein (GVGVP)$_n$ becomes more-ordered on hydrophobic association, as described in Eqns. (8) and (9), minus the same for (GXGVP).

As ΔS_t is directly calculated from the endothermic heat, ΔH_t of the experimental curve, the sought-after ΔG_{HA} can be equivalently stated as,

$$\Delta G_{HA}(GVGVP \rightarrow GXGVP) = \Delta H_t(GVGVP) - \Delta H_t(GXGVP). \tag{14}$$

It should be appreciated that such a relationship holds only for the phase transition, hence the required subscript, t.

At whatever temperature the inverse temperature transition, ITT, occurs for a particular ECMP composition within the accessible aqueous temperature range, the ECMP-in-water heat engine is based upon a phase transition in which, on heating, water undergoes a transition from lesser to greater entropy. In particular, on heating, structured hydrophobic hydration, i.e., water arranged in pentagonal rings, becomes less-ordered bulk water.

When the temperature of the transition is driven by another energy input, such as chemical energy, the particular energy input causes the responsive functional group, and hence the ECMP, to become more hydrophobic. The consequence is more hydrophobic hydration, which lowers the transition temperature, T_t, as seen in Fig. 12.

6.2.4 Plot of the temperature transition vs the change in Gibbs free energy for hydrophobic association, ΔG_{HA}

It is convenient for a hydrophobicity scale of amino acid residues to choose the most neutral residue, neither hydrophobic nor polar, as the zero reference state. This is achieved simply by replacing $\Delta H_t(GVGVP)$ of Eqn. (14) by $\Delta H_t(GGGVP)$, i.e.,

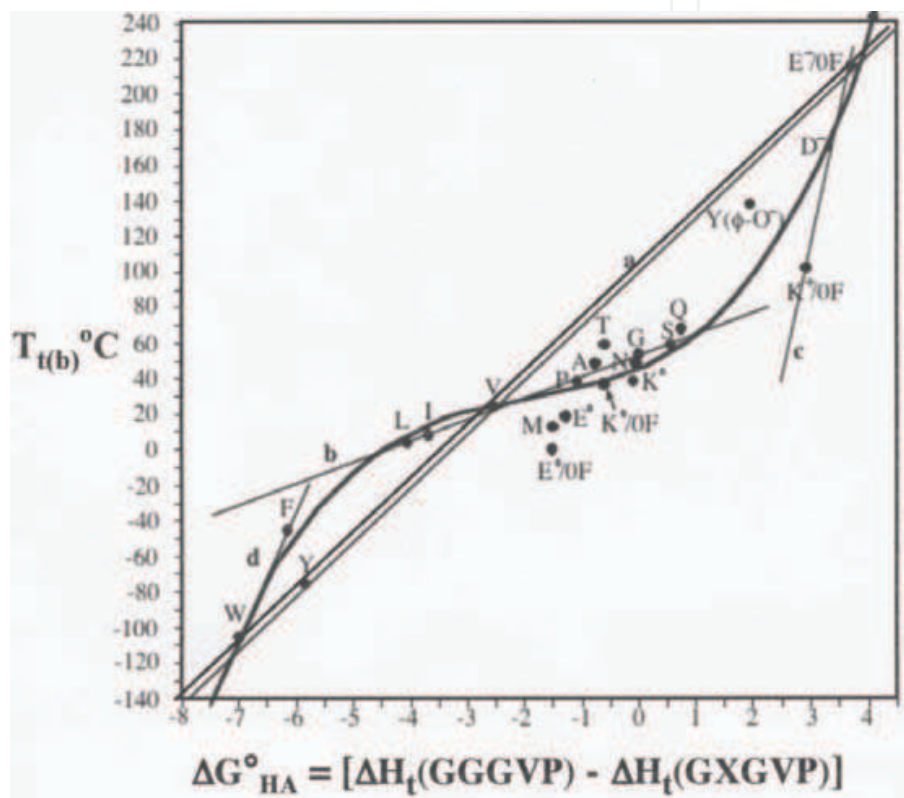Fig. 13. The plot of the change in Gibbs free energy for hydrophobic association, $\Delta G°_{HA}$, versus the onset temperature of the inverse temperature transition, T_t when using the midpoint of the temperature versus turbidity curve and T_b when using DSC to measure the onset of the heat of the phase transition. See text for further discussion. Adapted from (Urry, 2004).

$$\Delta G°_{HA} \equiv \Delta H_t(GGGVP) - \Delta H_t(GXGVP), \tag{15}$$

where ΔG_{HA} has been replaced by $\Delta G°_{HA}$ to indicate that the hydrophobicity scale has chosen G as the zero reference. Eqn. (15) is used for plotting the values in Fig. 13 of $T_{t(b)}$ versus $\Delta G°_{HA}$, where the data point for the G (glycine, Gly) is zero.

The doubled diagonal line, **a**, gives the T_t-based Hydrophobicity Scale approximation of the relationship between $T_{t(b)}$ and $\Delta G°_{HA}$, when in reality it is a sigmoid relationship. The sigmoid plot in Fig. 13 allows that a given value of T_t can be read from the sigmoid curve for a better approximation of $\Delta G°_{HA}$. This was done for the $\Delta G°_{HA}$ values of **Table 2**.

All of the amino acid residues with aliphatic hydrophobic groups – G, A, P, V, I, and L – fall on the straight line, **b**, i.e., they all exhibit the same linear temperature dependence of the inverse of the entropy, $(\Delta S_t)^{-1}$. All of the aliphatic hydrophobic side chains of amino acid residues, as well as the CH_2 in the backbone of G, have the same thermal stability of hydrophobic hydration, but the thermal stability of aliphatic hydrophobic hydration appears greater than that of the aromatic residues.

The temperature dependence of the amino acid residues with charged side chains, line **c**, gives the steepest slope. And E^-, D^-, and K^+ follow the relative capacity, in decreasing order, of charged side-chains to disrupt hydrophobic hydration.

The temperature dependence of the amino acid residues with aromatic side chains, line **d**, is much steeper than that of the aliphatic residues, which, as the slope is $(\Delta S_t)^{-1}$, suggests less thermal stability for the hydrophobic hydration of aromatic groups.

As seen in **Table 1** and Fig. 13, the biggest change in $\Delta G°_{HA}$ occurs on ionization of the carboxyl side chain of glutamic acid, i.e., $-CH_2-CH_2-COOH \rightarrow -CH_2-CH_2-COO^- + H^+$. From **Table 1**, the change in free energy of hydrophobic hydration, $\Delta G°_{HA} = [(GE°GVP) \rightarrow (GE^-GVP)] =$ is 5.22 kcal/mol-(GEGVP). Also, as seen in Fig.10C, this ionization disrupts 75% of the hydrophobic hydration, N_{hh}. Furthermore, in Fig. 12 partial neutralization of E^- by ion-pairing with calcium ion markedly increases N_{hh} in a manner that mirrors the decrease in T_t. This demonstrates how putting chemical energy into a protein-in-water heat engine drives *chemo-mechanical transduction*. It does so by increasing the amount of hydrophobic hydration, and thereby lowering T_t, until the phase transition falls sufficiently below the operating temperature to have completed the hydrophobic association of contraction. Just as with the dissolution of the alcohol series of Butler (1937), as more CH_2 moieties are added, more exothermic hydrophobic hydration builds up. This continues until the unfavorable, positive $[-T\Delta S]$ term of $\Delta G(dissolution) = \Delta H - T\Delta S$ becomes greater than the favorable, negative ΔH term, and solubility is lost. The thermodynamics is such that hydrophobic hydration builds until the tipping point (the phase transition to hydrophobic association) has been reached. Once the temperature of the system is some 10°C above the onset temperature for the transition, contraction is nearly complete.

The cumulative effect of neutral residues might also be noted. For example, when the hydrophobicity of a domain or structure of a protein is being considered, the $\Delta G°_{HA}$ of glutamine, Q, of 0.75 in **Table 1** and Fig. 13 can have a disruptive effect on hydrophobic association. The cumulative effect of some half dozen glutamine residues give a $\Delta G°_{HA}$ of 4.5 kcal/6 mol-Q, which contributes more than a single glutamate where from **Table 1**, $\Delta G°_{HA}$ reads 3.7 kcal/mol-E^-.

6.2.5 (T_t and $\Delta G°_{HA}$)-Hydrophobicity scales for biological functional groups attached to amino acid side-chains

A number of biological functional groups have been attached to amino, carboxyl, and -OH functions of designed ECMP. The T_t values are listed in **Table 2** and the $\Delta G°_{HA}$ values have been approximated using the sigmoid curve of Fig. 13. Of immediate interest are the redox functional groups and most particularly N-methyl nicotinamide, which has been used to determine the effect of increased hydrophobicity on reduction potential and positive cooperativity. As will be shown in section **6.2.8** the effects of increased hydrophobicity on reduction potential and cooperativity of redox functions parallel the effects of increased hydrophobicity on pK and positive cooperativity of the carboxyl and amino functions.

Residue X	ΔG°_{HA} from **Figure 13** (kcal/mol)[g]	T_t linearly extrapolated to $f_X = 1$
Lys (dihydro NMeN)[b,d]	− 7.0	−130°C
Glu(NADH)[c]	− 5.5	−30°C
Lys (6-OH tetrahydro NMeN)[b,d]	− 3.5	15°C
Glu(FADH$_2$)	− 2.5	25°C
Glu(AMP)	+ 1.0	70°C
Ser(-O-SO$_3$H)	+ 1.5	80°C
Thr(-O-SO$_3$H)	+ 2.0	100°C
Glu(NAD)[c]	+ 2.5	120°C
Lys(NMeN, oxidized)[b,d]	+ 2.5	120°C
Glu(FAD)	+ 2.5	120°C
Tyr(-O- SO$_3$H)[e]	+ 3.0	140°C
Tyr(-O-NO$_2^-$)[f]	+ 3.5	220°C
Ser(PO$_4^=$)	+ 8.0	860°C

[a]The usual conditions are for 40mg/ml polymer, 0.15N NaCl, 0.01M phosphate at pH 7.4.
[b]NMeN, N-methyl nicotinamide, attached to a lysyl side chain, i.e., N-methyl-nicotinate attached by amide linkage to the e-NH$_2$ of Lys. The most hydrophobic reduced state is N-methyl-1,6-dihydronicotinamide (dihydro NMeN), and the second reduced state is N-methyl-6-OH 1,4,5,6-tetrahydronicotinamide or (6-OH tetrahydro NMeN).
[c]For the oxidized and reduced nicotinamide adenine dinucleotides, the conditions were 2.5 mg/ml polymer, 0.2M sodium bicarbonate buffer at pH 9.2.
[d]For the oxidized and reduced N-methyl nicotinamide, the conditions were 5.0 mg/ml polymer, 0.1M potassium bicarbonate buffer at pH 9.5, 0.1M potassium chloride.
[e]The pK$_a$ of polymer bound -O-SO$_3$H is 8.2.
[f]The pK$_a$ of Tyr(-O-NO$_2$) is 7.2.
[g]Gross estimates (e.g., ± 0.5 kcal/mol) of ΔG°_{HA} using the T_t-values in the right column in combination with the $T_{b(t)}$ versus ΔG°_{HA} values from **Figure 13**. Adapted from Table 5.2 of Urry, 2006.

Table 2. Hydrophobicity Scales (preliminary T_t and ΔG°_{HA} values) for chemical modifications and prosthetic groups of proteins[a]. T_t is the temperature for the onset of the inverse temperature transition, and ΔG°_{HA} is the change in Gibbs free energy for hydrophobic association for poly[f_V(GVGVP),f_X(GXGVP)].

In particular, increases in hydrophobicity shift the pK and reduction potential values in a supra-linear manner toward the less polar, more hydrophobic state with the same changes in free energy that contribute to the increases in positive cooperativity.

The largest change in ΔG°_{HA} of the redox functions in **Table 2** occurs on reduction of oxidized N-methyl nicotinamide (NMeN$^+$) attached by amide linkage to the lysine side chain, i.e., ΔG°_{HA}[NMeN$^+$ → dihydro NMeN] = −9.5 kcal/mol-NMeN. This is greater than the change in the Gibbs free energy of hydrophobic association on reduction of oxidized nicotinamide adenine dinucleotide (NAD$^+$) to NADH, i.e., ΔG°_{HA}[NAD$^+$ → NADH] = −8 kcal/mole-NAD. Similarly for the reduction of flavin adenine dinucleotide (FAD) to FADH$_2$, ΔG°_{HA}[FAD → FADH$_2$] = −5 kcal/mole-FAD. These numbers are of the right order and magnitude for their biological functions. In the electron transport chain of the inner mitochondrial membrane, the oxidation of FADH$_2$ provides the energy to pump at a

maximum 66% of the number of protons as does the oxidation of NADH, and 100[(5 kcal/mole-FAD)/(8 kcal/mole-NAD)] = 63%.

Also, enzymatic phosphorylation of the serine residue of the serine kinase site, RGYSLG, within designed ECMP extrapolates to a $\Delta G°_{HA}$ of +8kcal-mol-phosphate. This finding provides evidence that the presence of phosphate disrupts hydrophobic association (See section 8.1.11 of Urry, 2006a). Also, the $K_{eq} \approx 1$ for the reaction, ATP + ECMP-S = ADP + ECMP-S-P, i.e., $\Delta G°_{HA}$[ECMP-S → ECMP-S-P] ≈ - $\Delta G°_{HA}$[ATP → ADP + P] ≈ 8 kcal/mol-P.

A.

Model protein I: (GVGIP GFGEP GEGFP GVGVP GFGFP GFGIP)₂₆(GVGVP)	2E/5F/2I
Model protein i: (GVGVP GVGVP GEGVP GVGVP GVGVP GVGVP)₃₆(GVGVP)	E/0F
Model protein ii: (GVGVP GVGFP GEGFP GVGVP GVGVP GVGVP)ₙ, n ≈ 40	E/2F
Model protein iii:(GVGVP GVGVP GEGVP GVGVP GVGFP GFGFP)₃₉(GVGVP)	E/3F
Model protein iv: (GVGVP GVGFP GEGFP GVGVP GVGFP GVGFP)₁₅(GVGVP)	E/4F
Model protein v: (GVGVP GVGFP GEGFP GVGVP GVGFP GFGFP)₄₂(GVGVP)	E/5F

Fig. 14A. Family of ECMP used below in the acid/base titration studies. **Model proteins i** through **v** are the same as in **Table 3**.
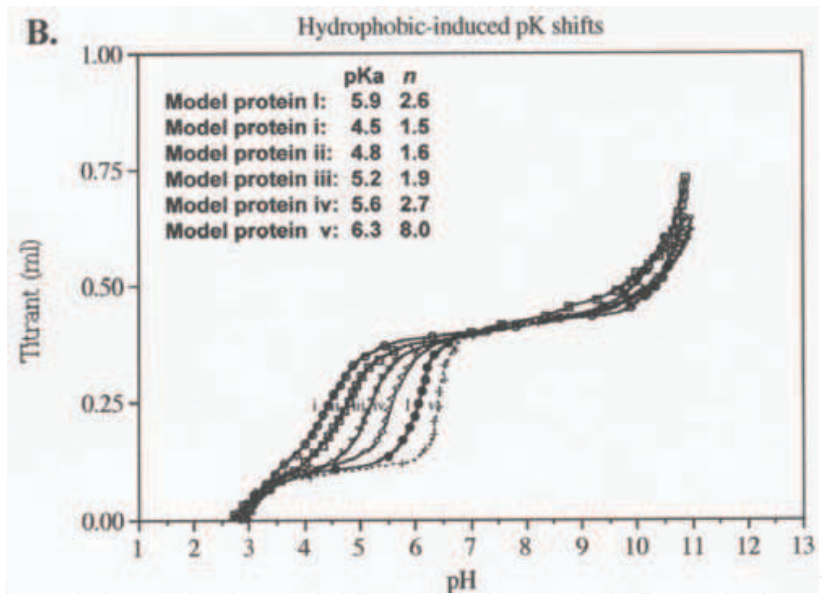

Fig. 14B. ECMP acid/base titrations exhibit supra-linear hydrophobic-induced pK & positive cooperativity shifts as V-residues are replaced by F-residues (Urry, 2006a).

6.2.6 The apolar-polar repulsive free energy of hydration, ΔG_{ap}

Three families of ECMP were designed (See **Table 3** below), each containing a different acid/base or redox function (Φ), containing a set of V → F increases in hydrophobicity, i.e., Φ/nF, where n = 0, 2, 3, 4, and 5, and V → functional groups (E, K, and NMeN). Acid/base and redox titrimetry data demonstrate systematic hydrophobic-induced pK, reduction potential, and positive cooperativity shifts. In general, five different experimental approaches used on these and other ECMPs exhibit apolar-polar group competition for hydration and quantify an apolar-polar repulsive free energy of hydration, ΔG_{ap}.

Generalized equations, containing the required terms for both apolar-polar (ap) and charge-charge (cc) repulsion, were derived for analysis of acid/base and redox titration data in

order to resolve charge-charge and hydrophobic-induced pK, reduction potential and positive cooperativity shifts (Urry, 1997; 2006a). Analyses used a specialized adaptation of a Hill plot to resolve the free energies of the charge-charge (cc) and apolar-polar (ap) cooperativity interactions, $[(\partial\Delta G/\partial\alpha)_T]_{cc}$ and $[(\partial\Delta G/\partial\alpha)_T]_{ap}$, and to result in determination of the appropriate values of ΔG. The free energies due to cooperativity interactions were found to be equivalent to those free energies of corresponding pK shifts, $\Delta G_{ap} = 2.3RT\Delta pK$, of the acid/base titrations and to those of the reduction potential shifts of the redox functions, i.e., $\Delta G_{ap} = z\mathscr{F}\Delta E$.

6.2.7 Analysis of the acid-base titration curves of Fig. 14

The family of model proteins, **Model proteins i** through **v**, of Fig. 14A are poly(30 mers) in which in all five model proteins the third basic repeat, (GVGVP), has been changed to (GEGVP), and in which the first and fourth repeats remain as (GVGVP). The other three pentamers contain one or two V-residues having been replaced by one or two more-hydrophobic F-residues.

The members of this family are identified as E/0F, E/2F, E/3F, E/4F, and E/5F. Their remarkable set of acid-base titration curves are reported in Fig. 14B, where the pK and positive cooperativity shifts increase in a supra-linear manner. In particular, substitution of the first two V-residues by F-residues, as in going from **Model protein i** to **ii**, i.e., E/0F to E/2F, results in a pK shift of 0.3 pH units and the Hill coefficient changes from 1.5 to 1.6. By adding a single substitution on going from E/4F to E/5F at the higher hydrophobicity, the pK shift is 0.7 pH units and the Hill coefficient increases from 2.7 to 8 to give a change of 5.3. Thus, the effect of the initial substitution of the first F would be a pK shift of the order of 0.15, the addition of the last F-residue on going from E/4F to E/5F gives a 4.7 (= 0.7/0.15) times larger pK shift and an increase of the Hill coefficient by a factor of 106 (= 5.3/0.05).

From the **$\Delta G°_{HA}$**-based Hydrophobicity Scale of **Table 1**, the change in (G(HA on replacing a single V-residue by a single F-residue, found by a linear process of plotting from $f_F = 0$ to $f_F = 1$, is -3.65 kcal/mol-pentamer, yet the effect of increasing numbers of F substitutions on pK and Hill coefficient of the E/nF series is supra-linear. By what mechanism does this supra-linearity occur? And how may an understanding of the underlying physical process be found? The physical process will be found to be fundamental in understanding the function of protein-based machines of biology.

The challenge is to express accurately these hydrophobic-induced changes in pK and positive cooperativity in terms of changes in Gibbs free energy and to obtain a physical basis for the observed effects. This problem is approached below, by first deriving a generalized acid/base titration equation, and then by developing a graphical means whereby the changes in Gibbs free energies may be obtained and compared.

6.2.8 Generalized acid/base titration equations that contain apolar-polar, ap, and charge-charge, cc, repulsion terms

The familiar Henderson/Hasselbalch equation for the titration of a dilute weak acid or base has the form, pH = pK + $\log[\alpha/(1-\alpha)]$, which is modified to introduce cooperativity by introduction of the Hill coefficient, *n*, to give the expression, pH = pK + $(1/n)\log[\alpha/(1-\alpha)]$ (Hill, 1913). The need to obtain a titration equation wherein the Hill coefficient, *n*, could be replaced by an explicit term for the change in Gibbs free energy reflected by a change in cooperativity has been addressed over the years by Overbeek, (1948), Katchalsky & Gillis

(1949), and Harris & Rice (1954). The result for charge-charge repulsion observed in polyelectrolyte solutions would be of the form,

$$pH = pK_{cc} + \log[\alpha/(1-\alpha)] + [(\partial\Delta G/\partial\alpha)_T]_{cc}/2.3RT, \qquad (16)$$

where pK_{cc} is the shifted pK due to charge-charge repulsion, and $(1/n)\log[\alpha/(1-\alpha)]$ is replaced by two terms, $\log[\alpha/(1-\alpha)] + [(\partial\Delta G/\partial\alpha)_T]_{cc}/2.3RT$.

It becomes apparent on considering the data of Fig. 14 that designed ECMP also exhibit, as discussed above, an apolar-polar repulsive free energy of hydration, ΔG_{ap}. The equation for acid/base titrations of designed ECMP requires inclusion of terms for both charge-charge and apolar-polar repulsion. The derivation may be found elsewhere (Urry, 1997; 2006a) to give the following,

$$(\partial\Delta G^{nF}/\partial\alpha) = -2.3RT(\Delta pH^{nF} - \Delta pH^{ref})/0.82$$
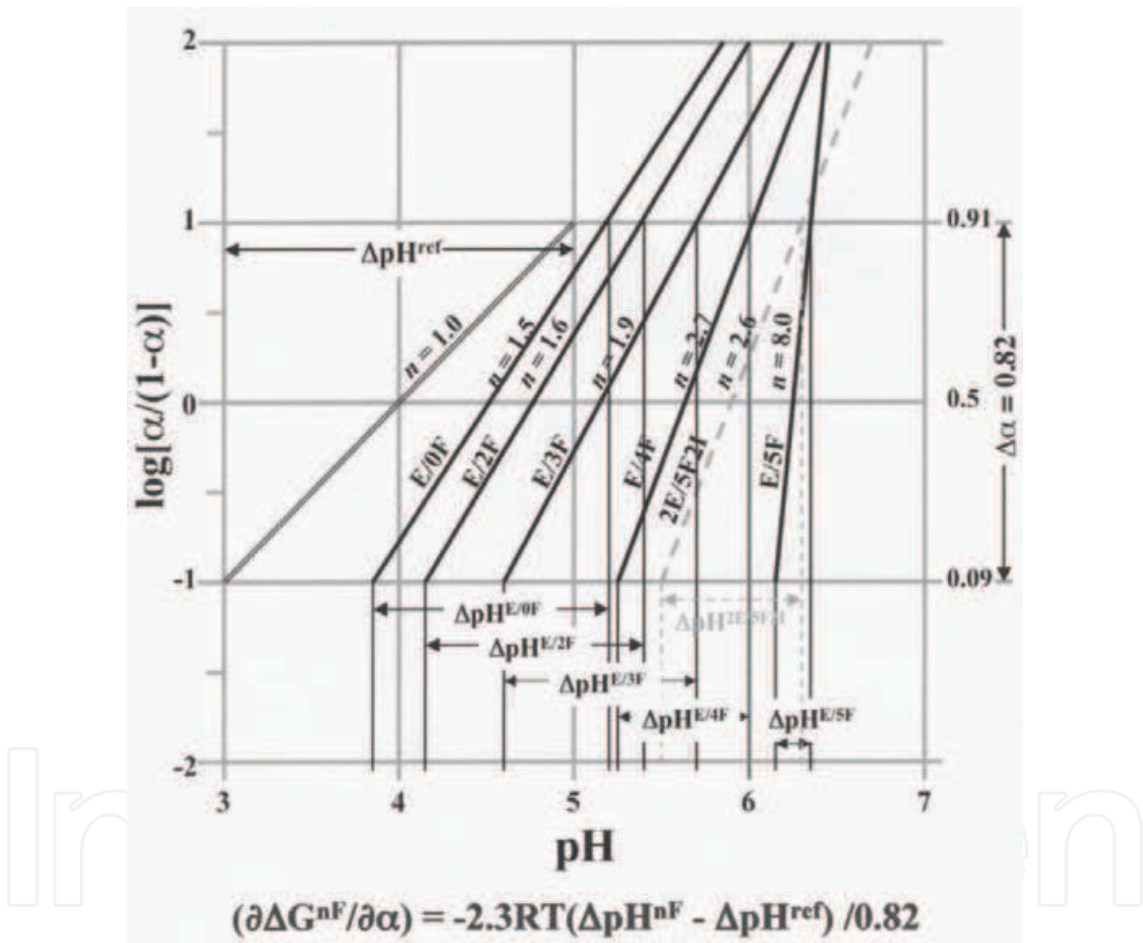
Fig. 15. Hill plots of the acid/base titration data Fig. 14B has been analyzed using Eqn. (18) to calculate cooperativity values as the stand alone term $(\partial\Delta G/\partial\alpha)_T/2.3RT$ to replace the factor, $1/n$, of the Hill coefficient, n. The thermodynamic expression, $(\partial\Delta G/\partial\alpha)_T$ is equivalent to ΔG_{ap}. It is calculated by the expression, $(\partial\Delta G^{nF}/\partial\alpha)_T = 2.3RT(\Delta pH^{ref} - \Delta pH^{nF})/0.82$, where the values of ΔpH^{ref} and ΔpH^{nF} are shown in the figure. $(\partial\Delta G^{nF}/\partial\alpha)$ is positive, i.e., repulsive, for positive cooperativity and negative for negative cooperativity. For the negative cooperativity of charge-charge repulsion the acid/base titration curve is broader than and the positive cooperativity curves due to apolar-polar repulsion are steeper than given by the Henderson-Hasselbalch Eqn., $pH = pK + \log[\alpha/(1-\alpha)]$. From (Urry et al., 2010).
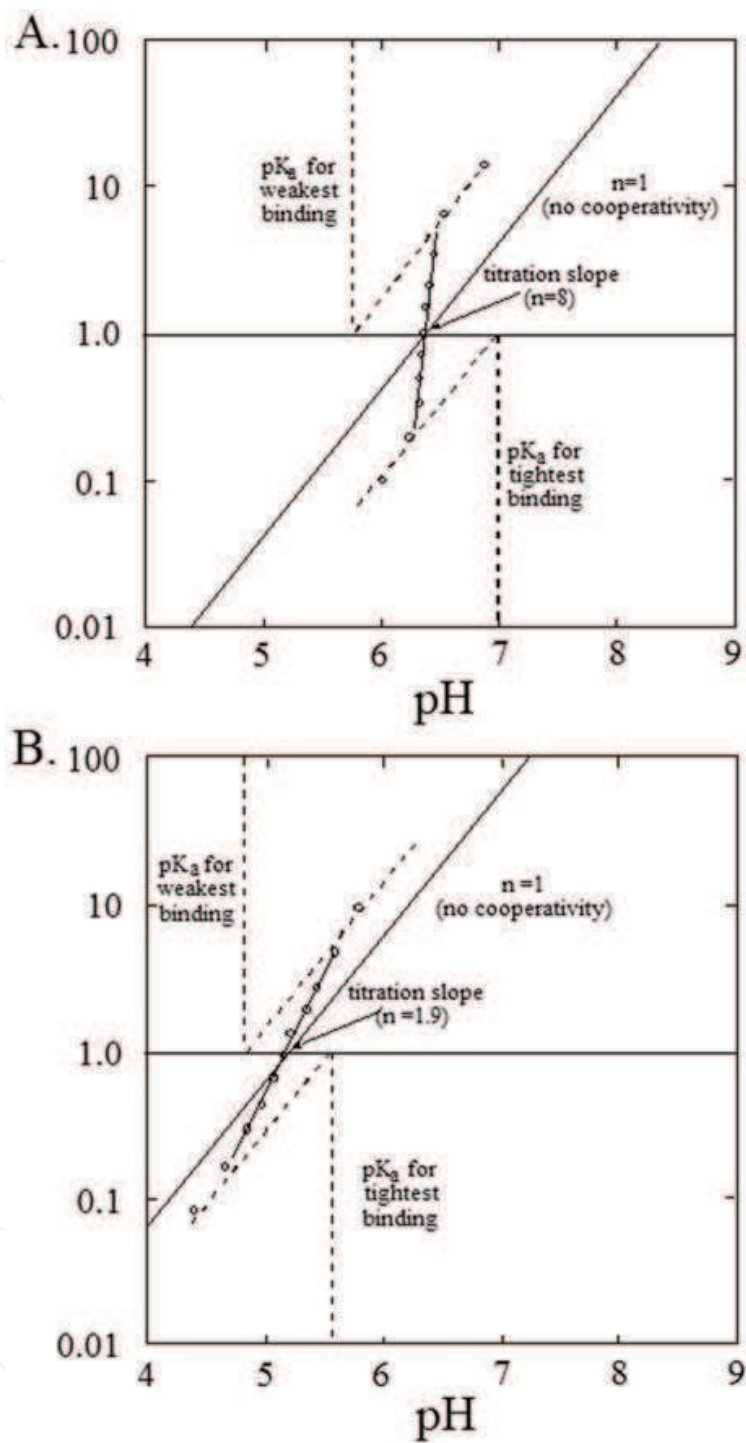
Fig. 16. Hill plots of the acid/base titration data of Fig. 14B used to estimate pK of the first and the last carboxyl to ionize, which demonstrate a residual pK shift for the last carboxyl to ionize. See text for discussion. Figure 5.31 of (Urry, 2006a).

$$pH = pK_o + \Delta pK_{cc} + \Delta pK_{ap} + \log[\alpha/(1-\alpha)] + \{[(\partial \Delta G/\partial \alpha)_T]_{cc} + [(\partial \Delta G/\partial \alpha)_T]_{ap}\}/2.3RT. \quad (17)$$

For **Model proteins i** through **v**, where the ionizable functions are separated by 90 backbone bonds plus 6 side chain bonds, charge-charge repulsion is negligible and the data for **Model proteins i** through **v** in Fig. 14B may be analyzed using the following expression,

$$pH = pK_o + \Delta pK_{ap} + \log[\alpha/(1-\alpha)] + \{[(\partial \Delta G/\partial \alpha)_T]_{ap}\}/2.3RT, \qquad (18)$$

where pK_o for the unperturbed glutamic acid is taken as 4.0.

For the Hill plot, pH is plotted on the x-axis and $\log[\alpha/(1-\alpha)]$ is plotted on the y-axis as seen for Fig. 15. The $\log[\alpha/(1-\alpha)] = 0$ intercept gives pK_{exptl} and $\Delta pK = pK_{exptl} - pK_o$. The last term, $\{[(\partial \Delta G/\partial \alpha)_T]_{ap}\}/2.3RT$, measures the variation of the slope, *n*, from 1, which is the diagonal as plotted in Fig. 15. If *n* < 1, the slope is less steep than for *n* = 1 as occurs for negative cooperativity. If *n* > 1, the slope is steeper than for *n* = 1 as occurs for positive cooperativity.

The means, whereby $[(\partial \Delta G/\partial \alpha)_T]$ is calculated from the data as plotted in Fig. 15, is described in the footnote to **Table 3**. The results for the glutamic acid data in Fig. 14B, as calculated using Fig. 15, are given in the second and third columns of **Table 3**.

A qualitative comparison of the pK and positive cooperativity data suggest equivalent supra-linearity of hydrophobic-induced responses when plotted against linear replacement of V by F. The quantitative results of columns 2 and 3 of **Table 3** strongly suggest that the same physical process is responsible for both hydrophobic-induced pK and positive cooperativity shifts. In our view the physical process in common is the apolar-polar repulsive free energy of hydration, ΔG_{ap}. Positive cooperativity as carboxyls ionize, where ionization of subsequent carboxyls is greatly facilitated by the earlier ionizations, becomes possible due to competition for hydration between hydrophobic groups and carboxylates. The first ionization is delayed because the first carboxylate does not obtain sufficient hydration. As seen with another feature of a Hill plot, For E/5F in Fig. 16A the first carboxylate forms with of pK 7, and the last carboxylate of the titration forms with a pK of 5.7.

Accordingly, the last carboxylate of the titration of E/5F forms with a pK of 5.7 and indicates an ongoing apolar-polar repulsion, $\Delta G_{ap} = 2.3RT\Delta pK = 2.3RT(5.7 - 4.0) = 2.3$ kcal/mol-E, calculated for 298K. Even the last carboxylate of E/3F with a pK of 4.8, seen in Fig. 16B, retains a substantial apolar-polar repulsion, i.e., $\Delta G_{ap} = 2.3RT\Delta pK = 2.3RT(4.8 - 4.0) = 1.1$ kcal/mol-E. These residual apolar-polar repulsion terms reflect an extent of elastic deformation of the elastic-contractile model protein from the more nearly random chain distribution relevant to $(GVGVP)_n$ below T_t. The residual pK (and positive cooperativity) shifts warrant further discussion not possible with the present time and space limitations, but they reflect the richness of the data available from designed ECMP.

Before going on to the equation for redox titrations of designed ECMP, it may be noted that the data for **Model protein I** in Fig. 15, with both relevant charge-charge and apolar-polar repulsion terms, can be analyzed using the complete Eqn. (17). The close sequence proximity of the two E-residues in **Model protein I**, as seen in the 2E/5F/2I composition of Fig. 14A, ensures a charge-charge repulsion term that can be seen in Fig. 15. In particular, the curve for 2E/5F/2I exhibits a greater pK shift and yet a smaller slope than that of E/4F.

The first of two pieces of information that enable the resolution of all the terms is that ΔpK_{cc} and ΔpK_{cc} are of the same sign, whereas $[(\partial \Delta G/\partial \alpha)_T]_{ap}$ and $[(\partial \Delta G/\partial \alpha)_T]_{cc}$ are of opposite signs. This is apparent by comparison of the curves for E/4F and 2E/5F/2I. The second piece of information comes from the demonstration that $\Delta G_{ap} = 2.3RT\Delta pK$ equals $[(\partial \Delta G/\partial \alpha)_T]_{ap}$, as seen in **Table 3**, and the expectation that $\Delta G_{cc} = 2.3RT\Delta pK$ equals $[(\partial \Delta G/\partial \alpha)_T]_{cc}$. With this perspective, all of the terms in Eqn. (17) can be determined, i.e., $\Delta G_{ap}(2E/5F/2I) = [(\partial \Delta G/\partial \alpha)_T]_{ap}(2E/5F/2I) = 2.32$ kcal/mol-E and $\Delta G_{cc}(2E/5F/2I) = [(\partial \Delta G/\partial \alpha)_T]_{cc}(2E/5F/2I) = 0.23$ kcal/mol-E (See Urry et al., 2009; 2010). This demonstrates for the ECMP-in-water system how much more significant apolar-polar repulsion is than charge-charge repulsion, as previously shown for f_X versus pK plots for

poly[f_V(IPGVG),f_E(IPGEG)] (Urry et al., 1993) and for poly[f_V(IPGVG),f_K(IPGKG)] (Urry et al., 1994). Again, while warranted, present time and space limitations do not permit further discussion here, but Figure 5.30 and associated text in (Urry, 2006a) provide further analyses.

Model protein i : [GVGVP GVGVP GΦGVP GVGVP GVGVP GVGVP]$_n$(GVGVP);　　Φ/0F

Model protein ii : [GVGVP GVGFP GΦGFP GVGVP GVGVP GVGVP]$_n$(GVGVP);　　Φ/2F

Model protein iii: [GVGVP GVGVP GΦGVP GVGVP GVGFP GFGFP]$_n$(GVGVP);　　Φ/3F

Model protein iv: [GVGVP GVGFP GΦGFP GVGVP GVGFP GVGFP]$_n$(GVGVP);　　Φ/4F

Model protein v: [GVGVP GVGFP GΦGFP GVGVP GVGFP GFGFP]$_n$(GVGVP);　　Φ/5F

Φ(function)	E(glutamic acid, -COOH)		K(lysine amino, -NH$_2$)		K{NMeN}-(redox)	
Energy term kcal/mol	ΔG_{ap} [§] (pKa shift)	$(\partial\Delta G/\partial\alpha)$ slope; (n)	ΔG_{ap} (pKa shift)	$(\partial\Delta G/\partial\alpha)$ slope; (n)[†]	$z\mathscr{F}\Delta E$ redox shift	$(\partial\Delta G/\partial\alpha')$ slope; (n)[*]
Φ/0F	0.7	1.1 (1.5)	0	0 (0.9)	0	0 (1.0)
Φ/2F	1.0	1.3 (1.6)	0.3	0.3 (1.1)	0.8	0.5 (1.2)
Φ/3F	1.6	1.7 (1.9)	0.6	0.7 (1.2)	1.7	1.1 (1.5)
Φ/4F	2.2	2.2 (2.7)	1.4	1.2 (2.1)	2.5	2.7 (4.8)
Φ/5F	3.1	3.0 (8.0)	2.0	2.1 (2.7)	-----	-----

The numbers in parentheses in the table are the Hill coefficients, n, and Hill plots of $\log[\alpha/(1-\alpha)]$ versus pH for acid base titrations and $\log[\alpha'/(1-\alpha')]$ versus ΔE for the redox titrations are used, respectively, to calculate $(\partial\Delta G/\partial\alpha)$ and $(\partial\Delta G/\partial\alpha')$. $\partial\alpha$ and $\partial\alpha'$ are determined by graphical means using the y-axis intercept values of $\log[\alpha/(1-\alpha)] = 1$ (α=0.91) and -1(α=0.9), giving the graphically derived values of the divisors of 0.82 (= 0.91 – 0.09) for both $\Delta\alpha$ and $\Delta\alpha'$. The corresponding x-axis reference values are a ΔpH of 2 with $\Delta G = -2.3RT\Delta pH$ for the acid-base titrations and a ΔE of 59 mV with $\Delta G = -z\mathscr{F}\Delta E$ for the redox titrations. The expressions for acid base titrations become $(\partial\Delta G/\partial\alpha) = -2.3RT(\Delta pH^{exptl} - \Delta pH^{ref})/0.82$ with $\Delta pH^{ref} = 2$ and ΔpH^{exptl} being the run corresponding to the $\Delta\alpha = 0.82$ rise for a readily defined interval of the Hill plot (See section **4.4.5**). Analogously for redox titrations, $(\partial\Delta G/\partial\alpha') = -z\mathscr{F}(\Delta E^{exptl} - \Delta E^{ref})/0.82$ with $\Delta E^{ref} = 59$ mV and ΔE^{exptl} being the run corresponding to the rise of $\Delta\alpha' = 0.82$ for the specified interval. As ΔpH^{exptl} approaches 2 and as ΔE^{exptl} approaches 59, the slope approaches one and the terms $(\partial\Delta G/\partial\alpha)$ and $(\partial\Delta G/\partial\alpha')$ approach zero, which is $n = 1$. The sign on the free energies is written as the repulsive free energy, ΔG_{ap}, in which an increase in hydrophobicity increases the free energy on going from the less polar to the more polar state, i.e., to the charged or the oxidized state. This results from an increase in ΔG due to the increase in apolar-polar repulsion.
[§] The pKa for the unperturbed glutamic acid is taken as 4.0.
[†] The Hill coefficient, n, for K/0F was experimentally found to be 0.9, possibly due to the effect of Cl$^-$-NH$_3^+$ ion pair formation during the titration. Since the interest is the change due to addition of more hydrophobic Phe (F) residues, K/0F is taken as the reference state (Woods, TC.; Hayes, L.; Xu, J.; McPherson, DT. & Urry DW., in preparation.).
[*] The Hill coefficient, n, for the reference state composition, K{NMeN}/0F, i.e., N-methyl nicotinamide (NMeN) attached by amide linkage to lysine (K) of **Model protein i**, is taken as 1.0 after including the term, 1/z of $2.3RT/z\mathscr{F}$, for the number of electrons (2) transferred in the overall reaction (See Eqn. 19). (Hayes, LC.; Woods, TC.; Xu, J.; Gowda, DC.; McPherson, DT. & Urry, DW. In preparation.) Adapted from (Urry & Luan, 2009).

Table 3. Comparison of increases in Hydrophobicity on pK and Reduction Potential Shifts and on Positive Cooperativity for different Functional Groups in the Basis Set.

6.2.9 Generalized redox titration equation that includes apolar-polar, ap, repulsion terms

For redox titrations, the equivalent expression to the familiar Henderson/Hasselbalch equation for acid/base titrations, is the Nernst equation, $E = E_0 + (2.3RT/z\mathscr{F})\log[\alpha'/(1-\alpha')]$, where E is the electrical potential in volts for dilute solutions of small non-interacting redox functions, E_0 is the electrical potential of the reference state (the unperturbed redox function), z is the number of electrons transferred during the redox reaction, $\mathscr{F}$ is the Faraday constant of 23,060 cal/volt, and α' represents the mole fraction of the redox species being formed during the titration.

In analogy to acid/base titrations, cooperativity effects can be introduced with the Hill coefficient to give $E = E_0 + \Delta E_{ap} + (1/n)(2.3RT/z\mathscr{F})\log[\alpha'/(1-\alpha')]$ for redox titrations of designed ECMP. Your author is unaware of hydrophobic-induced shifts in reduction potentials and cooperativity effects being treated in analysis of redox titrations. **Table 3**, however, clearly shows hydrophobic-induced reduction potential and positive cooperativity effects to be larger for designed ECMP with the NMeN redox function than with the E functionality. For example, compare data for E/4F (columns 2 and 3) with those of NMeN/4F (columns 6 and 7).

Accordingly, for our purposes Eqn. (19) will be stated using equivalent terms to those of Eqn. (18), as follows,

$$E = E_0 + \Delta E_{ap} + (2.3RT/z\mathscr{F})\log[\alpha'/(1-\alpha')] + (1/z\mathscr{F})[(\partial\Delta G/\partial\alpha')_T]_{ap}, \qquad (19)$$

Equation (19) neglects charge-charge interactions between redox functions, because the approximately 100 bonds between functional groups would argue charge-charge interactions to be negligible for this designed ECMP.

The values in columns 6 and 7 of **Table 3** were calculated using the titration data for the oxidation of NMeNH to NMeN$^+$ (Hayes, LC.; Woods, TC.; Xu, J.; Gowda, DC. McPherson, DT. & Urry, DW. Effect of the hydrophobicity of elastic-contractile model proteins on redox potential. In preparation.) and are plotted in analogy to the plots for titration of E/nF in Fig. 15, that is, E is plotted versus $\log[\alpha'/(1-\alpha')]$. As representative calculations, $[(\partial\Delta G^{NMeN/4F}/\partial\alpha')_T]_{ap} = (\Delta E^{ref} - \Delta E^{4F})_{ap}$ and $\Delta G_{ap}(NMeN/4F) = z\mathscr{F}\Delta E_{ap}(NMeN/4F)$. For the $\Phi/4F$ compositions of **Table 3**, $z\mathscr{F}\Delta E_{ap}(NMeN/4F) \approx [(\partial\Delta G^{NMeN/4F}/\partial\alpha')_T]_{ap} \approx 2.5$ kcal/mol-NMeN; $\Delta G_{ap}(E/4F) \approx 2.3RT\Delta pK \approx [(\partial\Delta G^{E/4F}/\partial\alpha)_T]_{ap} \approx 2.2$ kcal/mol-E, and $\Delta G_{ap}(K/4F) \approx 2.3RT\Delta pK(K/4F) \approx [(\partial\Delta G^{K/4F}/\partial\alpha)_T]_{ap} \approx 1.4$ kcal/mol-K (Woods, TC.; Hayes, LC.; Xu, J.; McPherson, DT. & Urry. DW. Lys-containing elastic-contractile model proteins: Biosynthesis and supra-linear increases in ΔpKa and in positive cooperativity with linear increases in hydrophobicity. In preparation).

Not only is the apolar-polar repulsive Gibbs free energy of hydration apparent for the N-methyl nicotinamide function in the ECMP composition, NMeN/4F, but it is 14% larger than for the glutamate function in the ECMP composition, E/4F, and 80% larger than the lysine function in the ECMP composition, K/4F. This might have been expected due to the large increase in hydrophobicity on reduction, i.e., $\Delta G°_{HA}(NMeN^+ \rightarrow$ dihydro NMeN$) = 9.5$ kcal/mol-NMeN in **Table 2**.

It seems quite apparent why biology so routinely utilizes redox functions in its energy conversion processes. In particular, the nicotinamide adenine dinucleotide (NAD), nicotinamide adenine mononucleotide (NMN) and flavin adenine dinucleotide (FAD) redox functions become reduced in the process of oxidation of foods, and especially NADH and FADH$_2$ enter into the electron transport

chain and reduce ubiquinol. Ubiquinol then becomes cyclically oxidized and reduced in the process of pumping protons across the inner mitochondrial membrane to the inner membrane space. These protons then flow back across the inner mitochondrial membrane through ATP synthase to produce 32 of the 36 ATPs formed on the oxidation of glucose, for example.

Section **7.1** below, presents the means whereby Complex III of the inner mitochondrial membrane utilizes cyclic reduction and oxidation of its protein-bound redox functions – heme b_H, heme b_L and an FeS center - in combination with the protein mechanisms discussed here - **ΔG_{HA}**, ΔG_{ap}, and single-chain elastic extension and contraction - to pump protons across the inner mitochondrial membrane. And section **7.2** below presents means whereby the F_1-motor of ATP synthase utilizes ΔG_{ap} to produce ATP from ADP and Pi(inorganic phosphate).

6.2.10 Elastic deformation on the hydrophobic association (extension) and on ΔG_{ap} (repulsion)

The elasticity of $(GVGVP)_n$ has been characterized by many physical methods with the necessity of delineating it from the random chain network theory of elasticity. The nature of ECMP elasticity is most conclusively demonstrated by means of single-chain force-extension experiments, see Fig. 6E, using the methodology of atomic force microscopy (Hugel, 2003; Urry et al, 2002). Instead of rastering in the x-y plane of the substrate surface, a single chain suspended between the substrate plane and the cantilever tip is pulled in the z-direction to demonstrate an overlay of the extension and relaxation curves. Thus, within the sensitivity of the force measurement, $(GVGVP)_n$ exhibits ideal elastic behavior. Because of a common observation of some very minor deviations of the relaxation curve from the extension curve, and because ideality is a goal approached but never quite obtained, we choose to refer to the "near ideal" elasticity of a single chain of $(GVGVP)_n$. Obviously, the random chain network theory of elasticity is not applicable to the single-chain force-extension results of Fig. 6E on $(GVGVP)_n$.

The polymer construct is central to a robust elasticity. The first mathematical expression for the propagation of a polymer (Eyring, 1932), depicted in Fig. 6A, demonstrates the two key features, the torsional, or dihedral, angle, ϕ, that provides the entropic component of elastic force, f_S, and the backbone angle, θ, and to a lesser extent the bond length, ℓ, that provide the internal energy component of elastic force, f_E.

The molecular mechanics ECEPP program due to Scheraga and coworkers (Momany et al., 1975) and molecular dynamics CHARMM program of Karplus and coworkers (Brooks, et al., 1983) both give the same value of five EU/pentamer-(GVGVP), (Urry, et al., 1982d; Urry & Venkatachalam, 1983; Chang & Urry, 1989), which satisfactorily calculate the magnitude of the entropic component of elastic force, f_S (Urry, 2006b). And the values, so obtained, for $(GVGVP)_n$ have been instructive in estimating the elastic force on extension of single protein chains on going from one functional state to another in the crystal structures of protein motors (Urry, 2006b; Urry et al, 2010). Here, the values from molecular dynamics calculations are listed in **Table 4** for the damping of torsional oscillations that occur on 130% extension of a single chain of β-spiral as described in the relaxed state in Fig. 5 and in relaxed and extended states in Figs. 6D1 and D2.

As seen in **Table 4**, the torsion angles for the suspended segment - ψ_{4i}, ϕ_{5i}, ψ_{5i}, and $\phi_{1(i+1)}$ -, indicated by rotational arrows in Fig. 6B, are the angles that exhibit large torsional oscillations in the relaxed state that become dramatically damped on extension. Fig. 6C

	Angle	Relaxed	Extended	Angle	Relaxed	Extended	Angle	Relaxed	Extended
β-turns	ψ_{16}	10.87	14.17	ψ_{26}	27.33	07.64	ψ_{36}	20.19	14.84
	ϕ_{17}	09.86	15.18	ϕ_{27}	11.71	08.33	ϕ_{37}	08.99	10.47
	ψ_{17}	47.59	46.68	ψ_{27}	11.70	13.51	ψ_{37}	21.53	32.96
	ϕ_{18}	61.70	47.41	ϕ_{28}	08.61	10.36	ϕ_{38}	11.15	10.66
	ψ_{18}	09.37	16.05	ψ_{28}	09.33	08.16	ψ_{38}	11.09	27.29
	ϕ_{19}	14.25	08.67	ϕ_{29}	09.70	07.31	ϕ_{39}	12.70	10.24
Suspended	ψ_{19}	44.09	10.99	ψ_{29}	47.32	10.48	ψ_{39}	52.00	12.50
	ϕ_{20}	41.94	09.29	ϕ_{30}	48.57	11.39	ϕ_{40}	55.88	08.37
Segments	ψ_{20}	14.50	11.15	ψ_{30}	42.56	10.62	ψ_{40}	40.67	11.08
	ϕ_{21}	27.13	24.17	ϕ_{31}	11.43	11.38	ϕ_{41}	36.44	19.06
β-turns	ψ_{21}	09.39	22.73	ψ_{31}	12.17	09.21	ψ_{41}	12.97	14.80
	ϕ_{22}	09.94	08.00	ϕ_{32}	09.90	08.93	ϕ_{42}	11.59	07.33
	ψ_{22}	11.58	16.13	ψ_{32}	15.30	10.80	ψ_{42}	11.34	13.17
	ϕ_{23}	16.37	09.33	ϕ_{33}	09.60	07.62	ϕ_{43}	09.23	09.76
	ψ_{23}	14.33	14.25	ψ_{33}	09.88	09.43	ψ_{43}	10.60	12.53
	ϕ_{24}	11.39	29.20	ϕ_{34}	11.86	09.71	ϕ_{44}	11.06	12.82
Suspended	ψ_{24}	19.53	37.87	ψ_{34}	63.80	08.36	ψ_{44}	41.89	35.22
	ϕ_{25}	25.02	23.06	ϕ_{35}	91.70	10.20	ϕ_{45}	48.98	31.31
Segments	ψ_{25}	49.32	32.10	ψ_{35}	15.03	11.51	ψ_{45}	42.05	56.89
	ϕ_{26}	31.43	27.24	ϕ_{36}	21.49	18.66	ϕ_{46}	21.55	30.33

Data from Chang & Urry, 1989, and tabulation from Urry & Parker, 2002.

Table 4. Comparison of the root mean square (RMS) fluctuations of torsion angles (ϕ and ψ) of VP(GVGVP)$_{10}$GVG for the non-extended and 130% extended states. Large decreases on extension in the amplitude of the ϕ and ψ torsional oscillations of the suspended segments are readily apparent, particularly when compared to the ϕ and ψ of the β-turns.

schematically demonstrates with the product of three torsion angle oscillations - $\Delta\phi_i$ x $\Delta\psi_I$ x$\Delta\phi_{i+1}$ – the large decrease of volume in configuration space that can occur on damping of the amplitude of three torsional oscillations. This decrease in volume represents a decrease in entropy, but instead of just three angles the computation will utilize the 31 internal torsion angles listed in **Table 4**. The equation, as written for extended, **e**, and relaxed, **r**, states, $\Delta S = R \ln[\Pi_i\Delta\phi_i^e \Delta\psi_i^e / \Pi_i\Delta\phi_i^r \Delta\psi_i^r]$, calculates the decrease in entropy due to a 130% extension to be -1.1 cal/mol-deg-residue. From looking at the decreases in amplitudes of the angles in **Table 4**, the suspended segments overwhelmingly give rise to the decrease in entropy. Using the relationship, $f_S = -T(\partial S/\partial L)_{VT}$, at 10 K for an extension, ΔL, of 3.5 to 8.0 nm per pentamer gives an f_S of 24 pN (Urry et al., 2002; Urry, 2006b). Very similar ΔS values were obtained for ΔS(GVGVP) in water (Wasserman & Salemme, 1990) using yet a third computational approach, the Kollman molecular dynamics program, for such calculations. Single-chain extension for elastomeric force development has been implicated in the function of several proteins - the Rieske Iron Protein component of Complex III of the electron transport chain discussed in section **7.2** below, e.g., the myosin II motor of muscle contraction (Urry, 2006a, 2006b), and the kinesin bipedal motor (Urry, 2005).

7. ECMP-derived thermodynamics of protein hydration and of elasticity describe function of biology's protein-based machines!

The above described thermodynamics of protein hydration ($\Delta\mathbf{G_{HA}}$ and ΔG_{ap}) and of elasticity (f_E and f_S), which with displacement give ΔG(elastic deformation), provide insight into key details of the function of biology's protein-based machines. Considered in this section are: Complex III (cytochrome bc$_1$/Rieske Iron Protein) of the inner mitochondrial membrane, the

F_1-motor of ATP synthase also of the inner mitochondrial membrane, and the full-length KcsA potassium ion channel of *Streptomyces lividans*. Function in each protein-based machine involves trans-membrane structures of decreasing complexity. At this stage, the thermodynamic quantities describe individual events at each site of action, but integration of events into a complete image of trans-membrane transport is in the future. Example of how this may be achieved occurs in section **8. Eyring's Absolute Rate Theory applied to biological trans-membrane transport**, whereby a single image, the free energy profile for ion passage through the monovalent cation selective Gramicidin A channel, contains all of the information required to calculate current for a chosen ion activity and trans-membrane potential.

7.1 Complex III of the electron transport chain of the inner mitochondrial membrane

There are five complexes within the inner mitochondrial membrane that achieve oxidative phosphorylation. Four complexes couple electron flow to proton translocation from the matrix side of the membrane to the inter-membrane space, i.e., cytosolic side. The fifth complex, ATP synthase, utilizes the proton concentration developed in the inner-membrane space by the first four complexes to synthesize ATP from ADP and Pi as the protons re-cross the inner membrane to the matrix side. Treated below are Complex III, of the four complexes, and the fifth complex, ATP synthase, emphasizing its F_1-motor.

7.1.1 Complex III (cytochrome bc_1/Rieske Iron Protein) of the inner mitochondrial membrane

Also referred to as the cytochrome **bc_1** complex, Complex III of yeast is a homodimeric integral membrane protein comprised of 22 subunits. The structure of Fig. 17A contains the 22 protein subunits plus a single molecule of cytochrome **c**, where it is positioned to be reduced before diffusing to the fourth complex, cytochrome **c** oxidase, to release its electron, which passes through copper ions to the two hemes, **a** and **a_3**.

A stereo view of the redox functions are given in Fig. 17B, positioned exactly as in the complete complex in part A. There are two reaction sites to note, the Q_o site and the Q_i site. At the Q_o site on the cytosolic side of the membrane, ubiquinol meets and transfers one electron to the FeS center and a second electron to heme **b_L**; this leaves the ubiquinol with two positive charges which it releases to the cytosolic side of the membrane as protons to become ubiquinone and the FeS center returns to the heme **c_1**. The ubiquinone leaves and a second ubiqiunol enters to repeat the process. The net result at the Q_o site is a tightly coupled receipt of four electrons and the release of four protons to the cytosolic space, by means of the three thermodynamic processes presented in section **6** and as depicted in Fig. 17C.

At the Q_i site on the matrix side of the membrane, heme **b_H**, having received an electron from heme **b_L**, passes it on to ubiquinone. This step occurs twice to give a double negative charge to ubiquinone, and to a second ubiquinone, which pick up four protons from the matrix side of the membrane to become become two ubiquinols that can each diffuse through the lipid bilayer to enter the Q_o site.

7.1.2 The cyclic domain movement of the Rieske Iron Protein FeS center between cytochrome b and c_1

Using each of the three thermodynamic processes developed in section **6**, represented as **ΔG_{HA}**, ΔG_{ap}, and single chain stretching/contracting, the tightly coupled cyclic reaction at the Q_o site is depicted in three steps in Fig. 17C.
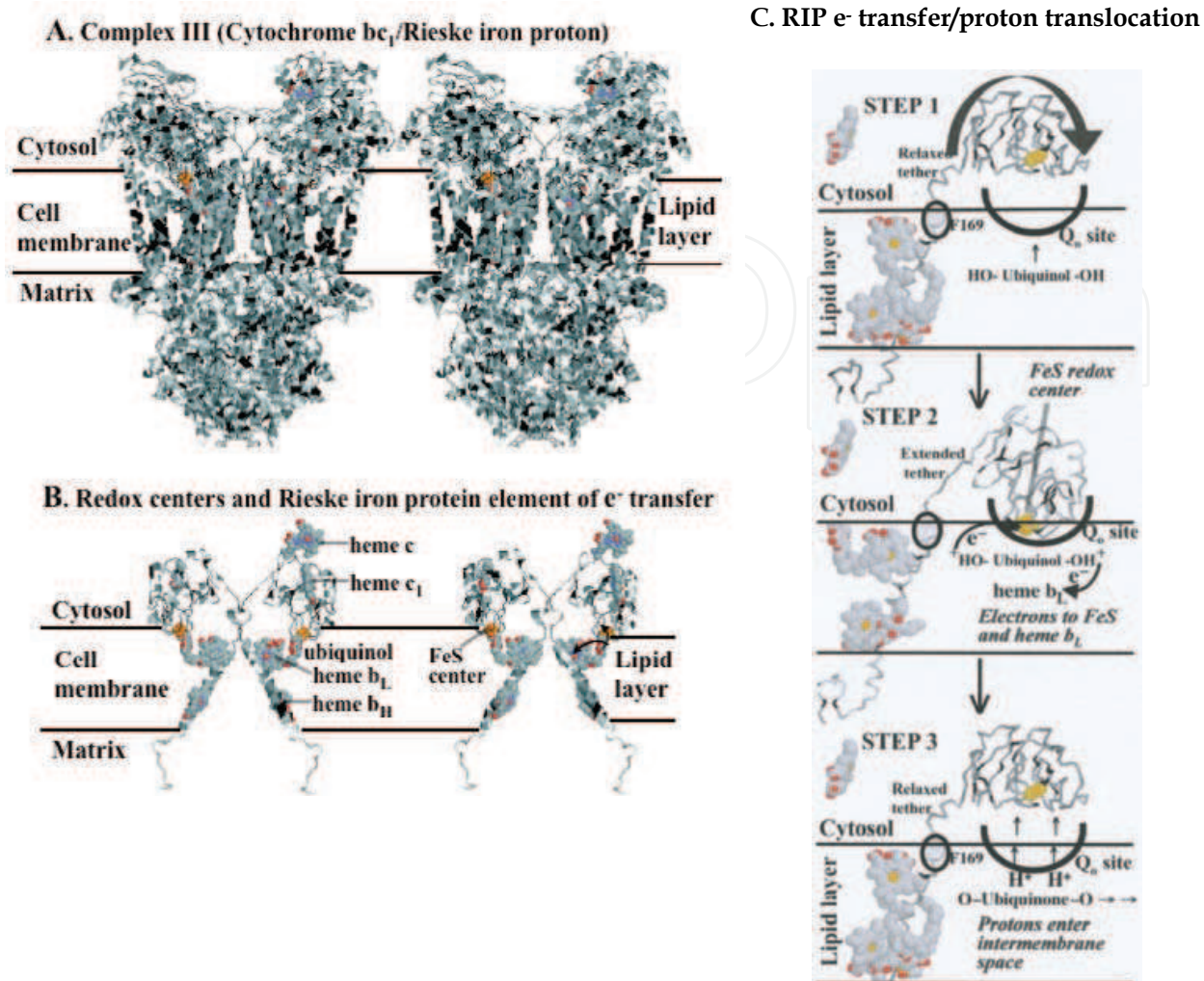
Fig. 17. **A**. Stereo pair of complete homo-dimeric structure of Complex III from yeast, plus one molecule of its substrate, cytochrome c (at front upper right). Given in ribbon representation with gray code for residues - charged white, neutral light gray, aliphatic hydrophobics gray, and aromatics black. The location of cell membrane and its lipid bilayer are indicated as well as the cytosolic (inner membrane space) and matrix sides of the membrane. Complex III functions by translocating protons from the matrix side to the cytosolic side of the membrane, as it oxidizes ubiquinol of the lipid layer at the Q_o site on the cytosolic side of the membrane and reduces ubiquinone at the Q_i site on the matrix side.
B. Stereo pair of homodimeric Rieske Iron Protein (**RIP**) with labeled redox components of Complex III (positioned exactly as in part **A**) and electron transfers at right. Note: While the globular component of RIP and its FeS center are in one monomer, its anchor in the membrane occurs with the transmembrane helices of the other monomer. **A** and **B** (Urry et al., 2010) utilize the crystal structure data of Lange & Hunte (2002). PDB accession code, 1KYO.
C. Rieske Iron Protein (RIP) and redox components of the monomer of Complex III showing 3 Steps in the cycle of electron transfer/proton translocation achieved by domain movement into and out of the Q_o site with stretching of its anchored tether as the globular tip of RIP with its FeS redox center is drawn into the Q_o site by hydrophobic association. The three steps are discussed in detail in the text, utilizing the crystal structure data of Zhang et al., 1998. Protein Data Bank, accession code 1BCC & 3BBC. From Urry et al., 2010.

STEP 1: The hydrophobic ubiquinol enters the Q_o site and, on making the site more hydrophobic, induces the globular component of RIP with its hydrophobic side and tip to roll into the Q_o site increasing its hydrophobic association as it goes. *This lowers ΔG_{HA}, the the change in Gibbs free energy for hydrophobic association (the first thermodynamic process).*

STEP 2: In the thermodynamic process of lowering ΔG_{HA} as the RIP globular component rolls into the Q_o site, the relaxed single chain tether with its end segment anchored in the cell membrane becomes stretched, *thereby utilizing the second thermodynamic process of storing energy in the stretching of the single chain.* This positions the FeS center in the Q_o site to receive one electron from ubiquinol, which transfers a second electron to heme $\mathbf{b_L}$ and on to heme $\mathbf{b_H}$ at the Q_i site. The result is a ubiquinol with two positive charges.

STEP 3: The two positive charges of ubiquinol exert an apolar-polar repulsion, ΔG_{ap}, bringing *into play the third thermodynanamic process,* that weakens the hydrophobic association, allows the stretched tether to contract and lift the globular component with FeS center to heme $\mathbf{c_1}$ for transfer of its electron. This vacating of the Q_o site opens access for release of two protons to the inner-membrane space. The resulting ubiquinone diffuses into the lipid layer, and is replaced by another ubiquinol, which returns the Q_o-site to the state for STEP 1.

*Thus, the three thermodynamic processes developed in section **6** (ΔG_{HA}, ΔG_{ap}, and single chain stretching/contracting) are seen to be the basis for the tight coupling of electron transport to proton translocation performed by Complex III (cytochrome bc_1/Rieske Iron Protein) of the inner mitochondrial membrane in the essential function of energy conversion in the mitochondria, the essential energy factory of the cell.*

7.2 The F_1-motor of ATP synthase of the inner mitochondrial membrane
7.2.1 Partial structure of ATP synthase as obtained by electron diffraction
(Stock et al. 1999)

Fig. 18 gives a stereo view of the structure of ATP synthase of yeast mitochondria as determined by electron diffraction with residues represented as spheres. The spheres are gray-coded with charge residues white, neutral residues light gray, aliphatic hydrophobic residues gray and aromatic residues black. Missing, however, are the a-subunit, which is a partial sleeve on the F_0-rotor (the c_{10}-subunit) that completes the proton channel from cytosol to matrix, and the stator (b_2-subunit) that locks from the sleeve to the $(\alpha\beta)_3$-catalytic housing. This ensures that the F_0-rotor-couplings-$F_1(\gamma)$-rotor assembly may rotate without rotation of the $(\alpha\beta)_3$-catalytic housing.

At the top-side of Fig. 18 is the cytosolic side of the inner mitochondrial membrane, i.e., the inter-membrane space into which Complex III of Fig. 17 pumps protons. One such proton from the inter-membrane space then passes through a proton channel between the a-subunit sleeve and the 10-fold symmetric F_0-rotor to bind at the D61 carboxylate, e.g., the left most of the two white dots seen on the left-hand side of F_0-rotor just below the midline.

Drawing from the mechanism due to Fillingame and coworkers (Fillingame, 1999; Fillingame et. al., 2002), as a proton from the inner membrane space flows through the channel to bind at the dot on the left, an already protonated D61, e.g., the white dot at the right, releases a proton to the matrix side of the membrane, resulting in 36° clockwise rotation (as seen from the top) of the F_0-rotor. The translocation of 10 protons completes a 360° rotation of the F_0-rotor, which by the noted couplings of Fig. 18 drives a complete 360° rotation of the F_1-(γ)-rotor within the $(\alpha\beta)_3$-catalytic housing.

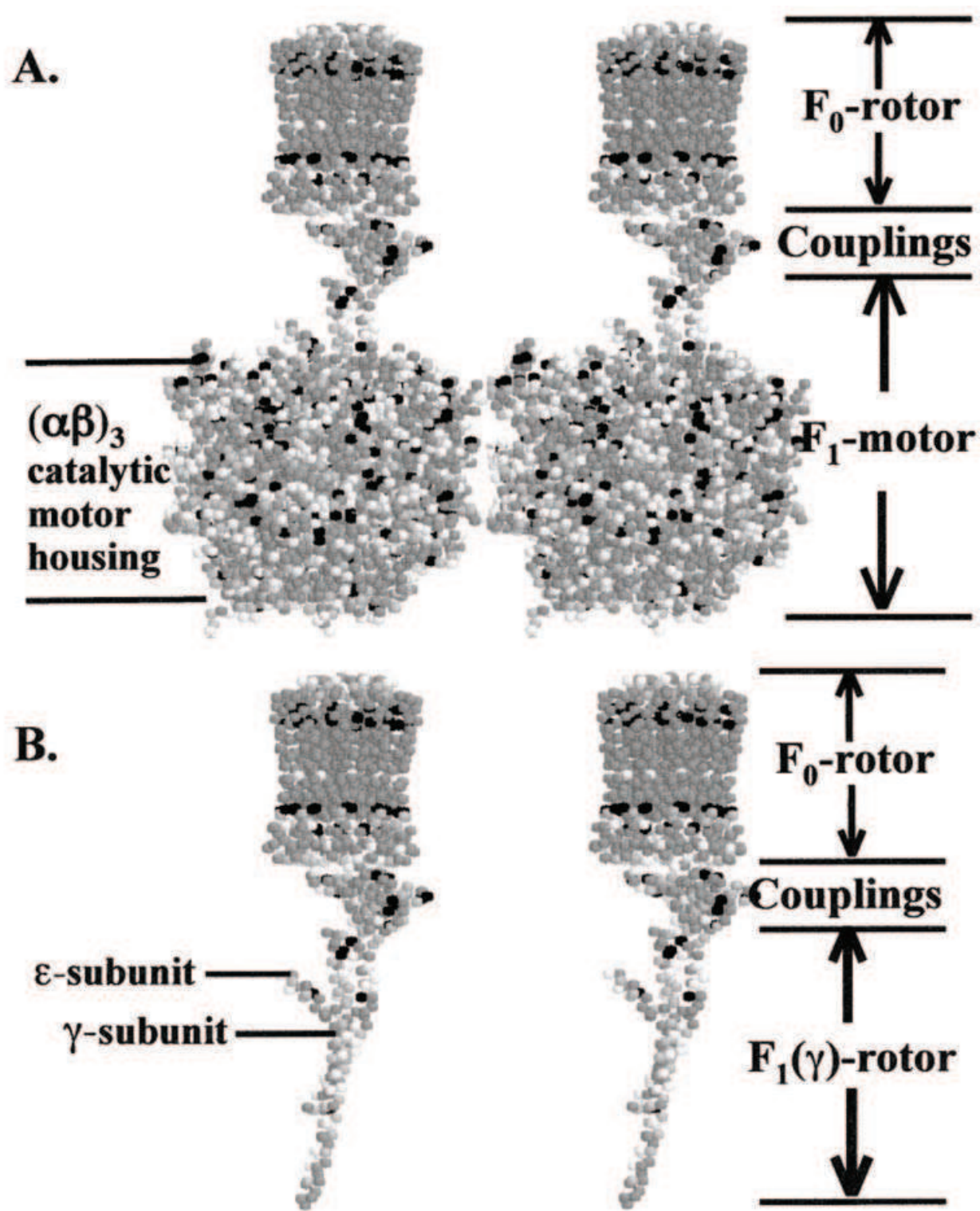Fig. 18. Partial structure of ATP synthase obtained by electron diffraction with residues given as spheres.
A. Missing are the a-subunit and the stator (b_2-subunit).
B. The complete F_0-rotor-couplings-$F_1(\gamma)$-rotor assembly.
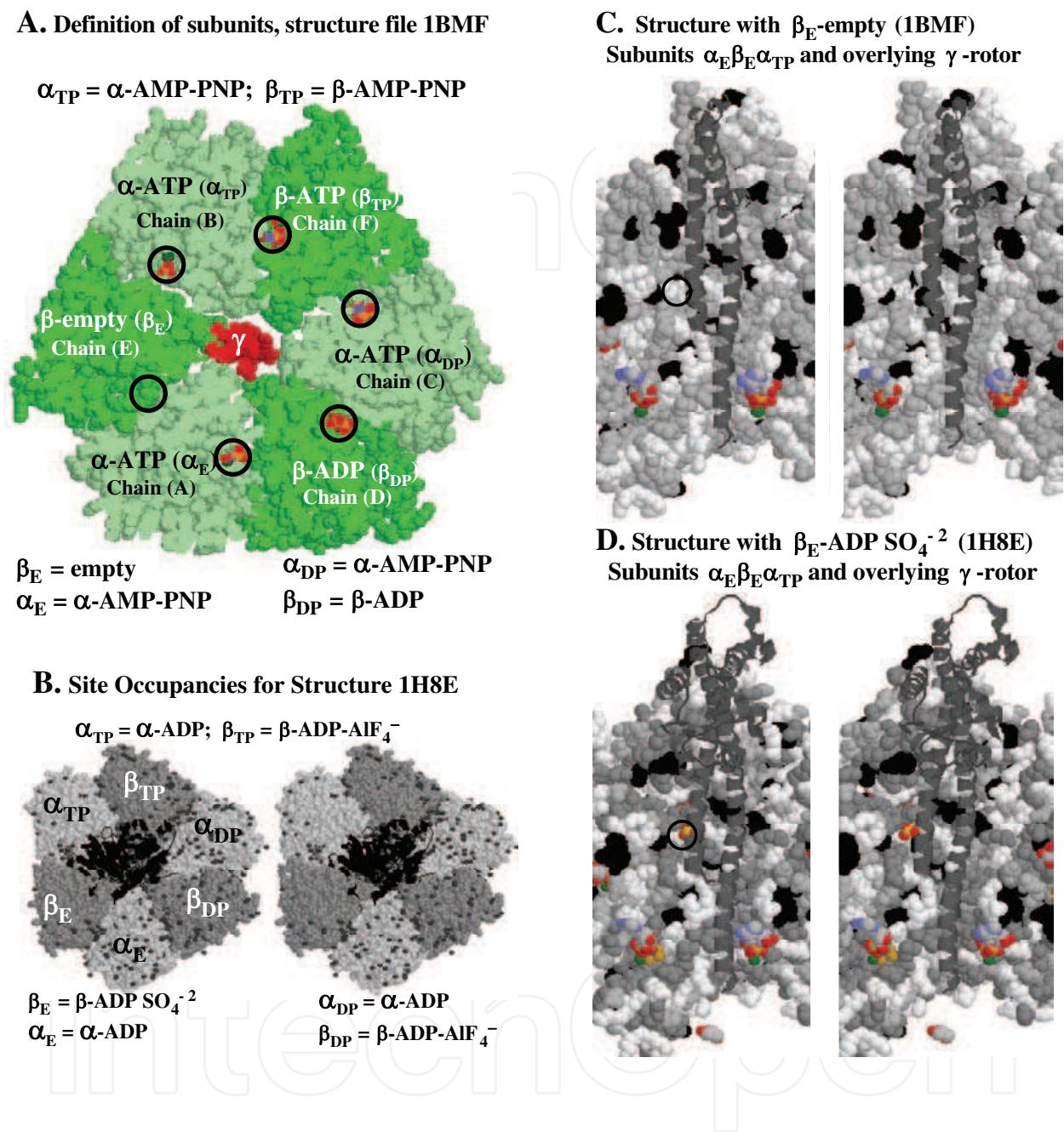Protein Data Bank, accession code 1QO1. Adapted from Figure 8.23 of Urry, 2006a.

A. Definition of subunits, structure file 1BMF

$\alpha_{TP} = \alpha\text{-AMP-PNP};\ \beta_{TP} = \beta\text{-AMP-PNP}$

α-ATP (α_{TP}) Chain (B)
β-ATP (β_{TP}) Chain (F)
β-empty (β_E) Chain (E)
γ
α-ATP (α_{DP}) Chain (C)
α-ATP (α_E) Chain (A)
β-ADP (β_{DP}) Chain (D)

$\beta_E = \text{empty}$ $\alpha_{DP} = \alpha\text{-AMP-PNP}$
$\alpha_E = \alpha\text{-AMP-PNP}$ $\beta_{DP} = \beta\text{-ADP}$

B. Site Occupancies for Structure 1H8E

$\alpha_{TP} = \alpha\text{-ADP};\ \beta_{TP} = \beta\text{-ADP-AlF}_4^-$

β_{TP}
α_{TP}
α_{DP}
β_E
β_{DP}
α_E

$\beta_E = \beta\text{-ADP SO}_4^{-2}$ $\alpha_{DP} = \alpha\text{-ADP}$
$\alpha_E = \alpha\text{-ADP}$ $\beta_{DP} = \beta\text{-ADP-AlF}_4^-$

C. Structure with β_E-empty (1BMF) Subunits $\alpha_E\beta_E\alpha_{TP}$ and overlying γ-rotor

D. Structure with β_E-ADP SO$_4^{-2}$ (1H8E) Subunits $\alpha_E\beta_E\alpha_{TP}$ and overlying γ-rotor

Fig. 19. **A** and **B**. Nomenclature for the α- and β-subunits of the (αβ)$_3$-catalytic housing of the F$_1$-motor of ATP synthase as defined from the crystal structures with Protein Data Bank accession codes, 1BMF (Abrahams et al., 1994) and 1H8E (Menz et al., 2001). The F$_1$-motor, when separated from ATP synthase, functions as an ATPase, named the F$_1$-ATPase. **C**. Looking at the inside of the catalytic housing of structure 1BMF from behind the γ-rotor toward the three subunits, $\alpha_E\beta_E\alpha_{TP}$, into a cleft, marked by small black circle, where the SO$_4^{-2}$ analogue of HPO$_4^{-2}$ would exist in structure 1H8E. **D**. Looking at the same internal view as in **C** to see the location of the highly charge sulfate, SO$_4^{-2}$, peeking out of the cleft. Adapted from Urry, 2006c.

7.2.2 Demonstration of apolar-polar repulsion, ΔG_{ap}, between phosphate analogue and the short helix of the γ-rotor

The views of Fig. 19 were developed from the structures listed in the Protein Data Bank as 1BMF (Abrahams et al., 1999) and 1H8E (Menz et al., 2001) for the purpose of demonstrating the ΔG_{ap}, the apolar-polar repulsive free energy of hydration. The strong repulsion exists, between the very polar, doubly charged sulfate group (SO_4^{-2}), an analogue for biologically potent phosphate (HPO_4^{-2}), and the very hydrophobic side of the γ-rotor. The three sides were identified as those sides facing the β-catalytic subunits as defined in Fig. 19A. By inspection the least polar, most hydrophobic β-subunit would be the empty site, $β_E$, the site without negatively charged nucleotides. The site containing the less charged nucleotide, ADP, is labeled $β_{DP}$, and the most charged site containing ATP is labeled $β_{TP}$. Calculations of the sides utilized the $\Delta°G_{HA}$ values of **Table 1**, and gave -20 kcal/mole for the $β_E$ face of the rotor, +9 kcal/mol for the $β_{DP}$ face of the rotor, and 0 kcal/mol for the $β_{TP}$ face of the rotor. (See Urry, 2006a; 2006c). *Thus, a most hydrophobic face of the rotor was found, as necessary for ΔG_{ap}, to be an operative mechanism.*

This is the first prediction for ΔG_{ap} to be a factor in the mechanism of action of the F_1-motor of ATP synthase, namely, "***Prediction 1:*** *The rotor must be hydrophobically asymmetric.*" In what follows each "*Prediction*" will be mentioned, followed by a brief explanation.

"***Prediction 2:*** *In the static state the most hydrophobic side of the rotor faces the least polar side of the motor housing.*" As seen in Fig. 18A, the most hydrophobic side of the rotor faced the empty site of 1BMF. This should also hold for structure 1H8E, which would require that $β_E$ = β-ADP SO_4^{-2} would be less polar than $β_{DP}$ = β-ADP-AlF$_4^{-2}$ and $β_{TP}$ = β-ADP-AlF$_4^{-2}$ as defined in Fig. 18B. On the basis of the Pauling Electronegativity Scale (Pauling, 1932; 1960) ADP-AlF$_4^{-2}$ calculates to be more electronegative than ADP SO_4^{-2}.

"***Prediction 3:*** *Role of ATP in the non-catalytic α-ATP subunits is one of triangulation of repulsive forces to lessen visco-elastic drag between rotor and housing as required for efficiency.*" The long-standing question of why is it important to have ATP in the non-catalytic α-subunits has now been answered. The ΔG_{ap} from the very polar, but not most polar occupant of the non-catalytic subunits, acts to disrupt hydrophobic associations that would otherwise cause a significant visco-elastic drag.

"***Prediction 4:*** *Negative cooperativity for ATP binding.*" The three faces of the γ-rotor are of very different hydrophobicity. The face with a $\Delta G°_{HA}$ of +9 kcal/mol would be the most attractive for the ATP to enter the apposed β-catalytic site. The next ATP would add to the β-catalytic site apposed to the face with a $\Delta G°_{HA}$ of ~0 kcal/mol. And the slowest rate of ATP addition would be to the β-catalytic site with a $\Delta G°_{HA}$ of -20 kcal/mol. Thus, there would be the appearance of a negative cooperativity of ATP binding to the β-catalytic sites. For discussion of the biochemical kinetics see Boyer, 1993: 1997.

"***Prediction 5:*** *Positive cooperativity of increased ATP occupancy of catalytic sites on rate of hydrolysis (rotation).*" Just as the ATP occupancy of the α-non-catalytic sites would decrease visco-elastic drag by disrupting hydrophobic association and increase rate of γ-rotor rotation, so too would ATP occupancy of the β-catalytic sites. Thus, the positive cooperativity of ATP binding to β-catalytic sites would be reflected in dependence of rate of hydrolysis on ATP occupancy.

"***Prediction 6:*** *Increase in distance between rotor and housing due to ΔG_{ap} repulsion, acting through water, between the most hydrophobic side of the rotor and the ADP-SO$_4$ analogue of the most polar state*. As seen in Fig. 20, the short α-helix of the γ-rotor seems to wrap partially around the
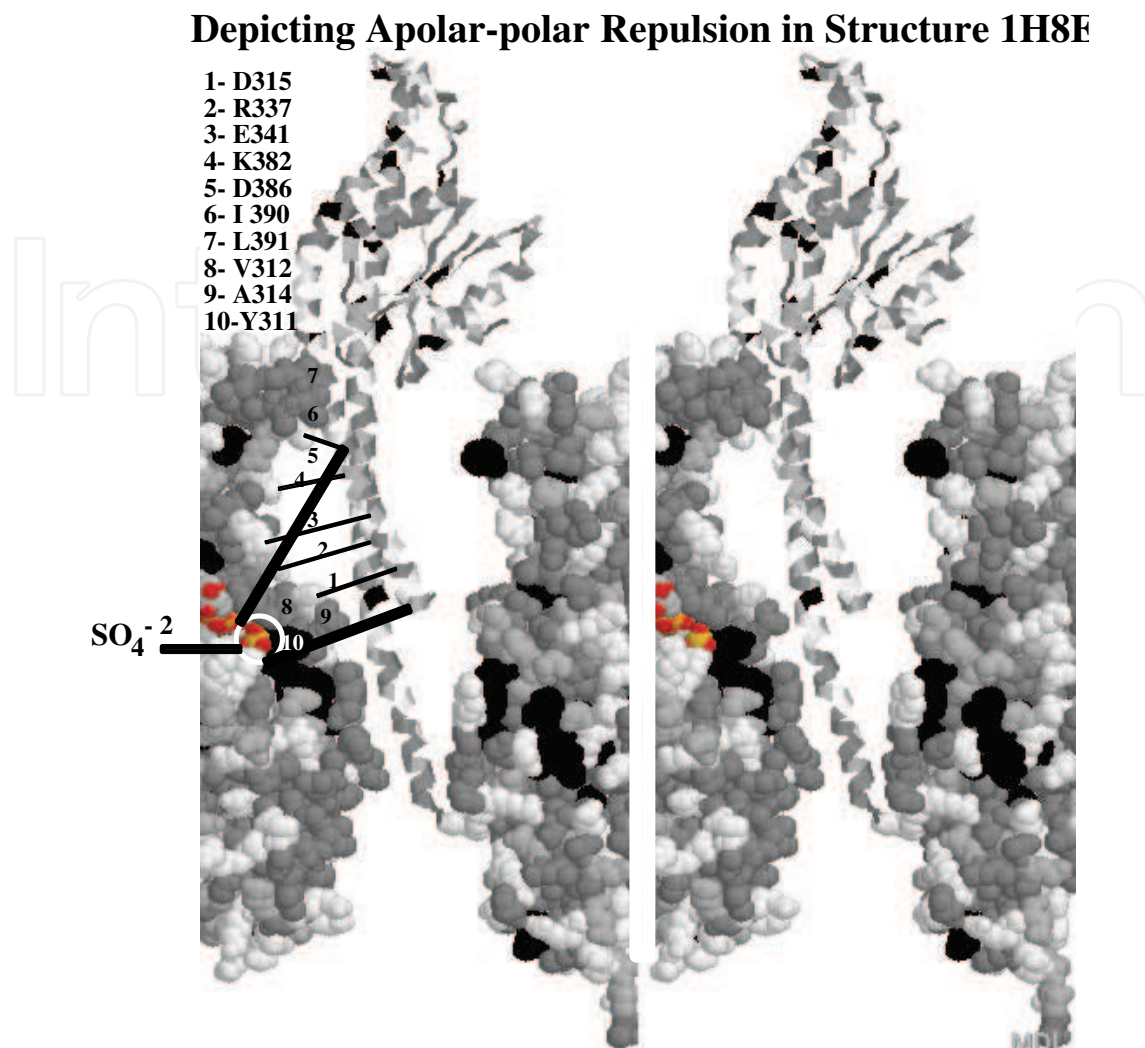
Depicting Apolar-polar Repulsion in Structure 1H8E

Fig. 20. Two subunits of 1H8E, as defined in Fig. 19B with β_E(β-ADP SO_4^{-2}) on the left and α_{DP}(α-ADP) on the right, to show the apolar-polar repulsive free energy of hyration between the very polar β_E(β-ADP SO_4^{-2}) on the left and the most hydrophobic face of the γ-rotor. The identified residues 8, 9, and 10 form one side of a cleft, identified by the black circle in Fig. 19 C and D. See text for further discussion. Protein Data Bank accession code 1H8E (Menz et al., 2001). Adapted from Urry, 2006c.

long α-helix of the γ-rotor, which is constrained at entry and at the bottom of the chamber. In addition to noting this, Menz et al. (2001) pointed out that the γ-rotor is displaced by an average of 3Å from the β-ADP SO_4^{-2} catalytic site. Both of these effects are remarkably well explained by ΔG_{ap}, the apolar-polar repulsive free energy of hydration, between the very polar β-ADP SO_4^{-2} catalytic site and the most hydrophobic face of the γ-rotor, as developed in section **6.2.6**.

"***Prediction 7:*** *A repulsive force acting through "waters of Thales" to store energy in elastic deformation provides the opportunity for high efficiencies of energy conversion by F₁ ATPase.*" The water between hydrophobic surfaces and polar, especially charged sites has been called the "waters of Thales" in honor of Thales of Miletus, father of the Ionian Enlightenment, who in the sixth century BC asked, "What is the world made of?" and answered that water is the basis of all matter. Water, as put forward here, provides the means whereby the unique protein-in-

water heat engine of biology with hydrophobicity dependence of T_t performs the work of the cell. ΔG_{ap} between ATP binding sites and the γ-rotor, providing energy for elastic deformation, would decrease visco-elastic drag and increase efficiency of energy conversion.

"**Prediction 8: ΔG_{ap}** *drives counter-clockwise rotation of the F_1 ATPase rotor*" follows from the relative positioning of the sulfate in the recess of a deep cleft and the orientation of γ-rotor, as seen in Fig. 19D. The rotation of the γ-rotor would be in a counter-clockwise direction due to the ΔG_{ap} even seen to cause an elastic deformation and displacement of the very polar β-ADP SO_4^{-2} catalytic site from the most hydrophobic face of the γ-rotor. This is seen more clearly in Fig. 20, where residues 8, 9, and 10 form a vein jutting out into the aqueous chamber and direct the apolar-polar repulsion, ΔG_{ap}, at the short α-helical limb of the γ-rotor. Looking down from the top, this would result in the counter-clockwise rotation of the γ-rotor. The remarkable work of Noji and coworkers (Noji, et al., 1997; Noji, 1998) demonstrated **Prediction 8** by directly observing the rotation by a video microscope. The rotation could be shown to occur in 120° steps as expected for a three-fold rotary motor. And the F_1-ATPase has been reported to rotate a long actin filament with an efficiency of near 100%. (Kinosita et al., 2000). See Epilogue, pages 551 - 555, of Urry, 2006a for more extensive discussion of the 8 predictions.

In your author's view, there could not be a more definitive demonstration of the prominent role of **$\Delta G°_{HA}$** and ΔG_{ap} in the description of the thermodynamics of protein function, and this has occurred with arguably the most important protein motor of biology that is responsible for nearly 90% of the ATP formed due to the oxidation of the representative food, glucose.

7.3 The full-length KcsA potassium-ion selective channel from Streptomyces lividans

The full-length KcsA potassium-ion selective channel from *Streptomyces lividans* has been reported recently by Uysal et al., 2009. As with the other protein structures obtained from the Protein Data Bank, KcsA has been analyzed using the program FrontDoor to Protein Explorer developed by Eric Martz (Martz, 2002).

7.3.1 Approach to the structure/function problem of the KcsA channel

The structural perspectives developed for KcsA will be in either space-filling or ribbon representation. Also a gray coding of amino acid residues will be used, where charged residues are white, neutral residues are light gray, aliphatic residues of intermediate hydrophobicity are gray, and aromatic residues, the most hydrophobic residues based on the **$\Delta G°_{HA}$**-Hydrophobicity Scale of **Table 1**, are black.

As our interest is in visually delineating between polar, e.g., charged, groupings and hydrophobic residue or domains, the gray coding scale allows for ready visualization of the distribution and locations of these disparate groups, whereby the darkness of the domain indicates the greater hydrophobicity. In particular, the argument has been developed that there exists a competition between hydrophobic and charged residues for hydration, which competition expresses as an apolar-polar repulsive free energy of hydration, a ΔG_{ap}.

7.3.2 Relevance of the thermodynamics of protein hydration to function of the KcsA channel

In particular, hydrophobic association develops as too much pentagonally structured water exists and the $[-T\Delta S]$ term of the Gibbs expression for dissolution in water, i.e.,
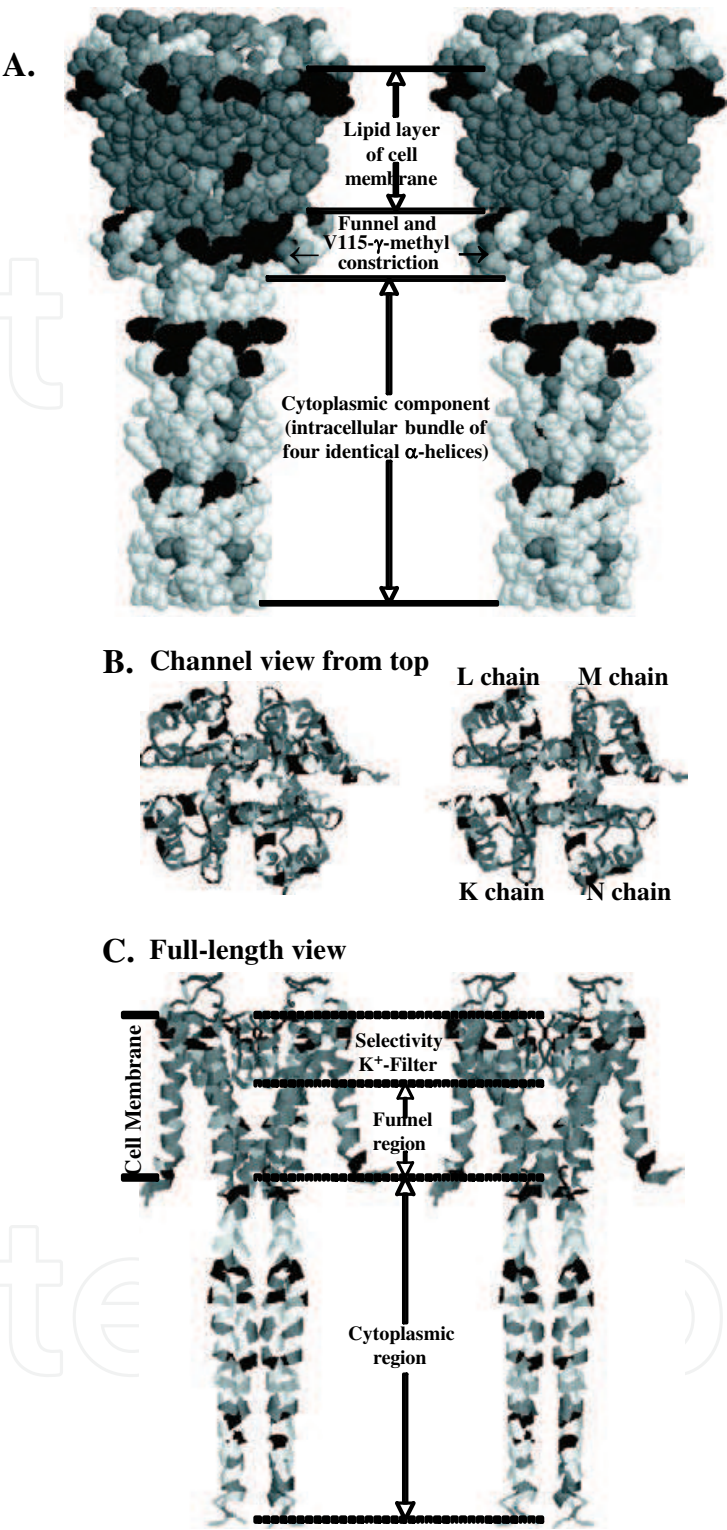
Fig. 21. KcsA potassium-ion channel of four identical chains with complete cytoplasmic component in cross-eye stereo view. **A**. In space-filling representation and gray scale where darker indicates greater hydrophobicity and white means charged residues. **B.** Channel axis view as seen from top showing four chains (KLMN) in ribbon representation. **C.** Full-length view, showing selectivity filter, funnel region, constriction due to close contact of γ-methyls of V115. PDB accession code 3EFF (Uysal et al., 2009). B. and C. from Urry et al., 2010.

Eqn. (4), $\Delta G(dissolution) = \Delta H - T\Delta S$, becomes too positive and solubility is lost. As a hydrophobic association fluctuates toward disassociation, too much hydrophobic hydration forms and solubility would be lost except when a charge forms during the fluctuation toward hydrophobic disassociation, wherein nascent charge recruits the pentagonal waters of hydrophobic hydration for its own hydration. The $[-T\Delta S]$-term decreases in magnitude and the fluctuation toward dissociation stands.

This perspective becomes immediately relevant to the KcsA channel due to its dependence of conduction on pH. As shown by Thompson et al., 2008, titrating the carboxyl function of glutamic acid from –COOH to –COO⁻ turns off conductance. With this experimental finding, one immediately looks for the formation of charged carboxylates that might disrupt hydrophobic associations that would hold the channel in the open state. So the intention is to progress from the overall representation in Fig. 21A to the details of interest.

The full structure of KcsA is given in Fig. 21 in cross-eye stereo pair and in space-filling representation with the gray coding mentioned above. Immediately apparent is the dark band with the designation of lipid layer of the cell membrane. The dark band serves to identify a ~30Å lipid-bilayer of the cell membrane that anchors the structure in the cell membrane.

By means of the ribbon representation without side chains in Fig. 21B, it is possible from the top of the channel to look from the extracellular side of the cell membrane into a continuous channel and also begin to gain a sense from this perspective of the folding of the four chains, K, L, M, and N.

The full-length view of the channel in Fig. 21C, allows a ready view of how the four chains form the superstructure of the channel. There is a specialized selectivity filter, the sequence of which provides the signature for a potassium-ion selective channel. And there is a funnel region ending in a constriction that closes the channel, and there is the lengthy protrusion into the cytoplasm of the cell. (See Uysal et al., 2009; Urry et al., 2010).

7.3.3 Carboxylate disruption of a key hydrophobic association

By means of a significant break from four-fold symmetry of the four identical chains of 3EFF (Uysal et al., 2009), the carboxyls of $E118_K$ and $E118_M$ are folded into and completely block the channel immediately below the V115 constriction. Without the apolar-polar repulsion of the $E118_K$ and $E118_M$ carboxylates, hydrophobic association occurs involving $W113_L$, interacting with $H25_L$ and $W26_L$ and nascent interaction of $W113_N$ with $H25_N$ and $W26_N$, as seen in Fig. 22B. When the $E118_L$ and $E118_N$ carboxylates are outside the channel structure, they are in a position exert a ΔG_{ap}, an apolar-polar repulsion, on $W113_K$, $H25_K$ and $W26_K$ and on $W113_M$, $H25_M$ and $W26_M$, respectively, that disrupts those hydrophobic associations as seen in Fig. 22A.

The $W113_L$ hydrophobic association with W26L and H25L, W113-(W26/H25), exerts a pull through the backbone sequence of $W113_L$-$F114_L$-$V115_L$ to draw the γ-methyl of V115 outward toward an opening of the constriction and of the selectivity filter (See Fig. 23F).

7.3.4 The effect of the $W113_L$-($W26_L$/$H25_L$) hydrophobic association on opening the Val115 γ-methyl constriction

The cross-section (slab cuts) at V115 γ-methyls are given in Fig. 23. From these the V115 γC-center to γC-center distances are obtained to give for the crystal structure 3EFF in Å, i.e., (N→L) = 6.322, (N→K) = 3.810, c(L→M) = 4.199, d(M→N) = 4.164, and e(L→N) = 4.864. By graphical analysis these distances allow estimates of channel closed and open states as shown in Fig. 23A and B, respectively.

Simply put the N and K γ-methyls of the V115 residues are in close contact, and completing them in square-planar arrangement gives the closed state in Fig. 23A, whereas the outward displacement $V115_N$ γ-methyl is made square-planar to give the open state represented in Fig. 23B.

7.3.5 Consider the hydrophobic association/dissociation (HA/HD) system, W113-(W26/H25), of the KcsA channel and its consequences

Consider, poised near 37°C, the W113-(W26/H25) hydrophobic association(HA) ↔ hydrophobic dissociation(HD) system with proximal carboxylates, **E118** and **E120**, of the KcsA channel in Fig. 24A. Decreasing charge increases the amount of hydrophobic hydration, N_{hh}, which lowers T_t below 37°C and drives HA (as seen in the lower part of Fig. 24A where the carboxylate of **E118** is missing and in general in Fig.12). On the other hand, increasing charge (by an increase in ΔG_{ap} due to the presence of the carboxylate of **E118**) decreases N_{hh}, which raises T_t and drives HD (as seen in the upper part of 24A and in general in Figs. 10, and 12). That the formation of carboxylates disrupt hydrophobic associations and that the removal of carboxylates allow hydrophobic association becomes apparent on studying Figs. 10C, 12, 14B, and 15, and **Table 3**, columns 2 and 3.
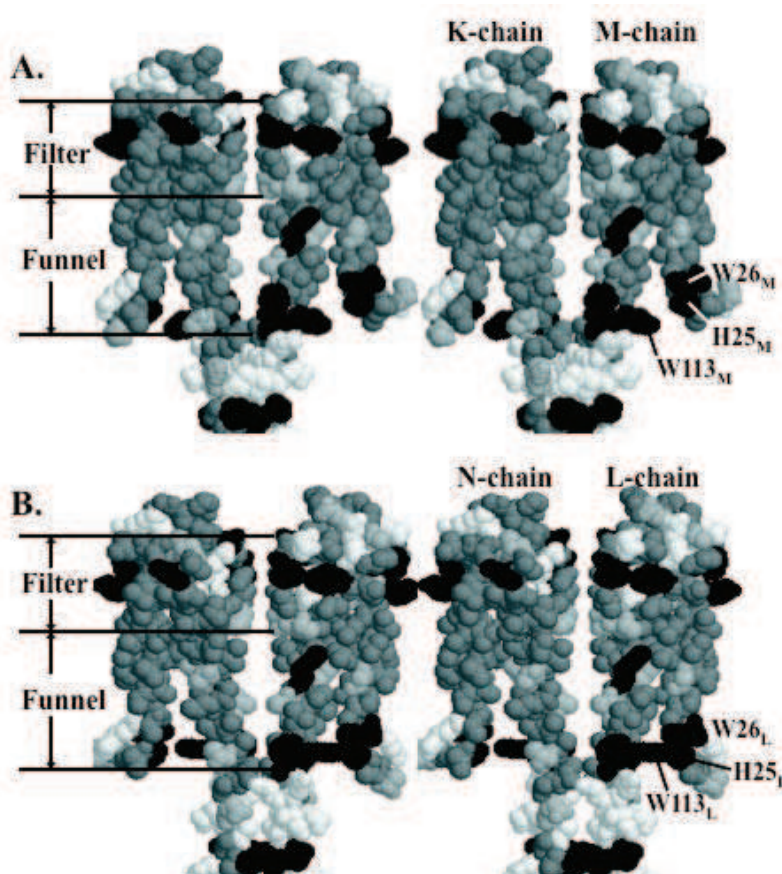
Fig. 22. Busts for the diagonally paired chains, K-M in A and L-N in B. The hydrophobic association of $W113_L$-($W26_L$/$H25_L$) pulls on the backbone sequence of $W113_L$-$F114_L$-$V115_L$ to draw the γ-methyl of $V115_L$ outward. That displacement is made square-planar to result in an open state in Fig. 23B. See text for further discussion. Protein Data Bank accession code 3EFF. From Urry et al., 2010.
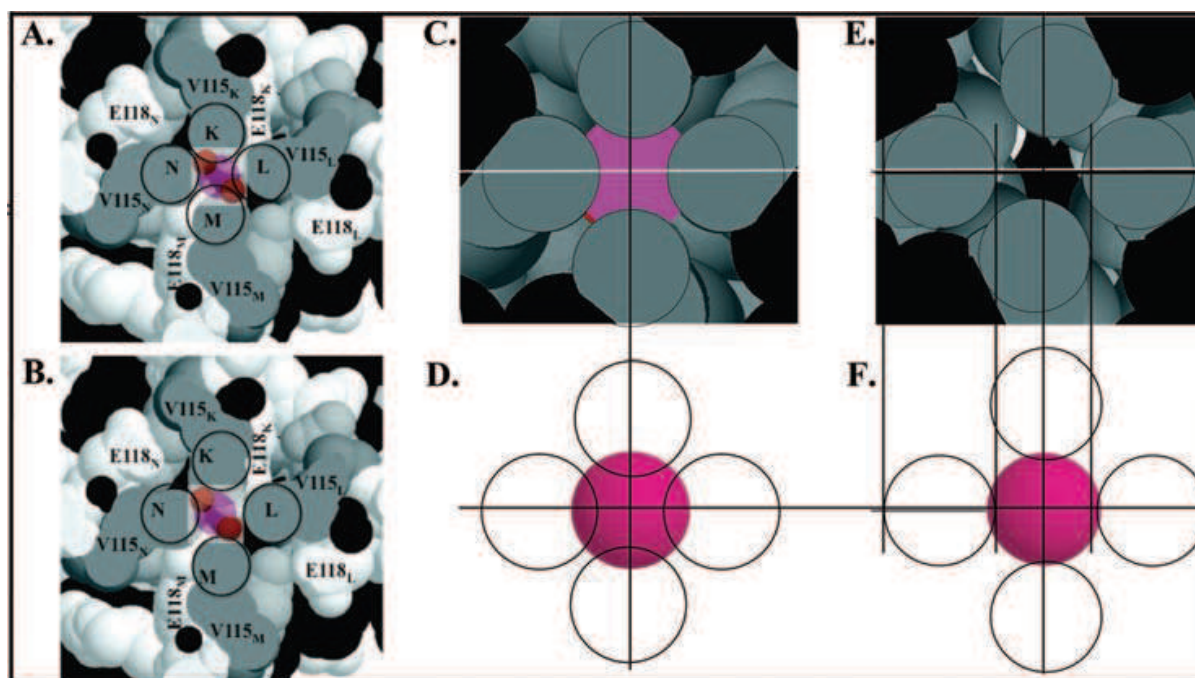
Fig. 23A and B. Cross-section at the V115 γ-methyl constriction. A. Representation of the closed state on making the N and K γ-methyl proximity square-planar. B. The open state by making the $V115_L$ γ-methyl displacement square-planar. C. A cross-section in the closed state of structure 1BL8 (Doyle et al., 1998) with representation in D. E. A cross-section at the G77 carbonyl oxygens of a closed structure, 3EFF (Uysal et al., 2009). But the displacement of the carbonyl oxygen on the left, on being made square-planar, represents an opening displacement when made in all chains, and either the lower left or the upper right oxygen pairs made square-planar give the closed state of D. See discussion.

The particular function of the W113-(W26/H25) hydrophobic association is to extend the backbone linkage $W113_L$-$F114_L$-$V115_L$ outward and thereby to move the γ-methyl of V115 outward. This outward displacement, when made square-planar for all four identical chains, opens the constriction at the base of the funnel of Fig. 21 (See Fig. 23B). A correlated outward displacement of the G77 carbonyl oxygen, also when made square-planar for all four identical chains, opens the selectivity filter as seen in Fig. 23E and F.

7.3.6 Developing the free energy profile for the open KcsA K$^+$-conducting channel

Fig. 24B becomes but a simple statement of the fraction of channels that will be in the open state for a given pH. Therefore, beyond a weighting of the probability of the open state, the problem of meaningful description of the pH dependence of potassium-ion conductance through the KcsA channel reduces to the state of the Gramicidin A channel discussed in section **8**.

The steps for developing a free energy profile for the KcsA channel would be similar to those listed in section **8.4.2** for the development of the free energy profile for ion passage through the Gramicidin A channel. The first challenge would be to obtain a suspension of stable lipid-bilayer membrane in which the KcsA channels could be incorporated and characterized by NMR and dielectric relaxation methods. For a detailed description of the process once the lipid-bilayer suspension of KcsA channels is obtained see section **8. Eyring's Absolute Rate Theory applied to biological trans-membrane transport** below.
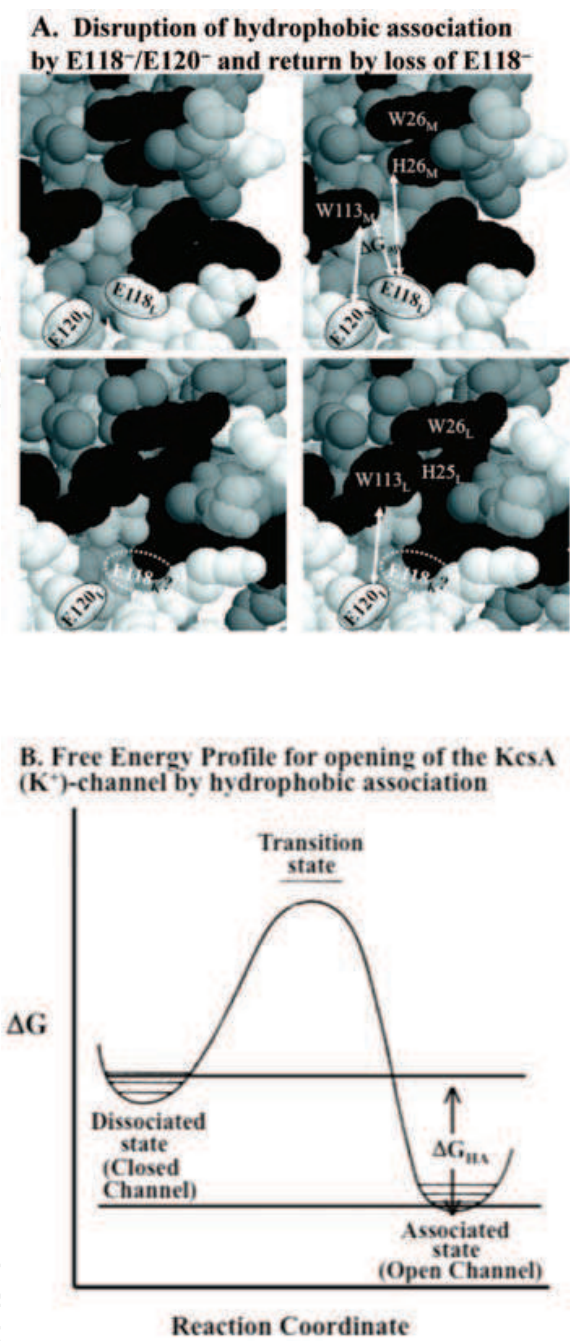
Fig. 24. A. Stereo view of hydrophobically dissociated (upper pair) and associated (lower pair) states proposed to be responsible, respectively, for the closed (Figs. 23A, C and D) and open (Figs. 23B and F) states of the KcsA (K⁺)-channel. By ΔG_{ap}, the apolar-polar repulsive free energy of hydration described in section **6.2**, the charge of the carboxylates, E118⁻ and E120⁻, disrupt hydrophobic association, and the loss of ΔG_{ap} due to absence of E118⁻ in the lower pair is seen to restore hydrophobic association.

B. Free energy profile representing the free energy change of hydrophobic association on protonation of the E118 carboxyl that restores the W113L,-(W26L/H25L) hydrophobic association and pulls on the backbone sequence of W113L-F114L-V115L to draw the γ-methyl of V115L outward and open the constriction. Thus, B provides a simple probability statement for the fraction of open channels. From Urry et al., 2010.

7.3.7 Looking forward to the remarkable potential of the Eyring Absolute Rate Theory to describe diverse biological trans-membrane transport processes

As will be seen in section **8**, once the image of the free energy profile is obtained, the channel conductance can be calculated as a function ion activity and trans-membrane potential. This has been demonstrated with the Gramicidin A Trans-membrane Channel as reviewed below. The entire process can be understood through the single visual image of the free energy profile of Fig. 27A. The challenge now before us is to reduce the essential and increasingly complex trans-membrane transport processes required for living organisms to visual images of free energy profiles. This potential to describe the essential energy converting trans-membrane systems of biology could result in one of the most profound legacies of the Eyring Absolute Rate Theory.

The sequence toward stepwise increasing complexity occurs in the preceding examples of the thermodynamics of biology's protein-based machines. The approach could be to begin with the KcsA channel, to proceed to Complex III of the electron transport chain of the inner mitochondrial membrane where the challenge would be in a coupled pair of visual images whereby proton flow from the matrix side would be coupled at the Q_o-site and the Q_i-site to the electron transport in the plane of the membrane, and then to proceed to ATP synthase with its pair of rotary motors, the F_0-motor and the F_1-motor, the first to use the return of proton to effect rotation of the rotor of the F_1-motor for making ATP.

8. Eyring's absolute rate theory applied to biological trans-membrane transport

8.1 The fundamental expression of Eyring's absolute rate theory

Application of the thermodynamics of Eyring's Absolute Rate Theory to essential trans-membrane transport processes of biology can result in a single figure of Gibbs free energy versus distance across the membrane that provides all of the information required to calculate transport as a function of concentration (or activity where relevant) of transported species and trans-membrane potential.

By means of Eyring's expression for the specific rate constant, k', (Eyring, 1935; Glasstone, et al. 1941; Eyring, 1969),

$$k' = \kappa kT/h \exp(-\Delta G\dagger/RT) = \kappa kT/h \exp(-\Delta H\dagger/RT + \Delta S\dagger/R), \qquad (20)$$

$$\Delta G\dagger = \Delta H\dagger - T\Delta S\dagger, \qquad (21)$$

where κ is the transmission coefficient; k is the Boltzman constant (1.38×10^{-16} erg/degree); T is the temperature in degrees Kelvin, K, which at physiological temperature of 37C would be 310K; h is Planck's constant (6.62×10^{-27} erg-sec); $\Delta G\dagger$ is the Gibbs free energy of activation for the chemical reaction or physical process being considered, and R is the gas constant (1.987 cal/deg-mol). Importantly, Eqn. (20) expresses the activation energy in terms of the Gibbs free energy, $\Delta G\dagger$, defined in Eqn. (21) where $\Delta H\dagger$ and $\Delta S\dagger$ are, respectively, the heat and entropy of activation that occur on achieving the activated state.

This is most fitting for the biophysical world where the essential processes of life occur at constant temperature and pressure, that is, where the experimentally obtained free energies are ΔG, and also where κ is commonly one. For special cases where κ differs from one, the rate process has been understood and κ calculated.
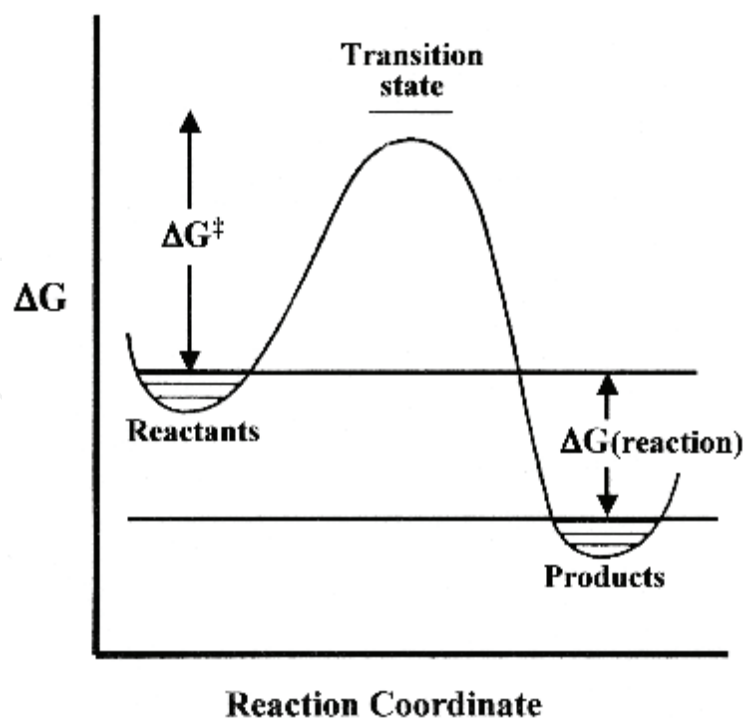
Reaction Coordinate

Fig. 25. The classic visual statement of Eyring's Absolute Rate Theory depicting reactants colliding to raise the free energy to that required for formation of the activated complex, now commonly called the transition state to include rate processes that may not involve chemical reactions, e.g., channel ion transport.

Fig. 25, the visual statement made by Eqn. (20), presents the archetypical image of Eyring's Absolute Rate Theory. As originally derived, it depicts the Gibbs free energy barrier that must be surmounted as reactants pass along the reaction coordinate to form products and may be called the *free energy profile* for the reaction. The reaction coordinate represents a splendid simplified plot of the distance between atoms or molecules in the gas phase flying at each other on collision course, passing over the high-energy barrier (the activated or transition state) and flying apart as product or products.

For ion transport through a trans-membrane channel the reaction coordinate is simply the length of the channel, such that plotting of the free energy profile for transit through a natural channel becomes a plot of the Gibbs free energy as a function of the actual distance along the channel. The channel state may be incorporated into a lipid-bilayer system at adequate concentrations wherein binding site locations can be determined by NMR data on individually C13-labeled carbonyl carbons of the channel. Also, by NMR methods the binding constants for single and multiple occupancy, the off-rate constants for single and multiple occupancy can be determined, and by dielectric relaxation rates for intra-channel ion translocations can even be experimentally determined.

Plotting these quantities as a function of free energy versus distance along the channel provides a free energy profile. Within a single image, the free energy profile for ion flow through the channel, the complete process of trans-membrane transport is described, and the calculated results may be compared with the single-channel currents determined by measurement of the single-channel currents in the so-called black lipid-bilayer membrane (BLM) obtained at appropriate applied potentials, and as a function of relevant ion

concentrations, corrected to molal ion activity (Urry et al. 1980a; Urry et al. 1980b; Urry, 1985). Successful calculation of the experimental single-channel currents using experimentally derived distances and rate constants from a macroscopic lipid-bilayer incorporated system can be used to substantiate the detailed mechanism and, of course, to substantiate the relevance of Eyring Absolute Rate Theory.

The reported example of a natural channel for ion transport, opens the door to the development of free energy profiles for trans-membrane transport of other ions and molecules required to sustain the cell. Thus, Eyring Rate Theory provides the opportunity to obtain within a single image the visualization of many trans-membrane transport processes of biology with the potential of medically relevant interventional insights that such would provide.

8.2 The trans-membrane channel as a unique example of a free energy profile

As the objective of our first example given below, Fig. 27A contains the image of a biophysical path often-enjoyed by Henry Eyring, one of diffusion through membranes. In the present case the reaction coordinate for ion transit through a trans-membrane channel becomes the length of the channel through which the ion passes. And the plot of ion position in the channel as a function of Gibbs free energy images a *free energy profile* of ion passage over a terrain of valleys and mountain passes. The valleys locate and quantify low-energy binding sites, and the mountain passes locate and quantify high-energy barriers of the transition states. The free energy profile contains in a single figure the complete physical process of ion passage through the channel. By passing through a biological channel, ions achieve a controllable transit through an otherwise ion-impenetrable lipid membrane.

8.3 Turning channels on and off becomes central to integrating life processes.

In order to correlate and integrate the functions required for life, there must be controlled channel opening and closing. Another plot of the same form as that of Fig. 25, given above in Fig. 24, depicts the process whereby protonation of a carboxylate effects hydrophobic association to open a channel and the reverse process closes the KcsA potassium channel of living organisms. In this example, hydrophobic association pulls the channel gate open, and hydrophobic dissociation allows the channel gate to return to its closed state (See section **7.3**). The equilibrium constant for this process allows calculation of the probability of the open state.

8.4 Construction of the free energy profile for the malonyl Gramicidin A trans-membrane channel and calculation of single-channel currents
8.4.1 A channel-containing lipid-bilayer state for determining structure, binding sites and rate constants

An aqueous suspension of the channel-containing lipid-bilayer state is prepared (Spisni et al. 1983; Pasquali-Ronchetti et al, 1983). This provides sufficient channel concentrations to use physical methods, such as nuclear magnetic resonance, to determine structure, channel-binding sites and rate constants. This data combines by means of Eyring rate theory to produce the free energy profile from which single-channel currents may be calculated, in a manner entirely independent of the BLM single-channel current measurement.

8.4.2 Steps in the development of a free energy profile with which to calculate single-channel currents

The steps are: **1**) Determination of structure and location of ion binding sites, as shown in Fig. 26A, B, and C (Urry et al., 1982a; Urry et al., 1982b; Urry et al., 1982c; Urry et al., 1982; Urry et al., 1983) for malonyl Gramicidin A (mal-GA). The data demonstrate the channel structure in the prepared lipid-bilayer state to be the single-stranded, head-to-head dimerized, left-handed $\beta^{6.3}$-helix. **2**) Derive the appropriate steady state equations for all occupancy states and the equation for the single-channel ion current (Urry, 1985; Urry et al., 1980a; 1980b) as given in Fig. 26D, E, and F. **3**) Construct the free energy profile for passage of ions through the trans-membrane structure by experimental determination of binding site locations and rate constants (Urry, 1985; Henze et al., 1982; Urry, et al. 1989; Urry, 1987), as in Fig. 27A, B, and C. **4**) Add to ΔG of Eqn. (20) the trans-membrane potential dependence appropriate to each rate constant with an assumed linear trans-membrane potential drop. And **5**) calculate the single-channel current as a function of ion activity and applied trans-membrane potential (Urry, 1985; Urry, 1984).

8.4.3 Comments on the structure(s) of Gramicidin A

As originally proposed in 1971 (Urry, 1971; Urry et al. 1971) and established now for three decades (Bamberg et al. 1977; Bamberg et al. 1978; Szabo & Urry 1979; Anderson & Koeppe II, 1992; Busath, 1993), the structure of the ion-conducting Gramicidin A channel in the BLM system for determining single-channel currents is a head-to-head hydrogen-bonded, single-stranded β^6-helix, a member of a new family of helices initially named π_{LD}-helices (Urry, 1971; Urry et al. 1971). The name was changed to β-helices as the hydrogen-bonded pattern between turns within the monomer is that of the parallel β-pleated sheet and between the turns at the head-to-head junction is that of the anti-parallel β-pleated sheet Urry, 1972. And the work, listed in part in the papers of reference (Urry, et al., 1982a, 1982b, 1982c, 1982e, 1983) showed the structure in lipid-bilayer suspensions (Pasquali-Ronchetti, et al. 1983; Spisni et al., 1983) to be the head-to-head hydrogen bonded, single-stranded and *left*-handed $\beta^{6.3}$-helix of Fig. 26A, B, and C, as originally proposed.

Nicholson and Cross (1989) using solid state ^{15}N NMR spectroscopy of Gramicidin A incorporated into a dimyristoyl phosphatidyl choline (DMPC) bilayer preparation, reported the same β-hydrogen-bonding pattern (β-helix) proposed in 1971, but concluded the *right*-handed rather than *left*-handed helix. We then incorporated malonyl Gramicidin A into dodecyl phosphocholine micelles, and utilized high resolution 2D NMR data to determine the handedness in this phospholipid system also to be *right*-handed (Jing & Urry, unpublished results), but with altered ion-binding interactions. Since Gramicidin A is now well-known for its many helical states (Anderson et al. 1999; Cross et al. 1999; Burkhart & Duax, 1999), the question continues to be, Is a determined Gramicidin A structure obtained at high channel concentrations relevant to the trans-membrane structure that gives rise to the single-channel current events of the (BLM) technique?

Without a methodology to observe directly the structure of a single trans-membrane channel in the BLM where the single-channel current is measured, application of Eyring's Absolute Rate Theory (ART) provides the opportunity to test a given structure by independent calculation of single-channel currents as reviewed here. Success would support the structure from which the rate constants and binding sites were derived and would be a remarkable validation of use of the Eyring rate equation for trans-membrane channel transport (with Gibbs free energies of activation for the barriers).

8.4.4 Development of the free energy profile for the malonyl Gramicidin A channel state

As depicted in the several components of Fig. 26, the malonyl-Gramicidin A trans-membrane channel - a covalent dimer with a two-fold symmetry axis perpendicular to the channel axis – contains two ion binding sites (a symmetrically positioned tight binding site for the first ion in the channel and a pair of weak binding site on entry of the second ion into the channel). Double occupancy results in repulsion between ions that weakens second ion binding. The result is two entry/exit barriers and a single central barrier for ion exchange between the two sites.

Therefore, description of ion transport through the channel requires five experimentally determinable rate constants. The following values were obtained using the lipid-bilayer suspension of malonyl GA channels: $k^t_{off} = 3 \times 10^5$/sec, $k^t_{on} = 3 \times 10^7$/M-sec, $k^w_{off} = 2 \times 10^7$/sec, $k^w_{on} = 2 \times 10^7$/M-sec and $k_{cb} = 4 \times 10^6$/sec. The two off-rate constants were obtained by means of sodium-23 nuclear magnetic resonance (NMR) longitudinal and transverse relaxation studies. And sodium ion-induced carbonyl carbon chemical shifts (CS), and sodium ion line width (LW), excess longitudinal relaxation (ELR) rate and excess line width (ELW) data (Urry et al., 1980a, 1980b; Urry et al. 1989; Urry, 1987) were used to obtain values for the tight and weak binding constants, $K^t_b = k^t_{on}/k^t_{off}$ and $K^w_b = k^w_{on}/k^w_{off}$, from which the on rate constants were determined. The magnitude of k_{cb} was obtained by means of thallium ion dielectric relaxation data for the ion jump inside the channel (Henze et al., 1982). Due to the two-fold symmetry and in the absence of an applied field the rate constants defined in Fig. 26D become, $k^t_{off} = k_{-1} = k_2$; $k^t_{on} = k_1 = k_{-2}$; $k^w_{off} = k_3 = k_{-4}$; $k^w_{on} = k_{-3} = k_4$; $k_{cb} = k_5 = k_{-5}$. An assumed linear applied potential drop is applied to these experimentally derived rate constants with the distances defined in Fig. 27A to be $a_1 = 10.5$ Å; $b_1 = 13$ Å; $d = 15$ Å, as utilized in the current equation of Fig. 26F.

The experimental Gibbs free energies of activation were calculated, using Eqn (20) in the form of $\Delta G^\dagger = 2.3RT(12.79 - \log k')$, from the experimental data to be as follows: $\Delta G^\dagger(t_{off})^{exp} = 10.1$; $\Delta G^\dagger(t_{on})^{exp} = 7.4$; $\Delta G^\dagger(w_{off})^{exp} = 7.6$; $\Delta G^\dagger(w_{on})^{exp} = 7.6$; $\Delta G^\dagger(cb)^{exp} = 8.6$. These values and binding site locations are used to plot the free energy profile of Fig. 27A.

In addition, a set of five "best fit" rate constants for the experimental single-channel currents were determined by allowing all five rate constants to vary in order to optimize the fit to the experimental BLM single-channel current data, as a function of ion activity and trans-membrane potential. The "best fit" single-channel current values were found to be: $\Delta G^\dagger(t_{off})^{fit} = 10.5$; $\Delta G^\dagger(t_{on})^{fit} = 7.3$; $\Delta G^\dagger(w_{off})^{fit} = 8.2$; $\Delta G^\dagger(w_{on})^{fit} = 8.0$; $\Delta G^\dagger(cb)^{fit} = 7.9$. The "best fit" $\Delta G^\dagger$ values for the experimental BLM single-channel current data compare favorably with the free energies of the experimentally determined rate constants using the lipid-bilayer suspension of channels without optimization.

8.5 Absolute rate theory calculates experimental single-channel currents using experimentally-derived rate constants

8.5.1 Experimental BLM single-channel currents of the malonyl Gramicidin A trans-membrane channel

We start with the malonyl Gramicidin A trans-membrane channel, the covalent dimer, formed by chemically connecting, by peptide linkage, the amino ends of two molecules of the 15 amino acid residue peptide, Gramicidin A, using the malonyl group, -OC-CH$_2$-CO-, and we measure the resulting single-channel currents in the black lipid-bilayer membrane
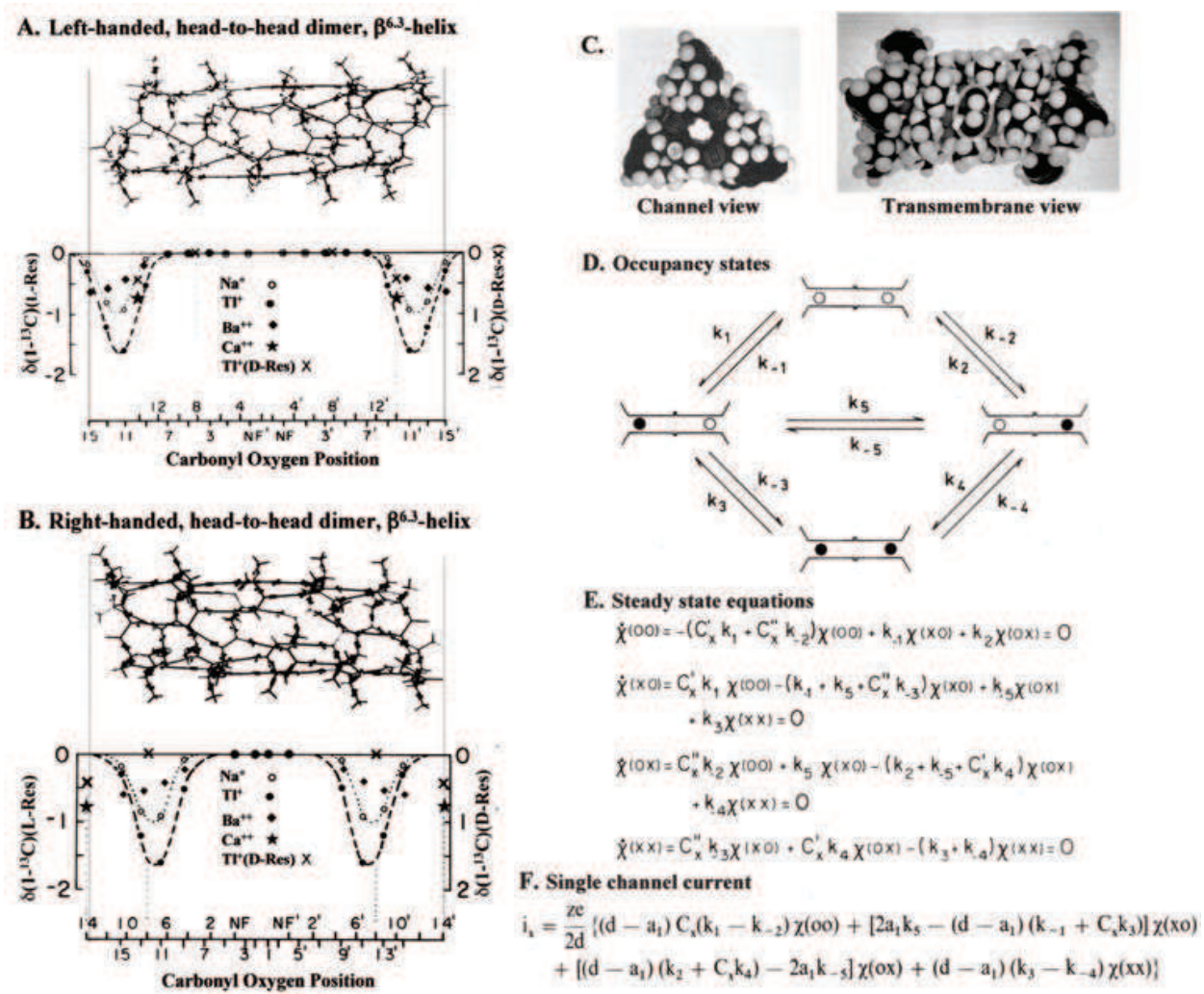
A. Left-handed, head-to-head dimer, β^{6.3}-helix

B. Right-handed, head-to-head dimer, β^{6.3}-helix

C.

Channel view   Transmembrane view

D. Occupancy states

E. Steady state equations

$$\dot\chi(OO) = -(C_x' k_1 + C_x'' k_{-2})\chi(OO) + k_{-1}\chi(XO) + k_2\chi(OX) = O$$

$$\dot\chi(XO) = C_x' k_1 \chi(OO) - (k_{-1} + k_5 + C_x'' k_{-3})\chi(XO) + k_5\chi(OX) + k_3\chi(XX) = O$$

$$\dot\chi(OX) = C_x'' k_2 \chi(OO) + k_5 \chi(XO) - (k_2 + k_5 + C_x' k_4)\chi(OX) + k_4\chi(XX) = O$$

$$\dot\chi(XX) = C_x'' k_3 \chi(XO) + C_x' k_4 \chi(OX) - (k_3 + k_4)\chi(XX) = O$$

F. Single channel current

$$i_s = \frac{ze}{2d}\{(d - a_1)\, C_x(k_1 - k_{-2})\, \chi(oo) + [2a_1 k_5 - (d - a_1)(k_{-1} + C_x k_3)]\, \chi(xo)$$
$$+ [(d - a_1)(k_2 + C_x k_4) - 2a_1 k_{-5}]\, \chi(ox) + (d - a_1)(k_3 - k_{-4})\, \chi(xx)\}$$

Fig. 26. A. Upper image: Wire model of the single-stranded *left*-handed, head-to-head hydrogen bonded dimeric $\beta^{6.3}$-helix, indicating the β-sheet hydrogen-bonded pattern made possible by the L-D repeating sequence, namely HCO-L-Val[1]-Gly[2]-L-Ala[3]-D-Leu[4]-L-Ala[5]-D-Val[6]-L-Val[7]-D-Val[8]-L-Trp[9]-D-Leu[10]-L-Trp[11]-D-Leu[12]-L-Trp[13]-D-Leu[14]-L-Trp[15]-NHCH₂CH₂OH, with 6.3 residues per turn of helix, as proposed in 1971 (Urry et al., 1971; Urry, 1971, 1972). From Urry et al., 1982e.

Lower part: Plot of experimental carbon-13 carbonyl carbon chemical shifts as a function of carbonyl oxygen position in the structure for the single-stranded *left*-handed, head-to-head hydrogen bonded dimeric $\beta^{6.3}$-helical structure above. Data obtained by chemical synthesis of Gramicidin A with one carbonyl carbon-13 enriched per chain synthesized for each of the 8 L-residues and the amino terminal malonyl carbonyls and for each of two D-residues, D-Val[8] and D-Leu[14]. Adapted from Urry et al., 1982a; 1982b; 1982c; 1982e; Urry, 1985.

B. Upper image: Wire model of the single-stranded *right*-handed, head-to-head hydrogen bonded dimeric $\beta^{6.3}$-helix, indicating the β-sheet hydrogen-bonded pattern made possible by the alternating L-D repeating sequence with 6.3 residues per turn of helix.

Lower part: Plot of experimental carbon-13 carbonyl carbon chemical shifts as a function of carbonyl oxygen position in the sequence for the *right*-handed, head-to-head hydrogen bonded dimeric $\beta^{6.3}$-helical structure immediately above. From Urry et al., 1982e; Urry, 1985. In the plot for the *left*-handed structure in A, all of the Na⁺ and Tl⁺ data points and the single Ca⁺⁺ data point consistently define the location of two binding sites, including the data points for the D-residues, D-Val[8] and D-Leu[14]. On the other hand, for the plot of the *right*-handed structure in B, D-Val[8] shows no ion interaction in the middle of the binding site as defined by the L-residue carbonyl carbon chemical shifts. Furthermore, for the *right*-handed structure, the D-Leu[14] residue carbonyl carbon chemical shifts are substantial where there is no binding site again as defined by the 8 L-residue carbonyl carbon chemical shifts. Accordingly, we believe that the structure in our bilayer preparations of the malonyl Gramicidin A is the single-stranded, *left*-handed, head-to-head hydrogen bonded dimeric $\beta^{6.3}$-helix.

C. The single-stranded *left*-handed, head-to-head hydrogen bonded dimeric $\beta^{6.3}$-helical structure of the Gramicidin A transmembrane channel: in channel view on left and in transmembrane view on the right, using CPK (Corey-Pauling-Koltun) space-filling molecular models. The oval encompasses the two formyl hydrogens at the head-to-head junction.

D. Occupancy states: The information in A and C above, define the four occupancy states, which with the ten defined elemental rate constants, provide the information required to state the steady state equations in E. From Urry, 1985.

E. Steady state equations: As the single-channel currents are determined under steady state conditions, the four steady state equations are stated here for the four occupancy states and ten elemental rate constants of D above. From Urry et al., 1980b.

F. Single-channel current: With steady state equations and defined elemental rate constants, the single-channel current may be expressed, but, if written correctly, it yields no current until a transmembrane potential is applied. With binding site locations as in Fig. 27C, with the distances defined in Fig. 27A, with the positioning of the channel in relation to the membrane as in Fig. 27B, and with the indicated fraction of the transmembrane potential applied to each experimentally determined rate constant, the single-channel current is stated as given here in F. From Urry et al., 1980b.
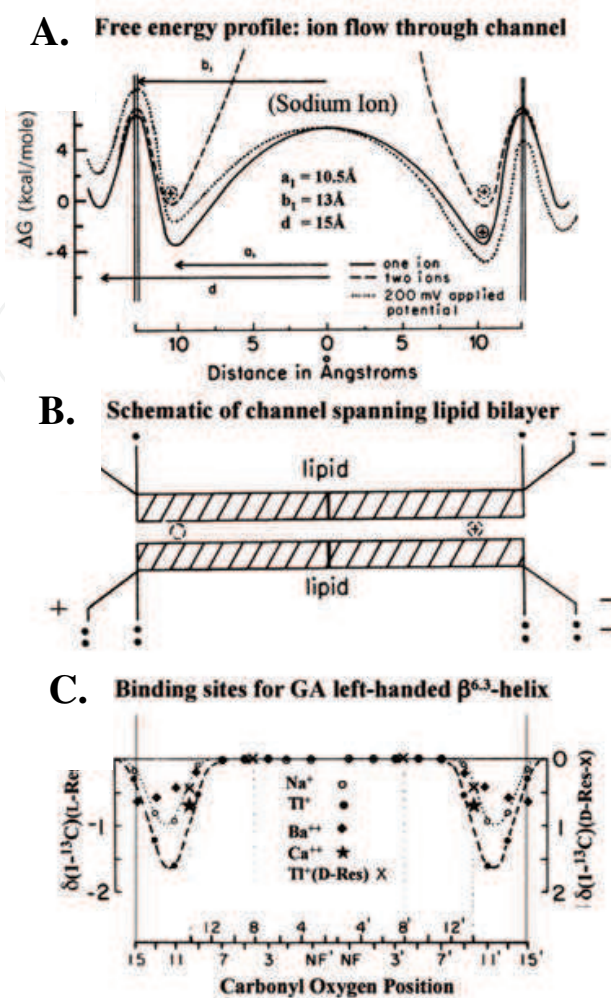
Fig. 27. A. <u>Free Energy Profile</u>: With five experimentally determined rate constants obtained from suspensions of transmembrane channels in bilayer preparations and the defined distances, the decrease in Gibbs free energies of binding sites and increase in Gibbs free energies of barriers are plotted here as well as the bias added by the linear applied potential drop of a 200 mV transmembrane potential, given as the dotted line for single ion occupancy, and also a similar bias added to the dashed curve for double occupancy. All the data is contained in the single image of the free energy profile with use of the expression in Fig. 26F to calculate the single-channel currents of Fig. 28A for comparison with the experimental single-channel currents given in Fig. 28B. B. Schematic representation of the Gramicidin A transmembrane channel spanning the 30Å lipid bilayer. The binding sites are noted within the channel and the charge distribution across the membrane has the left hand side indicated as positive and the right hand side as negative. Thus, the applied transmembrane potential is such that for the positive sodium ion the free energy is lower on the right hand side and raised on the left hand side of the membrane, as seen by the free energy profile in part A above. A. and B. from Urry, 1982b.

C. The lower component serves to align the binding sites in the channel and uses the outermost channel carbonyls to define the outermost reaches of the schematic representation in part B and the entrance barrier of the Gramicidin A transmembrane channel spanning the lipid bilayer in part A in order to clarify the relationship of the free energy profile of part A to the lipid bilayer being spanned by the Gramicidin A channel. Adapted from Urry et al., 1982a; 1982b; 1982c; 1982e; Urry, 1985.

(BLM) obtained at four applied potentials, 50 mV, 100 mV, 150 mV, and 200 mV, and as a function of ion concentrations, 0.1, 1, 3, and 5.5 M, corrected to molal ion activity.

It is called a black lipid membrane (BLM), because as the lipid membrane thins to a single 30Å wide lipid bilayer, the membrane is seen to go black, due to the interference of light reflected from each surface of the thin flat membrane. The 30Å wide lipid-bilayer can be spanned by a single channel-forming covalent dimer, the malonyl Gramicidin A trans-membrane channel, which allows measurement of single-channel currents from a histogram of single channel conductances.

8.5.2 Using Eyring Absolute Rate Theory to calculate the experimental BLM single-channel currents

The experimentally-derived rate constants (without any adjustment or fine-tuning of experimental values obtained on channel incorporated lipid bilayer suspensions) can be used within the formalism of Eyring Absolute Rate Theory to calculate successfully the sodium ion single-channel currents for four different trans-membrane potentials and over a wide range of ion activities, as seen in Fig. 28(a). Comparison with the directly measured sodium ion single-channel currents in Fig. 28(b) is particularly satisfying, especially for the 150 mV curve. Furthermore, also calculated were the conductance ratios for the series of alkali metal ions – Li$^+$, Na$^+$, K$^+$, Rb$^+$, and Cs$^+$ – and found to be within experimental error (Urry et al., 1980a; Urry et al. 1989; Urry, 1987).
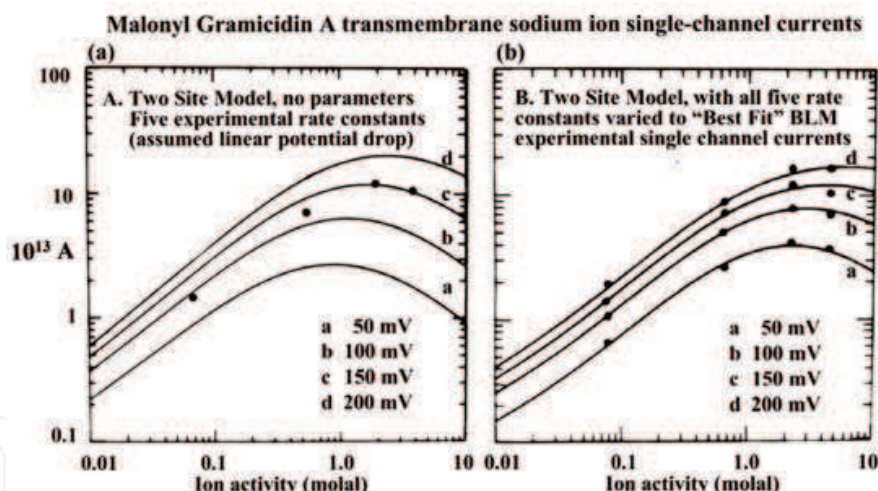

Fig. 28. Part (a): The calculated single-channel currents using the single-channel current equation of Fig. 26F with the data of the free energy profile of Fig. 27A, including a dotted curve adding the 200 mV potential bias and similarly for the dashed curve for double occupancy, that is, the five experimental rate constants and the assumed linear potential drop. The four data points for 150 mV applied potential were transferred laterally from the aligned part (b) to (a) using PowerPoint. Adapted from Urry et al., 1980a.

Part (b): Single-channel currents of Fig. 7A of Urry et al., 1980a. Data points from single channel current measurements at different ion activities and applied transmembrane potentials obtained using the black lipid membrane (BLM) approach, and solid lines are calculated "best fit" curves using a single set of five rate constants. From Urry, 1980a.

The data in Fig. 26A demonstrate the head-to-head hydrogen-bonded, single-stranded, *left*-handed β$^{6.3}$-helical structure of incorporated malonyl Gramicidin A transmembrane channel to occur in what has been verified as a lipid bilayer suspension (Spisni et al., 1983; Pasquali-Ronchetti et al., 1983). These findings also demonstrate the remarkable capacity of Eyring Absolute Rate Theory to construct in a single image of the free energy profile all the information with which to calculate trans-membrane transport for a number of important variables central to biological function.

The data of Fig. 26A - including the divalent ion binding data, for which the channel is impermeable - argue that the head-to-head hydrogen-bonded, single-stranded, *left-handed* β$^{6.3}$-helix gives rise to the experimental single-channel currents obtained in BLM experiments. *The most salient point to make here, however, is the remarkable capacity of the Eyring rate equation, Eqn. (20), to treat biologically important ion trans-membrane transport processes.*

8.6 Eyring Legacy: Absolute Rate Theory for thermodynamic description of diverse biological trans-membrane transport processes

Absolute Rate Theory is applicable to virtually all that happens in living organisms. Here we utilize Eyring's rate equation to construct a free energy profile for transit of sodium ion through a natural trans-membrane channel. Without resorting to BLM measurements of sodium ion single-channel currents through the channel, independent physical determinations of channel structure and of five separate rate constants were obtained and to each rate constant was applied an appropriate fraction of a trans-membrane potential; all of which were treated and assembled within the framework of the Eyring rate equation to construct a single free energy profile (See Fig. 27A). And the single image of the free energy profile (Fig. 27A) contains all of the information required to calculate the single-channel currents as a function of sodium ion activity and trans-membrane potential. In my mind, this stands as a demonstration of the significance and power of Eyring rate theory, embodied within Eqn. (20). To the best of my knowledge, such a capacity has been demonstrated by no other equation.

Following Henry Eyring, one might look toward, for example, quantitative description of the processes of Complex III, so central to the energy conversions that sustain living organisms. One might consider capturing the process of proton flow across the inner mitochondrial membrane in a single image by construction of the free energy profile, and similarly for electron transfer. Then there would be introduction of the coupling processes, which for the Q_o site are the naturally visual mechanical processes of hydrophobic association/dissociation and single-chain extension/relaxation. The capacity to think in such visual and comprehensive ways to convey information and understanding comes to us through the contributions of Henry Eyring.

9. Summarizing comments

9.1 The fundamental physical principle underlying the protein-in-water heat engine of biology

The steam-powered heat engine that set in motion The 19th Century Industrial Revolution heats water at the 100°C *water-to-vapor phase transition to perform mechanical work by expansion*. The fundamental physical process is the increase in entropy of water on heating at a phase transition where more-ordered (lower entropy) molecules of water become highly disordered (high entropy) molecules of water vapor.

On the other hand, the heat engine of biology heats a two-component system, protein-in-water, *to perform mechanical work by protein contraction due to hydrophobic association* (See Fig. 1). The fundamental physical process is again an increase in entropy of water, $\Delta S(H_2O)$. Heating at the phase transition causes pentagonal rings of hydrophobic hydration, N_{hh}, to become less-ordered (higher entropy) bulk water as a *much smaller decrease in entropy* occurs on the protein hydrophobic association of contraction. Due to this latter effect, the protein-in-water phase transition has been called an inverse temperature transition (ITT), wherein the protein component becomes more-ordered on raising the temperature.

The enabling feature of the protein-in-water heat engine of biology is the ease with which the state of a "biological functional group" changes the temperature of its protein-in-water phase transition, i.e., of the ITT.

A biological functional group can exist in two or more states. Invariably those states may be characterized as more-hydrophobic (m-h) and less-hydrophobic (l-h). On becoming more hydrophobic the protein of which it is part immediately develops more hydrophobic hydration. *On formation of hydrophobic hydration, $|T\Delta S| > |\Delta H|$, and at the phase transition, $\Delta H_t \approx T_t \Delta S_t$. Because of these thermodynamic relationships, the result of introducing a chemical or electrochemical energy that makes a functional group more-hydrophobic is that the phase transition shifts to a lower temperature. In particular, at the phase transition, $T_t \approx \Delta H_t/\Delta S_t$ and on formation of more hydrophobic hydration, $T_t(m\text{-}h) \approx (\Delta H_t + \delta H)/(\Delta S_t + \delta S)$, but since $|\Delta H_t + \delta H| < |T(\Delta S_t + \delta S)|$, $T_t(m\text{-}h) < T_t(l\text{-}h)$.*

Thus, instead of having to raise the temperature from below to above that of the phase transition to drive contraction by hydrophobic association, making a functional group more-hydrophobic lowers the temperature from above to below physiological temperature to drive contraction by hydrophobic association.

Finally, by way of example, because of the dependence of pK and reduction potential on hydrophobicity, the free energy transduction of electrochemical energy into chemical energy, and vice versa, occur, and because hydrophobicity induced increases in positive cooperativity occur for both acid/base and redox titrations, the result is increased efficiency, i.e., the optimization of biological free energy transduction by the proteins of biology. And so it goes for all of the pair-wise energy conversions of Fig. 8 and of section **4.2**. These (on inclusion of transient "near ideal" elastic deformation, even of single chains) constitute the dominant energy conversions that sustain Life.

Using herein-derived thermodynamic elements of the change in Gibbs free energy of hydrophobic association, $\mathbf{\Delta G_{HA}}$, of the apolar-polar repulsive free energy of hydration, ΔG_{ap}, and of "near ideal" elastic deformation of protein chains, this article discusses the function of key proteins involved in the trans-membrane transport energy converting processes of biology, and they point to the Eyring Theory of Rate Processes Legacy to demonstrate how the complete trans-membrane transport process may be captured in a single image of the free energy profile for transport from one side to the other of the cell membrane.

10. Acknowledgements

11. References

Abrahams, JP.; Leslie, AGW.; Lutter, R. & Walker, JE. (1994). Structure at 2.8 Å of F_1–ATPase from bovine heart mitochondria. *Nature* (London), 370, 621-628. Protein Data Bank, Structure File 1BMF.

Anderson, OS.; Apell, H-J; Bamberg, E.; Busath, DD.; Koeppe, RE.; Sigworth, FJ.; Szabo, G.; Urry DW. & Woolley, A. (1999). Gramicidin channel controversy – the structure in a lipid environment. *Nature Structural Biology*, 6, 609.

Anderson, OS. & Koeppe II, RE. (1992). Molecular determinants of channel function," *Physiol. Rev.* 72, S89-S158.

Anfinsen, C.B. (1973). Principles that govern the folding of protein chains. *Science*, 181, 223-230.

Bamberg, E.; Apell, H.J. & Alpes H. (1977). Structure of the gramicidin A channel: Discrimination between the $\pi_{L,D}$ and the β helix by electrical measurements with lipid bilayer membranes. *Proc. Natl. Acad. Sci. USA*, 74, 2402-2406.

Bamberg, E.; Apell, H-J.; Alpes H.; Gross, E.; Morrell, JL.; Harbough, JF.; Janko K. & Läuger, P. (1978). Ion channels formed by chemical analogs of gramicidin A. *Fed. Proc.*, 2633-2638.

Boyer, PD. (1993). The binding change mechanism for ATP synthase – some probabilities and possibilities. *Biochim. Biophys. Acta*, 1140, 215-250.

Boyer, PD. (1997). The ATP synthase – a splendid molecular machine. *Annu. Rev. Biochem.*, 66, 717-749.

Brooks, BR.; Bruccoleri, RE.; Olafson, BO.; States, DJ.; Swaminathan, S. & Karplus, M. (1983). CHARMM: A program for macromolecular energy, minimization, and dynamics calculations. *J. Comp. Chem.* 4, 187-217.

Busath, DD. (1993). "The use of physical methods in determining gramicidin channel structure and function," *Ann. Rev. Physiol.* 55, 473-501.

Burkhart BM. & Duax, WL. (1999). Gramicidin channel controversy – reply. *Nature Structural Biology*, 6, 611-612.

Butler, JAV. (1937). The energy and entropy of hydration of organic compounds. *Trans. Faraday Soc.*, 33, 229-238.

Carnot, S. (1992). *Reflections on the Motive Power of Fire*, Peter Smith Publisher, ISBN-13: 978-0844618098, Gloucester, MA

Chang DK. & Urry, DW. (1989). Polypentapeptide of Elastin: Damping of internal chain dynamics on extension. *J. Computational Chem.* 10, 850-855.

Cook, WJ.; Einspahr, HM.; Trapane, TL.; Urry, DW. & Bugg, CE. (1980). Crystal Structure and Conformation of the Cyclic Trimer of a Repeat Pentapeptide of Elastin, Cyclo-(L-Valyl-L-prolylglycyl-L-valylglycyl)3. *J. Am. Chem. Soc.* 102, 5502-5505.

Cross, TA.; Arseniev, A.; Cornell, BA.; Davis, JH.; Killian, JA.; Koeppe II, RE.; Nicholson, LK.; Separovic, F. & Wallace, BA. (1999). Gramicidin channel controversy – revisited. *Nature Structural Biology*, 6, 610-611.

Doyle, DA.; Morais-Cabral, J., Pfuetzner, RA.; Kuo, A.; Gulbis, JM.; Cohen, SL.; Chait, BT. & MacKinnon, R. (1998). The structure of the potassium channel: Molecular basis of K^+ conduction and selectivity. *Science*, 280, 69-77.

Dzyaloshinskii, IE.; Lifshitz, EM. & Pitaevskii, LP. (1961). General theory of van der Waals' forces. *Sov. Phys. Uspekhi*, 4, 153–176.

Eddington, A. S. (1958). The Running-Down of the Universe. Chapter IV, In: *The Nature of the Physical World*, Ann Arbor Paperbacks, The University of Michigan Press, p. 69. First published by Cambridge University Press. Also, Kessinger Publishing LLC, ISBN-10: 1417907185, ISBN-13: 978-1417907182, Whitefish, MT

Eyring, H. (1935). Activated Complex in Chemical Reactions. *J. Chem. Physics*, *3*, 107-115.

Eyring, H. (1969). Models in research. *Int. J. Quant. Chem.*, IIIs, 5-15.

Eyring, H.; Walter, J. & Kimball, GE. (1944, 1958 printing). *Quantum Chemistry*, Chapter XVIII, 18a. van der Waals' forces, pp 351-355.

Fillingame, RH. (1999). Molecular rotary motors. *Science*, 286, 1687-1688.

Fillingame, RH.; Angevine CM. & Dmitriev, OY. (2002). Coupling proton movements to c-ring rotation in F1F0 ATP synthase: Aqueous access channels and helix rotations at the a-c interface. *Biochim. Biophys. Acta*, 1555, 29-36.

Glasstone, S., Laidler, KJ. & Eyring, H. (1941). *The Theory of Rate Processes, The Kinetics of Chemical Reactions, Viscosity, Diffusion and Electrochemical Phenomena*, McGraw-Hill Book Company, Inc. New York and London.

Harris, FE. & Rice, SA. (1954). A chain model of polyelectrolytes. *J. Phys. Chem.* 581 725–732.

Henze, R.; Neher, E.; Trapane TL. & Urry, DW. (1982). Dielectric relaxation studies of ionic processes in lysolecithin-packaged Gramicidin channels. *J. Membr. Biol.*, 64, 233-239.

Hill, AV. (1910). The possible effect of the aggregation of hemoglobin on its dissociation curves, *Proc. Physiol. Soc, J. Physiol.* 40 iv-vii; Hill, AV. (1913). *J. Biochemistry* 7 471-480.

Hobbs, ME.; Jhon, MS. & Eyring, H. (1966). The Dielectric Constant of Liquid Water and Various Forms of Ice According to Significant Structure Theory. *Proc. Natl. Acad. Sci., USA*, 56, 31-38.

Hugel, T. (2003). Towards synthetic molecular motors interfaced by AFM. Dissertation, LMU München, Faculty of Physics.

Jhon MS. & Eyring, H. (1976). Liquid Theory and the Structure of Water. *Ann. Rev. Phys. Chem.*, 27, 45-57.

Katchalsky, A. & Gillis, J. (1949). Theory of the potentiometric titration of polymeric acids. *Recl. Trav. Chim. Pays-Bas.* 678 879.

Kinosita Jr., K.; Yasuda, R.; Noji, H. & Adachi, K. (2000). A rotary motor that can work at near 100% efficiency. *Phil. Trans. R. Soc. Lond. B*, 355, 473-489.

Lange, C. & Hunte, C. (2002). Crystal structure of the yeast cytochrome bc_1 complex with its bound substrate cytochrome c, *Proc. Nat. Acad. Sci.* USA 99 2800-2805. Protein Data Bank, accession code, 1KYO.

Luan, C-H.; Dean Harris, R.; Prasad, KU. & Urry, DW. (1990). DSC studies of the inverse temperature transition of the polypentapeptide of elastin and its analogues. *Biopolymers*, 29, 1699-1706.

Luan, C-H. & Urry, DW. (1910). Solvent deuteration enhancement of hydrophobicity: DSC study of the inverse temperature transition of elastin-based polypeptides. *J. Phys. Chem.* 95, 7896-7900.

Martz E. (2002). FrontDoor to Protein Explorer; http://proteinexplorer.org; 1.982Beta.

McPherson, DT. Xu, J. & Urry, DW. (1996). Product purification by reversible phase transition following *E. coli* Expression of genes encoding up to 251 repeats of the elastomeric pentapeptide GVGVP. *Protein Expression and Purification* 7, 51–57.

Menz, RI.; Walker, JE. & Leslie, AGW. (2001). Structure of bovine mitochondrial F_1-ATPase with nucleotide bound to all three catalytic sites: Implications for mechanism of rotary catalysis. *Cell* 106, 331-341. Protein Data Bank, Structure File 1H8E.

Momany, FA.; McGuire, FF.; Burgess, AW. & Scheraga, HA. (1975). Energy parameters in polypeptides. VII. Geometric parameters, partial atomic charges, nonbonded interactions, hydrogen bond interactions, and intrinsic torsional potentials for the naturally occurring amino acids. *J. Phys. Chem.* 79, 2361-2381.

Nicholson, LK. & Cross, TA. (1989). Gramicidin cation channel: an experimental determination of the right-handed helix. *Biochemistry*, *28*, 9379-9385.

Noji, H.; Yasuda, R.; Yoshida, M. & Kinosita, K. (1997). Direct observation of the rotation of F_1–ATPase. *Nature (London)*, 386, 299-302.

Noji, H. (1998). AMERSHAM PHARMACIA BIOTECH & SCIENCE PRIZE: The Rotary Enzyme of the Cell: The Rotation of F_1-ATPase. *Science*, 282, 1844–1845.

Overbeek, JThG. (1948). The dissociation and titration constants of polybasic acids. *Bull. Soc. Chim. Belg.* 57 252-261.

Pasquali-Ronchetti, I.; Spisni, A.; Casali, E.; Masotti, L. & Urry, DW. (1983). Gramicidin A induces lysolecithin to form bilayers. *Biosciences Reports*, 3, 127-133.

Pauling, L. (1932). The energy of single bonds and the relative electonegativities of atoms. *J. Amer. Chem. Soc.*, 54, 3570-3582.

Pauling, L. (1960). *The Nature of the Chemical Bond and the Structure of Molecules and Crystals: An Introduction to Modern Structural Chemistry.* Third Edition, Cornell University Press, Ithaca, New York, 1960, page 93.

Prigogine, I. & Stengers, I. (1984a). *Order Out of Chaos: Man's New Dialogue with Nature.* Bantam Books, ISBN: 0553340824, New York, p. 103.

Prigogine, I. & Stengers, I. (1984b). *Order Out of Chaos: Man's New Dialogue with Nature.* Bantam Books, ISBN: 0553340824, New York, pp 12-13.

Rodríguez-Cabello, J.C.; Reguera, J.; Alonso, M.; Parker, T.M.; McPherson, D.T.; & Urry, D.W. (2004). Endothermic and exothermic components of an inverse temperature transition for hydrophobic association by TMDSC. *Chem. Phys. Letters* 388, 127-131.

Sanger, F. (1952). The arrangement of amino acids in proteins. *Adv. Protein Chem.*, 7, 1-66.

Sanger, F. & Thompson, EOP. (1953a). The amino-acid sequence in the glycyl chain of insulin. 1. The investigation of lower peptides from partial hydrolysates. *Biochem. J.*, 53, 353-366.

Sanger, F. & Thompson, EOP. (1953b). The amino-acid sequence in the glycyl chain of insulin. 2. The investigation of peptides from enzymic hydrolysates. *Biochem. J.*, 53,366-374.

Schrödinger, E. (1944a). *WHAT IS LIFE?: The Physical Aspect of the Living Cell with Mind and Matter and Autobiographical Sketches,* Cambridge University Press, 1944, (1967, edition, p. 68).

Schrödinger, E. (1944b). *WHAT IS LIFE?: The Physical Aspect of the Living Cell with Mind and Matter and Autobiographical Sketches,* Cambridge University Press, (1967, edition, p. 76).

Smith, CW. (1977). William Thomson and the creation of thermodynamics: 1840–1855. *Arch. Hist. Exact Sci.*, 16, 231-288. DOI: 10.1007/BF00328156.

Spisni, A.; Pasquali-Ronchetti, I.; Casali, E.; Lindner, L.; Cavatorta, P.; Masotti, L. & Urry, DW. (1983). Supramolecular organization of lysophosphatidylcholine-packaged Gramicidin A. *Biochim. Biophys. Acta*, 732, 58-68.

Stock D,; Leslie AGW, & Walker JE, (1999). Molecular architecture of the rotary motor in ATP synthase. *Science*, 286, 1700-1705. Protein Data Bank, Structure File 1QO1

Stackelberg, Mv. & Müller, HR. (1951). Zur Struktur der Gashydrate. *Naturwissenschaften*, 38, 456- .

Stackelberg, Mv. & Müller, HR. (1954). Feste Gashydrate II: Struktur und Raumchemie. *Zeitschrift für Elektrochemie*, 54, 25-39. (became *Berichte der Bunsengesellschaft für physicalische Chemie*).

Szabo, G. & Urry, DW. (1979). N-Acetyl Gramicidin: Single-Channel Properties and Implications for Channel Structure. *Science*, 203, 55-57.

Teeter, MM. (1984). Hydrophobic protein at atomic resolution: Pentagonal rings of water molecules in crystals of crambin. *Proc Natl Acad Sci USA*, 81, 6014–6018.

Thompson, AN.; Posson, DJ.; Parsa, PV. & Nimigean, C.M. (2008). Molecular mechanism of pH sensing in KcsA potassium channels. *Proc. Natl. Acad. Sci.* USA, 105 6900-6905.

Toffler, A. (1984). Forward, page xx. In: Prigogine, I. & Stengers, I. (1984). *Order Out of Chaos: Man's New Dialogue with Nature.* Bantam Books, ISBN: 0553340824, New York.

Urry, DW. (1971). The Gramicidin A trans-membrane channel: A proposed $\pi_{(LD)}$ Helix," *Proc. Natl. Acad. Sci.* USA, 68, 672-676.

Urry, DW. (1972). A Molecular Theory of Ion Conducting Channels: A Field-Dependent Transition Between Conducting and Nonconducting Conformations. *Proc. Natl. Acad. Sci. USA*, 69, 1610-1614.

Urry, DW. (1982a). Henry Eyring (1901-1981): A 20th Century Physical Chemist and His Models. *Mathematical Modelling* 3, 503-522.

Urry, DW. (1982b) On the Molecular Structure and Ion Transport Mechanism of the Gramicidin Transmembrane Channel, In: *Membrane and Transport*, Martonosi, A., (Ed.), 2, 285-294, Plenum Publishing Corporation, New York, New York.

Urry, DW. (1983). What is elastin; What is not. *Ultrastruct. Pathol.* 4, 227-251.

Urry, DW. (1984). Ionic mechanisms of the Gramicidin trans-membrane channel: cation nuclear magnetic resonance, dielectric relaxation, carbon-13 Nuclear Magnetic Resonance, and Rate Theory calculation of single-channel currents, In: *NATO Advanced Study Institute Series C, Spectroscopy of Biological Molecules*, Sandorfy, C. & Theophanides T., (Eds.), 511-538, D. Reidel Publishing Company, ISBN: 9789027718495, Dordrecht, Holland.

Urry, DW. (1985). Chemical Basis of Ion Transport Specificity in Biological Membranes. In *Topics in Current Chemistry*, (F.L. Boschke, Ed.) 128, 175-218, Springer-Verlag, Heidelberg, Germany

Urry, DW. (1987). NMR relaxation studies of alkali metal ion interactions with the Gramicidin A trans-membrane channel. *Bull. Magn. Reson.*, 9, 109-131.

Urry, DW. (1990). Elastomeric Polypeptide Biomaterials: Structure and Free Energy Transduction. *Mat. Res. Soc. Symp. Proc.* 174, 243-250.

Urry, DW. (1991). Protein Folding Controlled by Chemically Shifting the Temperatures of Inverse Temperature Transitions. In: *Proteins: Structure, Dynamics and Design*, Renugopalakrishnan, V.; Carey, PR.; Smith, ICP.; Huang, SG. & Storer, AC., (Eds.), Escom Sci. Publ. B.V., Leiden, The Netherlands, pp. 352-360.

Urry, DW. (1992). Free Energy Transduction in Polypeptides and Proteins Based on Inverse Temperature Transitions. *Prog. Biophys. Molec. Biol.*, 57, 23-57.

Urry, DW. (1995). Elastic Biomolecular Machines: Synthetic chains of amino acids, patterned after those in connective tissue, can transform heat and chemical energy into motion. *Scientific American*, January 44–49.

Urry, DW. (1997). Physical chemistry of biological free energy transduction as demonstrated by elastic protein-based polymers. (invited FEATURE ARTICLE) *J. Phys. Chem.B*, 101, 11007-11028.

Urry DW. (2004). The change in Gibbs free energy for hydrophobic association: derivation and evaluation by means of inverse temperature transitions. *Chem. Phys. Lett.*, 399, 177–183.

Urry DW. (2005). Hydrophobic and elastic mechanisms in Complex III/Rieske Iron Protein (RIP), walking protein motors and protein-based materials. In: *Peptide Science 2004*, Shimohigashi Y. (Ed.), The Japanese Peptide Society (2005), Proceedings of Asian Pacific International Peptide Symposium, APIPS-JPS 2004, pp. 115-118. (ISSN-1344-7661)

Urry DW. (2006a). *What Sustains Life? Consilient mechanisms for protein-based machines and materials*. Springer (Birkhauser), LLC, New York, ISBN: 08176 4346 X.

Urry DW. (2006b). Deciphering engineering principles for the design of protein-based nanomachines. In: *Protein-Based Nanotechnology*, Renugopalakrishnan, V.; Lewis, R. & Dhar PK. (Eds.), Springer, Chapter 9, 141-188.

Urry DW. (2006c). Function of the F_1-motor (F_1-ATPase) of ATP synthase by apolar-polar repulsion through internal interfacial water. *Cell Biol. Intl.*, 30, 44–55.

Urry, DW.; Goodall, MC.; Glickson, JD. & Mayers, DF. (1971). The Gramicidin A trans-membrane channel: Characteristics of head-to-head dimerized $\pi_{(LD)}$ helices. *Proc. Natl. Acad. Sci. USA*, *68*, 1907-1911.

Urry, DW.; Long, MM. & Sugano, H. (1978). Cyclic Analog of Elastin Polyhexapeptide Exhibits an Inverse Temperature Transition Leading to Crystallization. *J. Biol. Chem*. 253, 6301-6302.

Urry, DW.; Venkatachalam, CM.; Spisni, A.; Bradley, RJ.; Trapane, TL. & Prasad, KU. (1980a). The malonyl Gramicidin Channel: NMR-derived rate constants and comparison of calculated and experimental single-channel currents. *J. Membr. Biol.*, 55, 29-51.

Urry, DW.; Venkatachalam, CM.; Spisni, A.; Lauger, P. & Khaled, MA. (1980b). Rate Theory Calculation of Gramicidin Single-channel Currents using NMR-derived Rate Constants, *Proc. Natl. Acad. Sci. USA*, 77, 2028-2032.

Urry, DW.; Trapane, TL.; Sugano, H. & Prasad, KU. (1981). Sequential polypeptides of elastin: Cyclic conformational correlates of the linear polypentapeptide. *J. Am. Chem. Soc.* 103, 2080-2089.

Urry, DW.; Prasad, KU. & Trapane, TL. (1982a). Location of monovalent cation binding sites in the Gramicidin channel. *Proc. Natl. Acad. Sci. USA, 79*, 390-394.

Urry, DW.; Trapane, TL. & Prasad, KU. (1982b). Molecular structure and ionic mechanisms of an ion-selective trans-membrane channel: Monovalent versus divalent cation selectivity. *Int. J. Quant. Chem.: Quant. Biol. Symp.*, 9, 31-40.

Urry, DW.; Trapane, TL.; Walker JT. & Prasad, KU. (1982c) On the relative lipid membrane permeability of Na$^+$ and Ca^{2+}: A physical basis for the messenger role of Ca^{2+}. *J. Biol. Chem.*, *257*, 6659-6661;

Urry, DW.; Venkatachalam, CM.; Long M.M. & Prasad, K.U. (1982d). Dynamic β-Spirals and A Librational Entropy Mechanism of Elasticity," In: *Conformation in Biology,* Srinivasan R. & Sarma, RH. (Eds.) G.N. Ramachandran Festschrift Volume, Adenine Press, USA, 11-27.

Urry, DW.; Walker JT. & Trapane, TL. (1982e). Ion interactions in (1-^{13}C)D•Val^8 and D•Leu^{14} analogs of Gramicidin A, the helix sense of the channel and location of ion binding sites. *J. Membr. Biol.*, *69*, 225-231.

Urry, DW.; Trapane, TL. & Prasad, KU. (1983). Is the Gramicidin A trans-membrane channel single-stranded or double-stranded helix? A simple unequivocal determination. *Science,* 221, 1064-1067.

Urry, DW. & Venkatachalam, CM. (1983). A librational entropy mechanism for elastomers with repeating peptide sequences in helical array. *Int. J. Quant. Chem.: Quant. Biol. Symp*. 10, 81-93.

Urry, DW.; Trapane, TL.; Prasad, KU. & McMichens, RB. (1989). Ion interactions at membranous polypeptide sites using NMR: Determining rate and binding constants and site locations, In: *Methods in Enzymology*, Fleischer, S. (Ed.), 171, 286-342, ISBN-10: 0121820742, Academic Press, Inc., New York, New York.

Urry, DW.; Peng, S. & Parker, TM. (1993). Delineation of electrostatic-and hydrophobic-induced pka shifts in polypentapeptides: The glutamic acid residue. *J. Am. Chem. Soc.*, 115, 7509-7510.

Urry, DW.; Peng, S.; Gowda, DC.; Parker, TM. & Harris, RD. (1994). Comparison of electrostatic- and hydrophobic-induced pka shifts in polypentapeptides: The lysine residue. *Chem. Phys. Ltrs*, 225, 97-103.

Urry, DW.; Luan, C-H.; Harris, CM. & Parker, T. (1997a). Protein-based materials with a profound range of properties and applications: The elastin ΔT$_t$ hydrophobic paradigm, In: *Protein-Based Materials*, McGrath K. & Kaplan, D., (Eds.), Birkhauser, Boston, 133–177.

Urry, DW.; Peng, S.; Xu J. & McPherson, DT. (1997b). Characterization of waters of hydrophobic hydration by microwave dielectric relaxation. *J. Amer. Chem. Soc.*, 119, 1161–1162.

Urry, DW.; Hugel, T.; Seitz, M.; Gaub, H.; Sheiba, L.; Dea, J.; Xu J. & Parker, T. (2002). Elastin: A representative ideal protein Elastomer. *Phil. Trans. R. Soc. Lond.* B, 357, 169-184.

Urry, DW. & Parker, TM. (2002). Mechanics of elastin: Molecular mechanism of biological elasticity and its relevance to contraction. *J. Muscle Res. Cell Motility*, 23, 541-547. In: Special Issue: *Mechanics of Elastic Biomolecules*, Granzier, H.; Kellermayer M. Jr. &. Linke, W., (Eds.)

Urry, DW.; Urry, KD.; Szaflarski, W.; Nowicki M. & Zabel, M. (2009). Function and frustration of multi-drug ABC exporter protein and design of model proteins for drug delivery using protein hydration thermodynamics. *Current Pharmaceutical Design*, 15, 2833-2867.

Urry, DW.; Urry, KD.; Szaflarski, W. & Nowicki M. (2010). Elastic-contractile model proteins: Physical chemistry, protein function and drug design and delivery. doi:10.1016/j.addr.2010.07.001; *Adv. Drug Del. Rev.*, xxx, xxx–xxx.

Uysal, S.; Vásquez, V.; Tereshko, V.; Esaki, K.; Fellouse, FA.; Sidhu, SS.; Koide, S.; Peroz, E. & Kossiakoff, A. (2009). Crystal structure of full-length KcsA in its closed conformation. *Proc. Natl. Acad. Sci.* USA, 106, 6644-6649. Protein Data Bank accession code 3EFF.

Venkatachalam, CM.; Khaled, MA.; Sugano, H. & Urry, DW. (1981). Nuclear magnetic resonance and conformational energy calculations of repeat peptides of elastin: Conformational characterization of cyclopentadecapeptide, cyclo-(L-Val$_1$-L-Pro$_2$-Gly$_3$-L-Val$_4$-Gly$_5$)$_3$. *J. Am. Chem. Soc.* 103, 2372-2379.

Venkatachalam CM. & Urry, DW. (1981). Development of a Linear Helical Conformation From Its Cyclic Correlate. β-Spiral Model of the Elastin Poly(pentapeptide), (VPGVG)$_n$. *Macromolecules* 14, 1225-1229.

Volpin, D.; Urry, DW.; Pasquali-Ronchetti, I. & Gotte, L. (1976). Studies by Electron Microscopy on the Structure of Coacervates of Synthetic Polypeptides of Tropoelastin. *Micron* 7, 193-198.

Wasserman, ZR. & Salemme, FR. (1990). A molecular dynamics investigation of the elastomeric restoring force in elastin. *Biopolymers* 29: 1613–1631.

Zhang, Z.; Huang, L.; Shulmeister, VM.; Chi, YI.; Kim, KK.; Hung, LW.; Crofts, AR.; Berry, EA. & Kim, SH. (1998). Electron transfer by domain movement in cytochrome bc$_1$, *Nature* 392 677-684. Protein Data Bank, accession code 1BCC and 3BBC.

Zhou, Y.; Morais-Cabral, JH., Kaufman, A. & MacKinnon, R. (2001). Chemistry of ion coordination and hydration revealed by a K$^+$ channel-Fab complex at 2.0 Å resolution. *Nature*, 414, 43-48.
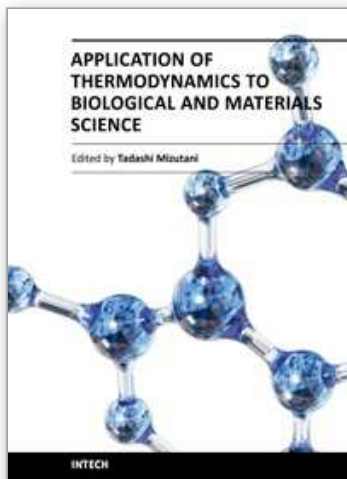
Application of Thermodynamics to Biological and Materials Science
Edited by Prof. Mizutani Tadashi

Progress of thermodynamics has been stimulated by the findings of a variety of fields of science and technology. The principles of thermodynamics are so general that the application is widespread to such fields as solid state physics, chemistry, biology, astronomical science, materials science, and chemical engineering. The contents of this book should be of help to many scientists and engineers.

How to reference

In order to correctly reference this scholarly work, feel free to copy and paste the following:

Dan W. Urry (2011). Thermodynamics of Protein Structure Formation and Function, Application of Thermodynamics to Biological and Materials Science, Prof. Mizutani Tadashi (Ed.), ISBN: 978-953-307-980-6, InTech, Available from: http://www.intechopen.com/books/application-of-thermodynamics-to-biological-and-materials-science/thermodynamics-of-protein-structure-formation-and-function

INTECH
open science | open minds